DIGITAL ACCESS TO SCHOLARSHIP AT HARVARD
DASH.HARVARD.EDU

HARVARD LIBRARY
Office for Scholarly Communication

Sensing flow when it matters: a behavioral and circuit analysis of mechanosensation in the larval zebrafish

Citation

ODSTRCIL, IRIS. 2018. Sensing flow when it matters: a behavioral and circuit analysis of mechanosensation in the larval zebrafish. Doctoral dissertation, Harvard University, Graduate School of Arts & Sciences.

Permanent link

http://nrs.harvard.edu/urn-3:HUL.InstRepos:42015869

Terms of Use

This article was downloaded from Harvard University's DASH repository, and is made available under the terms and conditions applicable to Other Posted Material, as set forth at http://nrs.harvard.edu/urn-3:HUL.InstRepos:dash.current.terms-of-use#LAA

Share Your Story

The Harvard community has made this article openly available.
Please share how this access benefits you. Submit a story .

Accessibility

Sensing flow when it matters: a behavioral and circuit analysis of mechanosensation in the larval zebrafish

A DISSERTATION PRESENTED
BY
IRIS ODSTRCIL
TO
THE DEPARTMENT OF MOLECULAR AND CELLULAR BIOLOGY

IN PARTIAL FULFILLMENT OF THE REQUIREMENTS
FOR THE DEGREE OF
DOCTOR OF PHILOSOPHY
IN THE SUBJECT OF
BIOLOGY

HARVARD UNIVERSITY
CAMBRIDGE, MASSACHUSETTS
MAY 2017

© 2017 - Iris Odstrcil
All rights reserved.

Florian A. Engert Iris Odstrcil

Sensing flow when it matters: a behavioral and circuit analysis of mechanosensation in the larval zebrafish

Abstract

When flying or swimming, animals must adjust their own movement to compensate for displacements induced by the flow of the surrounding air or water. These flow-induced displacements can most easily be detected as visual whole field motion with respect to the animal's frame of reference. In spite of this, many aquatic animals consistently orient and swim against oncoming flows (a behavior known as rheotaxis) even in the absence of visual cues. How animals achieve this task, and its underlying sensory basis, is still unknown. Here we show that in the absence of visual information, larval zebrafish (*Danio rerio*) perform rheotaxis by using flow velocity gradients as navigational cues. We present behavioral data that support a novel algorithm based on such local velocity gradients, that fish use to efficiently avoid getting dragged by flowing water. Specifically, we show that fish use their mechanosensory lateral line to first sense the curl (or vorticity) of the local velocity vector field to detect the presence of flow and, second, measure its temporal change following swim bouts to deduce flow direction. These results reveal an elegant navigational strategy based on the sensing of flow velocity gradients.

Such a refined sensitivity to velocity gradients underscores the need that animals have to correctly identify the source of sensory stimuli to guide appropriate responses. Because fluid drag during locomotion can strongly activate the lateral line, the accurate interpretation of mechanosensory inputs requires that animals distinguish between external and self-generated stimuli. To overcome this kind of challenge, most organisms have evolved to perform neural computations that can nullify or otherwise compensate for the expected self-generated stimulation. These involve efference copies,

which are signals from motor-command centers that inform the sensory pathway about impending movements. The existence of diverse centrifugal projections that contact the lateral line suggests that efference copy mechanisms are involved in this process, yet the circuitry and its consequences on behavior are not well understood.

Using retrograde labeling of the lateral line nerve, we identify two parallel descending inputs that can influence lateral line sensitivity. We perform functional imaging to show that cholinergic signals originating from the the hindbrain transmit efference copies that cancel out self-generated stimulation during locomotion, while dopaminergic signals from the hypothalamus may have a role in threshold modulation in response to locomotion and salient mechanosensory stimuli. We propose that this simple circuit is involved in state-dependent gain modulation and are currently investigating its importance for sensory processing during spontaneous locomotion and mechanosensory-guided behaviors.

Contents

Listing of figures

A mis estrellitas ⋆⋆

Acknowledgments

When Sir Isaac Newton famously stated "If I have seen further, it is by standing on the shoulders of giants", it was to acknowledge that the quest for truth requires building upon previous discoveries. This is also the case at the level of the individual. If I have been able to see at all, it is because I have had immense support from many people. I would like to thank:

Florian Engert, my advisor, for having given me the trust and the freedom to follow my curiosity. His lab, where he has instilled a sense of excitement for ideas and joyful camaraderie, has been a constant source of inspiration, intellectual growth and friendship. His unbounded generosity was particularly important during times of great personal strife. I am forever grateful.

The members of my advisory committee: Alex Schier, Nao Uchida, Chris Harvey, and Aravi Samuel. They have been incredibly generous with their time, their advice and their suggestions for improvement. They have become powerful role models for my years to come.

Pablo Oteiza, my lateral line teammate. It has been an immense joy to work side by side with a friend and trusted fellow scientist.

The three people who taught me everything I needed to accomplish this work: Isaac Bianco, Martin Haesemeyer and Ruben Portugues. Their rigor and guidance throughout my thesis has grounded my thinking and has helped me develop into a more mature scientist. All this, together with laughter, a healthy dose of cynicism, cod liver, and port.

Andre Valente, who has been a steadfast friend, supporter and sounding board for ideas.

Eva Naumann, whose infinite curiosity and vibrance has been a constant source of awe and comfort.

My brothers in the Engert Lab: Clemens Riegler and Tim Dunn, for their unwavering commitment to embark on adventures. Drago Guggiana-Nilo, for being always present to listen, dance or share a meal. Kristian Herrera, for grudgingly appreciating my humor, and sharing coffee and ideas.

The entire Engert Lab: I couldn't have wished for a lab that felt more like home than this one. Adam Douglass, Abhinav Grama, Alix Lacoste, Andrew Bolton, Armin Bahl, Caroline Wee, David Hildebrand, David Schoppik, Entela Nako, Haleh Fotowat, Hanna Zwaka, Holly Martz, Kuo-Hua Huang, Jared Wortzman, Jessica Miller, Kris Severi, Robert Evan Johnson, Max Nikitchenko, and Owen Randlett.

Sean Hardy, for having trusted me as a mentor for his senior thesis, and having put as much effort as enthusiasm into the process. It was a most rewarding experience

I would also like to thank members of the Schier Lab for having adopted me as an honorary member of their group and volleyball team. Thank you Jamie Gagnon, Andi Pauli, Tessa Montague, Adam Carte, Meg Norris, Vassilis Bitsikas, Jeff Farrell, Julien Dubrulle, Mehdi Goudarzi, Albert Pan, Shristi Pandey, Alyson Ramirez, Constance Richter, and Summer Thyme.

I have relied on technical support from Ed Soucy, Doug Richardson, Renate Hellmiss and Chuck Bilikas. They all have been happy to spend time and effort to teach me and have made my work infinitely easier.

The MCO training program and the people who make it happen: Catherine Dulac, Mike Lawrence, Patty Perez, and Fanuel Muindi.

My classmates in the MCO program: Phil Shiu, Eddie Wang, Guo-Liang Chew, Patrick Hsu, Nikki Collins, and Nick Weir. I have learned from you and laughed with you in equal measure. I would particularly like to mention Sara Leiman and Ezgi Hacisuleyman. Sara has been a loyal and devoted friend. In Ezgi I found a kindred spirit, whose passion is a continuous source of inspiration. They both have taken care of me and encouraged me in ways that only truly good friends can.

I would also like to acknowledge those people who, from far away, have been an invaluable presence throughout these years.

The teachers who instilled in me a sense of wonder of the world, who guided me as I tried to find my vocation and who encouraged me every step of the way. Thank you Principal Susana Price Cabrera, Dr. Raymond Day, Ms. Patricia Benmergui and Señor Humberto Lopez. My beloved Northlands School: I carry 'Friendship & Service' in my heart. In this school, I have made the strongest friendships I know and which I hold dearest: Virginia Teijeiro: our parallel paths have made her my trusted confidante and my reference point. She possesses the rare ability to combine strength with kindness. Mariana Grünthal: her unbounded loyalty and love gives me great strength. Florencia Escudero: I have greatly benefited from her groundedness and her unique view of the world. Belen Ayarra: she is pure joy and affection, her energy is infectious. Connie Balboni: our bond is that of children who have promised each other life-long friendship, and its strength lies in its innocence and truth.

Ryan Kabir. He has been my guide through the darkest of times. He pushes me to be the best version of my self.

Finally, I would like to thank my family.

My siblings Grisel and German. From teaching me how to read to making sure I did my homework, they put me on the path that led to where I am now. They have been my role models, my cheerleaders, my greatest sources of comfort and love. Pierrino and Michèle, who in marrying my siblings became my siblings, and who have always supported me and offered me help and advice. The little ones: James, Catherine and Florence. They have brought inexpressible joy and meaning to my life. My dear parents: with their DNA they have instructed my physical composition, and with their teachings they have instructed my values and ideals. Their stars are my beacons.

"He that would seriously set upon the search of truth, ought in the first place to prepare his mind with a love of it. For he that loves it not, will not take much pains to get it; nor be much concerned when he misses it."

John Locke

1 Introduction

1.1 Motivation

The brain and its creations (perceptions, thoughts, dreams) have been of interest to humans for a very long time. However, unlike most other organs in the body, we still do not have a satisfying, unified understanding of how it works. One might argue that this is because the brain is vastly more complex. Additionally, its largely homogeneous, sponge-like structure does not provide great clues about its function. Take the heart as a counterexample: a 4-chambered, muscular organ, filled with blood and directly connected to pipe-like vessels. By 1628, the English physician William Harvey had established that the heart's role was to propel blood through the arteries in order to irrigate the body [Harvey, 1628]. Two-hundred years later, the scientific community still had not reached a consensus regarding how information flow occurred within the brain. Eventually, histological studies pioneered by Santiago Ramón y Cajal using Camillo Golgi's method of sparse labelling, revealed that the nervous system, like all other systems in the body, is made up of cells that in this case, possess

specialized structures that allow for information transfer between them.

Since then, we have attacked the problem at different levels of abstraction in the hopes that this piecemeal approach will enable us to have a complete picture one day. Efforts have ranged from the cataloguing of neuronal types and developmental descriptions of the origins of nervous tissue all the way to mathematical models of information coding and decoding by neurons. At each step of the way, these lines of inquiry have led us to profound insights about the nature of brains, and have even allowed us to develop therapies to relieve psychiatric disorders.

There is one particular approach that I would like to focus on: the study of behavior. Ultimately, the output of the brain is behavior (and the definition of behavior here is large - thoughts are included in it, as well as things that we cannot easily see but are still regulated by the brain like autonomic functions). If we truly want to understand how the brain works, it is necessary to understand what it *does*. Once we have a thorough description of a behavior, we can then move on to measuring activity in the brain in order to find the neurons and circuits that sustain it. This strategy has given us some of the most fundamental principles in neuroscience.

Consider the gill withdrawal reflex of the sea slug *Aplysia*. Normally, sea slugs retract their gills in response to gentle touches to their siphon. Subsequent anatomical examinations revealed that this simple reflex is mediated by a small circuit of sensory neurons in the siphon that synapse directly onto motor neurons innervating gill muscles. This is already an example of matching behavior to its underlying circuit. But the experiments become even more interesting. If a slug is exposed to a noxious stimulus, such as an electric shock, and is then stimulated with the same touch to its siphon, then the gill retraction becomes significantly amplified [Pinsker et al., 1970]. The enhancement of the reflex by a single shock lasts for minutes, but if shocks are repeatedly paired with siphon simulations, then the enhancement of the gill retraction can last for days. This simple behavioral paradigm has since been thoroughly examined to discover the circuit and biochemical mechanisms that give rise to the creation and maintenance of memories [Kupfermann et al., 1970, Castellucci et al., 1970]. Fundamentally, it is the basis for our current understanding of memory (reviewed in Kandel et al. [2014]).

Something that becomes apparent from this example is that we can learn about the functioning of neurons from the most unexpected of organisms. Humans, birds, cats, rodents, bees, flies and worms have been recruited for this task - each with its own benefits and shortcomings. In recent years, the larval zebrafish (*Danio rerio*) has emerged as a worthy subject of study given two crucial

advantages: 1.it has a diverse set of robust behaviors, and 2. its brain is small and transparent, making it amenable to experimentation.

Zebrafish larvae engage in a variety of behaviors that are mostly innate and reflexive, but which can, in some cases, be modulated by previous experience. Behaviors include predator avoidance, prey-capture and feeding as well as locomotor and postural responses to visual or vestibular motion like the optomotor, the optokinetic and the vestibuloocular reflexes [Dunn et al., 2016a, Gahtan et al., 2005, Bianco et al., 2011, Naumann et al., 2016, Portugues et al., 2014, Beck et al., 2004, Bianco et al., 2012]. Furthermore, larvae respond to many other stimuli such as touch, sound, temperature, odors, water flow and pH (reviewed in Orger and de Polavieja [2017]). This makes them ideal subjects for research on sensory processing. Zebrafish larvae also produce movements with distinct kinematic features that depend on their environment or internal state, thereby making them good candidates to study circuits underlying motor-control and action selection [Budick and O'Malley, 2000, Burgess and Granato, 2007, Trivedi and Bollmann, 2013].

Perhaps the most striking advantage of working with zebrafish larvae comes from their translucent bodies. This allows for the non-invasive measurement and manipulation of neuronal activity throughout the entire brain at single-cell resolution [Ahrens et al., 2012, 2013]. All of this is possible due to the development of novel optical methods, which can be implemented with relative ease due to the genetic tractability of the animal. The first, is the advent of genetically encoded fluorescent calcium indicators that report increases in intracellular calcium concentration as a proxy for neuronal activity [Tian et al., 2012]. The second, is the development of optogenetic tools that can selectively activate or silence neurons via light pulses [Fenno et al., 2011, Del Bene and Wyart, 2012]. Taken together, it becomes clear that the strength of the larval zebrafish as a model organism in neuroscience arises from the power to systematically probe the patterns of brain activity that arise as the animal engages in behavior.

The work presented in this thesis is an attempt to do exactly that. In Chapter 2, we describe a behavioral algorithm that enables larvae to use hydrodynamic information to swim against the flow. In Chapter 3, we delve into the anatomy and function of neuronal circuits that modulate the animal's sensitivity to hydrodynamic cues, particularly in the context of distinguishing between external and self-generated stimuli.

1.2 Sensory systems

Behavior can be deconstructed and thought of as a sensorimotor transformation, whereby an organism extracts relevant information about its environment, process it to identify salient features, and then selects an appropriate response, normally in the form of a motor output (Fig.1.2.1). With this framework in mind, it is possible to explore the neuronal and biochemical mechanisms that are at play at every single step of the transformation. We will begin by examining the principal features of sensory systems and their role in behavior.

1.2.1 Sensory processing

Extracting information about the environment requires 1. the detection of physical features of said environment (stimulus detection) and 2. energy transformations that convert stimuli into electrochemical signals that nerve cells can transmit (sensory transduction). Given the wealth of physical features in the world, organisms have developed distinct sensory modalities to detect subsets of them. In general, detectable types of energies are broadly characterized as electromagnetic, chemical, mechanical and thermal [Hudspeth et al., 2013]. For instance: vision, is the detection of photons, olfaction, the detection of volatile compounds, and touch, the detection of pressure on the skin.

The entire process starts with the activation of molecular detectors (receptors) expressed in sensory cells. Whilst the mechanism of action of each receptor depends on the stimulus they are attuned to, their activation always results in the opening of ion channels that change the membrane potential of sensory neurons (Fig.1.2.1, blue) . As an illustration, let us consider mechano-receptors that respond to physical distortions of the skin. Pressure on the skin has a direct impact on the membranes of sensory neurons that innervate it. As the membranes flatten, are squeezed or get otherwise deformed, receptors embedded in the membranes are correspondingly tugged and pulled to the point where their structures adopt an open conformation converting them into channels through which positive ions can flow (reviewed in Kung [2005]). In these cases, there is a significant relationship between stimulus strength and the magnitude of the membrane potential increase (see Montgomery and Bodznick [1994] for a review). Thus, information about pressure intensity gets translated into graded potentials. These receptor potentials can subsequently elicit vesicle release from sensory cells, resulting in the excitation of their post-synaptic partners to continue the relay of information

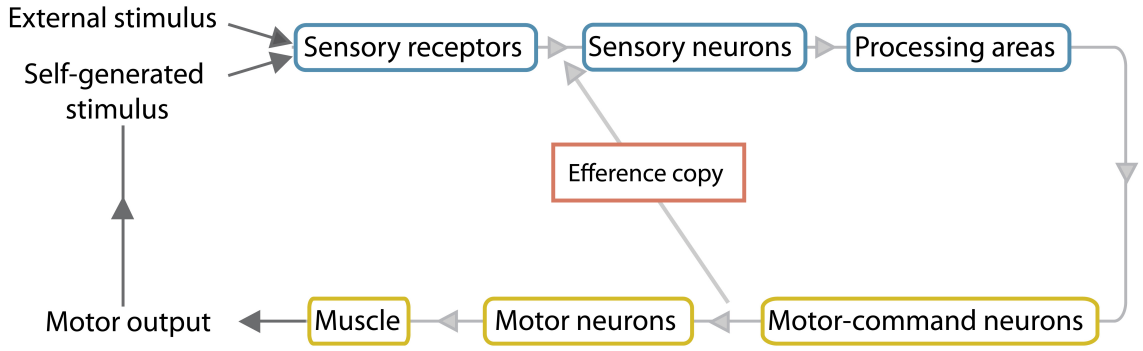

Figure 1.2.1: Efference copy signals bridge the motor and sensory pathways|Schematic of a sensorimotor circuit comprised of a sensory (blue) and motor pathway (yellow). Each pathway is organized hierarchically, where higher tiers denote increased processing complexity and distance from the periphery. Across the animal kingdom, efference copy signals (orange) or other types of corollary discharges have been observed to arise from almost all levels of the motor pathway and target any tier of the sensory pathway. In the larval zebrafish, centrifugal fibers originating from motor centers in the brain project along the lateral line nerve to the neuromasts (sensory receptors/ neurons). Adapted from Crapse and Sommer [2008].

to the central nervous system. Signals at these later stages are no longer graded, but are transmitted through all-or-nothing action potentials, which can encode information through their timing and their frequency.

In this way, energy in the outside world can be translated into signals that the nervous system is able to process and that are subsequently used to make sense of the environment to guide behavioral responses.

1.2.2 Efference copies

In the previous section, we have discussed how events occurring in an animal's environment can activate its sensory systems. This form of external activation is termed exafference. Interestingly though, sensory stimulation can also be generated by an animal's own movement (Fig.1.2.1). This form of reafferent stimulation poses a fundamental source of ambiguity for sensory encoding [Von Holst, 1954]. At the level of sensory receptors, it is physically impossible to discriminate between external and self-generated inputs. Receptors get activated whenever relevant stimuli impinge on them, regardless of their source. This poses a considerable challenge for an animal, which needs to identify the source of sensory stimulation to guide appropriate responses. In addition to informational am-

biguity, reafference also generates sensitivity challenges. Because movement can strongly drive sensory activity, it may mask external inputs that occur concurrently. Furthermore, it can result in the desensitization of primary afferents, leaving the animal unresponsive to stimuli following motion. In terms of information theory, the information content of any given signal is reduced as a function of how predictable it is. Therefore, a completely predictable signal such as a reafferent stimulus conveys no information [Shannon, 1938].

To overcome these problems, organisms have evolved different mechanisms that rely on the same basic strategy. Motor-command centers produce corollary discharges or efference copy signals to inform the sensory pathway about impending movements [Sperry, 1950]. Efference copies are a specific type of corollary discharge whereby an exact copy of the motor command destined for muscles is also transmitted to the sensory pathway (Fig.1.2.1, orange). Once received, the sensory organ or sensory processing area can nullify or otherwise compensate for the expected self-generated stimulation (Fig.1.2.1). Corollary discharge may result in reflex-inhibition or sensory filtration. Reflex-inhibition suppresses maladaptive triggering of reflexes by reafference. Sensory filtration, on the other hand, enables optimization of the information coding capabilities of sensory systems. Examples include increasing the threshold for sensory activation to prevent desensitization by motion or lowering the threshold during static reception (see Crapse and Sommer [2008]for review).

A classical example is given by the work of Curtis Bell on the electric fish *Gnathonemus Petersii*. Electric fish are so called because they emit electric organ discharges (EODs) that are used for electrolocation or communication [Bell et al., 1976]. These fish are also endowed with electrosensory organs that detect the EODs and electric fields created by other fish, together with organs that detect the distortions in the electric field of their own OED caused by objects in the environment [Szabo and Fessard, 1974]. In his experiments, Bell paralyzed fish and recorded cell activity from both the electric organ and from electrosensory brain areas [Bell, 1981]. Note that under paralysis, motor commands reach the electric organ but due to muscle inactivation, the organ fails to elicit an electric discharge. Under these conditions, Bell saw that electrosensory cells fired spontaneously, without any pattern with respect to the occurrences of electric organ discharges. He then proceeded to pair an external electrical stimulus whenever the electric organ was activated. In this case, electrosensory neurons were found to spike in response to the command-locked external stimulus. However, within 15 minutes, this phenomenon disappeared and sensory neurons returned to firing spontaneously and no longer in response to the command-locked stimulus. The most interesting experiment came

next. Bell then stopped delivering the stimulus after the motor-command. This cessation of a motor-locked stimulus, revealed that the spontaneous discharge of sensory neurons was inhibited immediately following a motor command. This beautiful negative image of the expected stimulus was significant evidence for efference copy signals that act to subtract self-generated stimulation.

It is important to note, however, that not all centrifugal projections to sensory areas generate subtractive corollary discharges. Some are involved in neuroprotective mechanisms that reduce or inhibit responsiveness to violent excitation, protecting the system from excitotoxicity caused by overstimulation [Darrow et al., 2007]. Others have been linked to learning or circuit modulation dependent on arousal states [Matsutani and Yamamoto, 2008].

Having discussed in broad terms how the nervous system encodes sensory signals and the general strategies for distinguishing between external and self-generated stimuli, we will turn our attention to the sensory cues that are significant for aquatic organisms such as the larval zebrafish, and their effects on behavior.

1.3 Rheotaxis

Water currents are an important feature of the ecology of most aquatic organisms and have been a driving force for the evolution of a wide variety of behavioral responses across the animal world. One prominent such behavior is that of rheotaxis: an unconditioned orienting response to water currents, that can be either in the upstream or downstream direction [Lyon, 1904]. In fact, orienting to fluids is a widespread behavioral output in the animal kingdom, and there exists an equivalent behavior to rheotaxis in the air, anemotaxis, which is performed by birds and insects [Vickers, 2000].

In a world that is constantly in motion, the benefits of being able to maintain body position to global current changes are many [Arnold, 1974]. Swimming against currents enables animals to avoid being dragged by them, resulting in the ability to stay in place in regions that are already known. Many species, including salmon and trout, are found to live in specific areas of natural rivers for considerable periods of time [Gerking, 1959]. These 'home ranges' are not only areas in which the fish will spend the majority of their time, but are also areas in which the animals will engage in defensive territorial behavior [Kalleberg, 1958]. The necessity to counteract currents that can remove animals from these home areas becomes obvious for such species.

However, water currents are not exclusively a force to fight against. Some organisms have evolved

to intercept prey that is drifting downstream. For example, trout stay in place in areas of low water velocity (close to the banks or behind rocks) to minimize energy expenditure while remaining within sight of areas of higher water velocities that bring the most amount of prey [Everest and Chapman, 1972]. Furthermore, currents also carry odors downstream, producing olfactory corridors that can be navigated to find food or sexual partners [Fraenkel and Gunn, 1961]. Finally, currents are strong directional factors for migrating animals. They can be a source of energetic savings for animals that drift passively downstream or with open sea currents [Jones, 1961, Jones et al., 1979, Arnold and Cook, 1984] . And they can also provide strong directional cues for adult fish who live in the sea and must return to fresh water to spawn [Fulton, 1897, Bowman, 1933, Meek, 1915].

While there is great variety in the rheotactic behavior across aquatic animals, zebrafish exhibit positive rheotaxis almost exclusively. That is, in the presence of water currents, zebrafish will orient and swim against them. In the wild, zebrafish have been found to live primarily in low and still waters, often connected to rice paddies [McClure et al., 2006]. In the cases where zebrafish were found in running currents, these were characterized by low flow regimes and the animals where often found near the banks or vegetation [Engeszer et al., 2007]. Given that zebrafish don't have a migratory life-cycle, and that their natural habitat is mostly still or slow waters, having the ability to orient and swim against water currents seems like an adequate behavioral response suited for their environment. Because the focus of our work is the larval zebrafish, henceforth discussions about rheotaxis will be limited to positive rheotaxis.

1.3.1 Sensory cues for rheotaxis

If we wish to understand the neuronal underpinnings of rheotaxis, and we consider the behavior a sensorimotor transformation, then it is necessary to think about the set of sensory stimuli that could be used to trigger and modulate it. Currents can directly stimulate fish via water displacements relative to their bodies, or indirectly, by visual, tactile or vestibular stimuli that arise from the displacement of the body in space. At this point, it is worth pointing out that motion is a relative concept; that is, the motion of an object can be determined only in comparison to another object. This implies that in order to detect motion, it is necessary to have access to external frames of reference or to experience changes in the velocity of such motion [Galilei, 1953].

Vision is a sensory modality that easily enables detection of external frames of reference. From

the point of view of a fish, when the flow is strong enough to displace the animal downstream, the fish perceives that the world around it (such as the banks of the river or the vegetation) is drifting away. Motion, thus, can be immediately detected. Indeed, when fish are presented with moving whole-field visual stimuli, they will turn and swim in the direction of perceived motion, even in the absence of water currents [Lyon, 1904]. These responses to displacement of visual images are termed optomotor responses (OMR) and have been widely used to study visuomotor processing in the brain of larval zebrafish [Cords, 1922, Ahrens et al., 2012, Portugues and Engert, 2011, Naumann et al., 2016]. In this scenario, to perform rheotaxis successfully, the animal must generate motor outputs that are sufficient to maintain the image of the external world as static as possible [Lyon, 1909]. While optic flow is a sufficient stimulus to trigger rheotactic behavior in many species, it is certainly not necessary. Blind cave-fish can perform rheotaxis, as well as sperm cells and bacteria [Baker and Montgomery, 1999, Bretherton and Lord Rotschild, 1961, Miki and Clapham, 2013, Fu et al., 2012].

In the absence of light, animals can detect currents by finding additional sources of external frames of reference or by being sensitive to changes in water speed. By touching the bottom of the river, for example, animals can sense if they are being dragged with respect to the more static river bed. Experimentally blinded *Fundulus* and minnows (*Phoxinus phoxinus*), have been found to swim in random directions in response to water flow until they come into contact with the bottom of the chamber or the stream [Lyon, 1904, Dijkgraaf, 1963]. In these experiments, even brief encounters with the bottom elicited rheotactic behavior and biased the localization of the animals to the bottom. Consistent with this finding, in the wild, salmonids keep position at night by moving to the bottom or to the banks of streams. In these locations, they have a tactile point of reference, as well as the added benefit of experiencing the lowest flow speeds due to the boundary layer [Davidson, 1949, Lindroth, 1956, Fabricius and Gustafson, 1955]. An extreme form of tactile adaptation in fishes that inhabit torrential mountain streams is the development of adhesive organs on their ventral surface [Hora, 1922].

Finally, we turn our attention to the detection of inhomogeneities in the fluid flow as sources of information about currents. Changes in flow velocity can be easily detected as periods of acceleration, which the vestibular system is exquisitely attuned for. Fish are known to respond to angular acceleration by counteracting rotations about any of the three main body axes [Jones, 1957, Howland and Howland, 1962, Ehrlich and Schoppik, 2017]. These kinds of responses, which are mediated by the

semicircular canals of the otic labrynth, do not seem to be involved in rheotaxis [Howland, 1971, Gray, 1937]. Furthermore, as of yet, experimenters have failed to find fish that respond to linear accelerations [Löwenstein, 1932, Gray, 1937].

So far, we have not considered that water flow itself can directly stimulate an animal. The presence of inhomogeneities that give rise to water motion relative to the fish's body result in direct stimulation that can guide behavior. Hydrodynamic changes in the immediate vicinity of a fish can be sensed by the lateral line system, a collection of external mechanosensory organs (akin to small whiskers) distributed along their bodies. We will examine this sensory modality at length in the next section. For now, it is sufficient to mention that experiments of freely-swimming *Menidia* larvae in water tunnels have shown that local water flow can provide enough force to bend (and activate) the mechanosensory organs [Cahn and Shaw, 1965]. The role of the lateral line in guiding rheotaxis, however, is contested. In some species, such as *Cheimarrichtys fosteri* and *Pagothenia borchgrevinki*, physical ablation of the lateral line results in the elimination of rheotactic behavior in the dark [Montgomery et al., 1997]. Conversely, studies in *Fundulus heteroclitus* and *Epinephelus striatus* show that fish with inactivated lateral lines are indistinguishable from wild-type siblings [Parker, 1903, Jordan, 1917]. The latter two experiments, however, are limited by the fact that they were conducted in the light, and therefore introduce optomotor responses as confounding factors. To completely avoid this problem, different groups have tested the necessity of the lateral line in the rheotactic behavior of the Mexican blind cave-fish (*Astyanax fasciatus*) without a clear consensus [Baker and Montgomery, 1999, Kulpa et al., 2015, Van Trump and McHenry, 2013]. It is possible that the role of the lateral line in rheotaxis is species-dependent. While it is understood that lateral-line mediated rheotaxis would involve the detection of changes in flow velocity within a stream, the mechanism by which this could be achieved and the behavioral reactions to changes in flow velocity are currently unknown. As we have seen, rheotaxis is a greatly varied behavior across species. Larval zebrafish, our focus of study, have been shown to engage in rheotaxis both in the light and in the dark [Olszewski et al., 2012, Olive et al., 2016]. Furthermore, they lose the ability to effectively rheotax in the dark without a functional lateral line [Suli et al., 2012]. Little is known about the navigational algorithms that give rise to rheotaxis in the dark, and these will be explored at length in Chapter 2.

1.4 The lateral line

As we have discussed, fish and amphibians use changes in water displacement around their bodies to sense objects in their vicinity and currents that could displace them [Dijkgraaf, 1963]. The lateral line system enables detection of such hydrodynamic stimuli and is engaged during behaviors such as schooling, prey capture, predator avoidance and rheotaxis [Partridge and Pitcher, 1980, McHenry et al., 2009, Montgomery et al., 1997, 2002, Suli et al., 2012]. In general, it is thought to mediate 'touch at a distance', and it becomes particularly important in conditions of turbidity or low luminance where sight cannot be used effectively [Dijkgraaf, 1963].

The lateral line is comprised of arrays of sensory organs, the neuromasts, distributed on the head and along the body in highly stereotyped species-specific patterns (Fig.1.4.1) [Webb, 1989a, Coombs et al., 1988]. The organs are further subdivided into external and canal neuromasts. External neuromasts are found in the epidermis and their apical surfaces protrude from the skin into the immediate external environment [Schulze, 1861, Webb, 1989b]. They can be directly stimulated by water flow relative to the animal's body, and their activation correlates with the strength of the flow [Schulze, 1870, Kroese and Van Netten, 1989]. Canal neuromasts, on the other hand, are found burrowed under the skin or bone, in fluid-filled cavities between two adjacent canal pores [Leydig, 1850]. Stimulation of canal neuromasts occurs when pressure differences between adjacent pores generate currents in the cavities that connect them. They essentially compute the derivative of the flow or pressure fields along the body. Only cartilaginous and bony fishes possess canal neuromasts [Chagnaud and Coombs, 2013]. These are not present in amphibians nor in fish larvae such as as the zebrafish larvae [Lannoo, 1985, Northcutt, 1989]. For this reason, we will continue our discussion of the lateral line only in reference to external neuromasts for the remainder of this work.

With respect to anatomy, neuromasts on the head form the anterior lateral line (ALL), while those on the trunk and tail form the posterior lateral line (PLL) (Fig.1.4.1a). In the larval zebrafish, neuromasts contain a core of 20 to 30 direction-selective mechanosensory hair cells intercalated with support cells and covered by protective mantle cells (Fig.1.4.1c, Ghysen and Dambly-Chaudiere [2004], Ma and Raible [2009]). The cupula, a gelatinuous structure made of proteins and polysaccharides, encases the filaments granting them stiffness and protection [Richardson et al., 1987]. Interestingly, cupulae have the ability to repair upon injury and are growing continuously [Vischer, 1989, Mukai and Kobayashi, 1995]. Furthermore, given that the hair bundle can be abstracted as a lever pivoting

on a fulcrum, it is generally believed that the physical properties of the cupula, such as length and stiffness, determine the sensitivity of each hair cell [Van Trump and McHenry, 2008].

1.4.1 Development

Developmental studies of the lateral line of zebrafish have almost exclusively been conducted with a focus on the posterior lateral line (PLL). The PLL originates as a placode posterior to the otic vesicle [Kimmel et al., 1995]. By 18-20 hours post-fertilization, the placode delaminates into two components. The first is a small compartment of about 20 cells that differentiates into the sensory neurons of the PLL ganglion that will eventually receive information from hair cells in the periphery and transmit it to the brain [Metcalfe, 1985]. The second compartment, the PLL primordium primI, contains about 100 cells and migrates along the horizontal myoseptum towards the end of the tail. As it migrates, the primordium deposits clusters of immature cells that develop into individual neuromasts within hours [Gompel et al., 2001]. Once it reaches the end of the tail, primI forms three characteristic terminal neuromasts that lie in close proximity to each other. At around the same time, a second primordium emerges and divides to form primII, which migrates towards the tail following prim I, and primD, which pioneers the dorsal component of the PLL [Sapède et al., 2002, Sarrazin et al., 2010]. As the primordia migrate, they are followed by axons from the PLL ganglion and by glial cells that myelinate the PLL nerve [Metcalfe, 1985, Gilmour et al., 2004, Brösamle and Halpern, 2002].

While the animal continues to grow into its juvenile and adult forms, additional neuromasts are deposited. Furthermore, the original lines derived from primI, II and D, migrate ventrally and new lines form to occupy the original positions [Nuñez et al., 2009, Haehnel et al., 2012]. Finally, individual neuromasts amplify to form elongated clusters of new neuromasts termed stitches. Stitches continue to grow throughout the animal's lifetime, ensuring that the lateral line system consistently covers the entire length of the animal's body. Interestingly, upon injury, regeneration of both the neuromasts and the lateral line nerve occurs even during adulthood, which has made the lateral line system a deeply studied subject in the field of regeneration (reviewed in Coffin et al. [2013]).

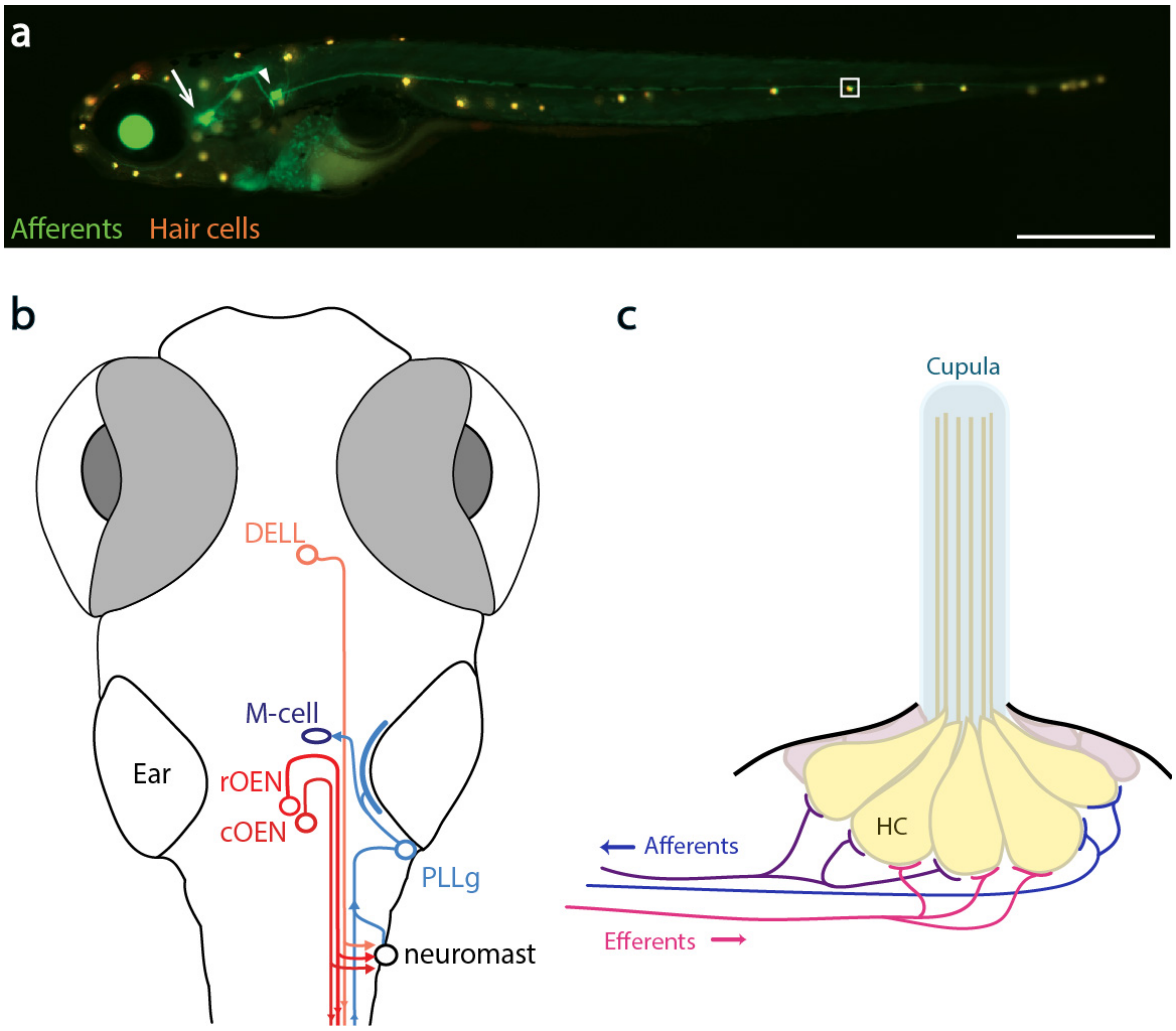

Figure 1.4.1: Anatomy of the lateral line system of zebrafish larvae| a. Side view of a 7 days post-fertilization (dpf) Hgn39D transgenic larvae expressing GFP in primary sensory neurons (green), in which hair cells have been stained using the vital dye DiASP [Pujol-Martí et al., 2012, Schuster and Ghysen, 2013]. Arrow: anterior LL ganglion. Arrowhead: posterior LL ganglion. White box: example neuromast, schematized in c. Scale bar: 0.5 mm. **b.** Diagram showing the major components of the LL circuit. Peripheral sensory organs, neuromasts (black), are activated by mechanosensory stimuli. Upon neuromast activation, signals are transmitted to primary sensory neurons/afferents whose cell bodies reside in the Posterior Lateral Line ganglion (PLLg, light-blue) and whose axonal projections extend to the hindbrain and might make connections with the Mauthner cell (M-cell, dark blue). Descending inputs originate from the Diencephalic Efferents to the Lateral Line (DELL, orange) and from the rostral and caudal Octavomedial Efferent Nuclei (r/cOEN, red). **c.**Schematic of a neuromast. Neuromasts are comprised of hair cells (HC, yellow) that extend hair bundles into the exterior environment and can be deflected by hydrodynamic stimuli. Hair bundles are protected by a cupula made up of proteins and polysaccharides. Additionally neuromasts contain support and mantle cells (pink). Sensory neurons innervate hair cells of a single polarity (afferents, violet and blue) and transmit information from the periphery to the brain. Efferent neurons (magenta), provide descending inputs and can innervate hair cells of multiple polarities. Image inspired by Ghysen and Dambly-Chaudiere [2004].

1.4.2 Sensory processing: from sensory organ to brain

Anatomy & Morphology

Hair cells are not only the main components of neuromasts, but also make up the inner ear, and are key mediators of the sense of hearing and balance in vertebrates (see Fettiplace and Hackney [2006] for review). In fact, our ideas about the "canonical hair" cell are a composite of results obtained in the lateral line of various aquatic species in addition to the inner ear of fishes, amphibians and rodents. While the ultrastructural details might vary between these different organs and across species, the general characteristics are maintained. In all cases, these highly-specialized cells transduce mechanical force (generated by sound or moving fluids) into electrochemical signals. This is primarily achieved by means of their apical "hairs", long filaments that protrude out of the cell into its immediate environment (Fig.1.4.1c). Deflections of the hair bundles open cation-permeable channels, resulting in receptor potentials that can lead to vesicle release from the cell's basal surface [Corey and Hudspeth, 1979]. Importantly, hair cells are directionally sensitive, which means that they become maximally depolarized when stimulated in a preferred direction [Hudspeth and Corey, 1977]. Furthermore, they become hyperpolarized (inhibited) when stimulated against the preferred direction. In general, the magnitude of the electrical response is graded with respect to the magnitude and not with the velocity of deflection [Flock, 1965]. Stimuli that are not aligned to the hair cell preferred axis still elicit electrical responses, albeit of lower magnitude that those produced by stimuli along the preferred axis [Shotwell et al., 1981]. Consequently, oblique stimuli cannot be distinguished from lower intensity stimuli in the preferred axis. Therefore, unambiguous directional information emerges not by virtue of single receptors, but rather, when the output of two hair cells with perpendicular orientations are compared.

Directional preference is determined by the morphology of the hair bundle itself. In the lateral line, each bundle is made up of 30-100 actin-rich stereocilia, arranged in a hexagonal pattern behind a single kinocilium, and connected to each other via tip-links [Kindt et al., 2012, Pickles et al., 1984]. Within a bundle, the length of the stereocilia increases in a "stair-case" fashion towards the kinocilium. The arrangement is so aesthetically striking, that it was reported by light-microscopists as early as the 1800s [Retzius, 1884]. It is this structural asymmetry that confers direction selectivity to the hair cell: forces that deflect the bundle towards the kinocilium, become excitatory by stretching the tip-links and providing the force necessary to open the mechanosensory channels [Pickles et al.,

1984, Kindt et al., 2012]. Conversely, deflections away from the kinocilium alleviate tension and result in hyper-polarization. There exists an interesting non-linearity in stimulus coding, whereby deflections in the preferred direction elicit (excitatory) currents that are larger in magnitude that the (inhibitory) currents caused by equal deflections in the non-preferred orientation [Flock and Wersäll, 1962].

Further directional organization is imposed at the anatomical level given that neuromast hair cells are not positioned in random directions. Rather, each neuromast contains only two populations of hair cells of opposing polarities along either the rostro-caudal or dorso-ventral axis of the fish [Flock and Wersäll, 1962]. In zebrafish, head neuromasts are believed to be of the dorso-ventral kind. The tail, on the other hand, contains both types but preference for the rostro-caudal axis is more prevalent Ghysen and Dambly-Chaudière [2007]. Directional preference is established during development, where neuromasts that arise from the first primordium are always rostro-caudal, while those that arise from the second primordium are exclusively dorso-caudal [López-Schier et al., 2004, Sarrazin et al., 2010].

The afferent pathway

A considerable body of work has traced how mechanosensory information flows from the peripheral neuromasts through different regions in the brain of elasmobranchs, bony fish and amphibians (see Wullimann and Grothe [2013] for review). While in general terms central processing seems to be conserved, there are considerable differences between species. For this reason, I will examine work done exclusively in the larval zebrafish in this section.

As a consequence of deflection in the appropriate direction, hair cells release glutamate at specialized ribbon-synapses in close apposition to the terminals of bipolar afferent neurons [Obholzer et al., 2008]. The cell bodies of these afferent (or primary sensory) neurons are located in small cranial ganglia (Fig.1.4.1a). Neurons that innervate head neuromasts are located in the ALL ganglion, found posterior to the eyes. Neurons that innervate tail and dorsal neuromasts are located in the PLL ganglion, posterior to the ears [Corey and Hudspeth, 1979, Keen and Hudspeth, 2006, Raible and Kruse, 2000]. Single afferent neurons may innervate more than one neuromast but they connect exclusively to hair cells of the same polarity (Fig.1.4.1c ,Nagiel et al. [2008], Faucherre et al. [2009]). Importantly, afferent neurons do not cross the midline and only collect information from

hair cells on the ipsilateral side with respect to their somas, giving rise to a mirror-symmetric circuit through the fish's midline.

Physiological responses of primary sensory neurons are phase-locked to deflections of the hair cells they innervate [Trapani et al., 2009, Haehnel et al., 2012]. At rest, sensory neurons display stochastic spontaneous activity averaging 6.5spikes/sec, generated by the basal spontaneous excitatory transmission of hair cells [Trapani et al., 2009, Trapani and Nicolson, 2011]. Spontaneous spiking in sensory neurons is thought to be critical for information coding [Douglass et al., 1993]. By having an elevated resting state, neurons have a greater dynamic range with which to code for both increases and decreases of their inputs. This is particularly relevant for lateral line sensory neurons that innervate hair cells, which in turn can be depolarized or hyperpolarized depending on the direction of the mechanosensory stimulus.

Afferents from both the ALL and PLL then enter the brain and terminate on the ipsilateral medial octavolateralis nucleus (MON) of the hindbrain forming a somatotopic map, whereby dorsal axons correspond to more posterior neuromasts (Fig.1.4.1b, Alexandre and Ghysen [1999]). A limited number of afferents also converge close to the lateral dendrite of the Mauthner cell, a command neuron that triggers extremely quick escapes, consistent with the observation that the lateral line can mediate escape behaviors [Eaton et al., 1977, Kimmel et al., 1974, Haehnel et al., 2012, Pujol-Martí et al., 2012]. Given that sensory neurons terminate in at least two distinct regions in the hindbrain, recent studies have suggested the existence of two functionally segregated sensory streams [Liao, 2010, Haehnel et al., 2012, Pujol-Martí et al., 2012]. The first is comprised of large early-born afferent neurons that can innervate multiple neuromasts, and whose axonal projections converge onto medial regions of the hindbrain in proximity to the Mauthner cell. Their size confers them with a heightened threshold for activation, making them good candidates for Mauthner-mediated escapes to high intensity stimuli that impinge on large regions of the body. It is important to note, however, that to this date no anatomical nor physiological evidence has been provided to support the claim that synapses exists between lateral line sensory neurons and the Mauthner cell in the larval zebrafish. On the other hand, the second stream is made up of smaller, later-born neurons that innervate single neuromasts and project to the MON. In this case, neurons possess more limited receptive fields and heightened sensitivity, which would be useful to detect and localize subtler inhomogeneities in the water surrounding the animal.

Higher-order nuclei of the lateral line circuit of the larval zebrafish have not been characterized

in detail. Experiments using anterograde transport of dyes have identified higher order neurons in the ipsi- and contralateral hindbrain, the torus semicircularis (TS) and the optic tectum - the latter two being important sites of multisensory integration in the vertebrate brain [Fame et al., 2006]. In agreement with these anatomical studies, recent functional experiments using calcium imaging have have found distinct non-overlapping activation patterns in the tectum when animals where presented with water flow, auditive or visual stimuli [Thompson et al., 2016].

At this point, we have a very good characterization of the initial steps of sensory transmission in the lateral line. For example, the input-output relationships between mechanosensory stimuli and hair cell activity, as well as how hair cell activity relates to the firing patterns of sensory neurons. Nonetheless, significant gaps in our understanding still remain, even at early stages of the sensory pathway. For instance, it is currently unclear how signals from the different hair cell polarities get processed, or how and where inputs from the different branches of the lateral line converge. Our knowledge about the processing of lateral line information in the MON, TS, optic tectum and higher brain areas is severely lacking. Going forward, we believe that an improved characterization of the hydrodynamic stimuli that can stimulate fish, together with a careful dissection of lateral line mediated behaviors, will provide strong hypotheses about the types of computations and neuronal types that should be present in the circuit. These hypotheses can then be tested by means of electrophysiology or whole-brain calcium imaging.

1.4.3 The efferent pathway: from brain to sensory organ

Information is not only transferred in a feed-forward manner from the periphery to the central nervous system, but it can also descend from the central nervous system back to the periphery. In contrast to the afferent system, few studies have been conducted on the efferent system of the lateral line of zebrafish larvae. In this section, I will provide a review of experiments performed in amphibians and various fish species and will draw special attention to the cases where there is data from zebrafish. In fact, it was this lack of knowledge about the zebrafish efferent system that motivated the line of research presented in Chapter 3.

Electron microscopy studies in *Xenopus laevis*, in zebrafish and other fish species have shown that centrifugal axons from the brain terminate in vesicle-rich endings in close proximity to the bases of hair cells and afferent fibers in neuromasts [Hama, 1965, Yamada and Hama, 1972, Toyoshima and

Shimamura, 1982, Dow et al., 2015].

Retrograde labeling with dyes injected into the lateral line nerve of eel, goldfish and zebrafish has revealed that these projections originate from three small nuclei [Meredith and Roberts, 1987, Zottoli and Van Horne, 1983, Metcalfe et al., 1985]. The rostral and caudal efferent nuclei (REN and CEN, respectively) located in the hindbrain are cholinergic, and are normally referred to collectively as the octavolateral efferent nucleus (OEN) (Fig.1.4.1b, red). The third nucleus, the diencephalic efferent of the lateral line (DELL) is catecholaminergic, and is found in the ventral hypothalamus (Fig.1.4.1b, orange, Bricaud et al. [2001], Tay et al. [2011]). In addition to acetylcholine and catecholamines, immunostains of vestibulocochlear efferents exhibit terminals containing GABA, opioids and calcitonin gene related peptide (CGRP), a small peptide ligand involved in nociception and vasodilation via G-protein coupled receptors [Adams et al., 1987]. We currently don't know how similar the auditory and lateral line efferent systems are and if, for example, neuromasts also receive GABA- or opioidergic inputs. Studies that have looked at descending inputs through the lateral line nerve have consistently found the DELL and OEN nuclei as the sole efferent nuclei. Additionally, efferent neurons that innervate the lateral line and ear of the eel have been found to produce both acetylcholine and CGRP, suggesting that the already identified efferent nuclei could account for multiple transmitters [Roberts et al., 1994].

Physiologically, centrifugal activity on the lateral line of fish and amphibians has a major inhibitory component mediated by acetylcholine. In *Xenopus*, the burbot *Lota lota*, and dogfish *Scyliorhynus*, stimulation of efferents in the PLL nerve inhibits spontaneous and evoked activity of afferents by generating inhibitory postsynaptic potentials (IPSPs) in hair cells [Russell, 1971a, Russell and Roberts, 1972, Flock and Russell, 1976]. These effects are not observed when stimulating in the presence of acetylcholine antagonists [Russell, 1971b, Flock and Russell, 1973].

Furthermore, there is direct evidence to suggest that the efferent system is fundamental in distinguishing between exafference and reafference. This evidence hinges upon the finding that efferent activity is closely correlated with the motor output of the animal. In the dogfish, efferent fibers are activated when animals are subject to stimuli that normally cause motor responses but not when the body is passively bent or when neuromasts are exposed to gentle water puffs [Roberts and Russell, 1972]. In addition, electrical stimulation of the Mauthner cell and other reticulospinal neurons also drives the efferent system, suggesting that signals in mid and hindbrain premotor neurons are relayed to the lateral line efferent system [Russell and Roberts, 1974]. A similar effect is observed in goldfish

(*Carassius auratus*), where efferent fiber activity is recorded following excitation of spinal-projecting neurons, including the Mauthner cell [Russell, 1976]. Other movements such as fin, eye and respiratory movements can also drive efferent discharge [Paul and Roberts, 1977, Art and Kroese, 1982, Montgomery and Bodznick, 1994]. This data strengthens the idea that motor commands, including non-locomotive ones, can induce efferent activity in order to counteract self-induced stimulation. It is worth noting that reafference cancellation may occur at multiple sites within the circuit. While hair cells have been shown to be inhibited directly by stimulation of the lateral line nerve, stimuli associated with respiratory movements seem to be processed upstream in the cerebellum-like structure of the medial octavolateral nucleus (MON) [Montgomery and Bodznick, 1999].

Additionally, some reports suggest an excitatory role for efferent fibers. Stimulation of the PLL nerve while blocking cholinergic action unmasks a slowly-developing increase in afferent spontaneous discharge that can persist for minutes after stimulation [Sewell and Starr, 1991]. Paradoxically, application of CGRP onto *Xenopus* neuromasts increases afferent spontaneous firing rate but also suppresses stimuli-evoked responses when hair cells are mechanically stimulated [Bailey and Sewell, 2000a,b]. The physiological and environmental conditions under which CGRP is released is currently unknown and it is unclear why it would be co-released with acetylcholine.

More conclusive results on the excitatory role of efferent neurons comes from a study on dopaminergic modulation in the lateral line of larval zebrafish [Toro et al., 2015]. Through immunohistochemistry and fluorescence microscopy, it was observed that hair cells express the dopamine receptor D1b and that dopaminergic efferents target hair cells but do not seem to form direct synapses with them. Stimulation of hair cells in the presence of D1-receptor agonists resulted in enhanced excitatory currents, which could be decreased by D1-receptor antagonists. These results suggest that dopamine positively modulates activity of hair cells in a paracrine fashion. Adding to our understanding of the context in which these neurons are recruited, independent electrophysiological recordings of dopaminergic efferent neurons in awake, paralyzed larvae uncovered phasic bursting patterns that are tightly correlated with locomotor output [Jay et al., 2015]. Again, we see a correlation between efferent activity and the occurrence of motor outputs.

The wealth of neurotransmitters found at neuromasts is suggestive of various levels of efferent control, with presumably different roles. While we have a significant amount of information about the system, it is fragmented and incomplete.An important shortcoming of previous physiological experiments is that they relied on stimulation of the entire PLL nerve, which we know is a heteroge-

neous collection of axons. Under these conditions, effects observed in afferent and hair cell activity might not be physiologically representative, but rather, a composite response of activity patterns that would normally be elicited independently of each other. In addition, correlations between motor state and efferent activity have been done by recording exclusively from the OEN. If we are to understand the role of efferent modulation on lateral line activity, then we must study efferent nuclei individually and probe their effects systematically. This topic will be the focus of Chapter 3.

"The program of scientific experimentation that leads you to conclude that animals are imbeciles is profoundly anthropocentric. It values being able to find your way out of a sterile maze, ignoring the fact that if the researcher who designed the maze were to be parachuted into the jungles of Borneo, he or she would be dead of starvation in a week... If I as a human being were told that the standards by which animals are being measured in these experiments are human standards, I would be insulted."

John Maxwell Coetzee

2

A novel mechanism for mechanosensory based rheotaxis in larval zebrafish

2.1 Preface

A shorter version of this chapter is published in the journal Nature (Oteiza et al., 2017). This work was performed in equal partnership by Pablo Oteiza and myself, with contributions from Ruben Portugues, George Lauder and Florian Engert. More specifically, P.O. conceived the project, built the rig, performed the experiments and analyzed the data. P.O, I.O. and F.E. designed the experiments. I.O. performed the chemical and 2-photon Lateral Line ablations. P.O. and R.P. designed the software for the behavioral rig. P.O. and G.L. performed the Particle Image Velocimetry experiments. R.P., F.E. and I.O. contributed to the mathematical and theoretical considerations. I.O. and F.E. wrote the model. P.O., I.O. and F.E. wrote the manuscript with the assistance of R.P. and G.L. All authors discussed the data and the manuscript.

2.2 Introduction

When flying or swimming, animals must adjust their own movement to compensate for displacements induced by the flow of the surrounding air or water [Chapman et al., 2011]. These flow-induced displacements can most easily be detected as visual whole field motion with respect to the animal's frame of reference [Lyon, 1904]. In spite of this, many aquatic animals consistently orient and swim against oncoming flows (a behavior known as rheotaxis) even in the absence of visual cues [Dijkgraaf, 1963, Montgomery et al., 1997]. How animals achieve this task, and its underlying sensory basis, is still unknown. Here we show that in the absence of visual information, larval zebrafish (*Danio rerio*) perform rheotaxis by using flow velocity gradients as navigational cues. We present behavioral data that support a novel algorithm based on such local velocity gradients, that fish use to efficiently avoid getting dragged by flowing water. Specifically, we show that fish use their mechanosensory lateral line to first sense the curl (or vorticity) of the local velocity vector field to detect the presence of flow and, second, measure its temporal change following swim bouts to deduce flow direction. These results reveal an elegant navigational strategy based on the sensing of flow velocity gradients and provide a comprehensive behavioral algorithm, also applicable for robotic design, that generalizes to a wide range of animal behaviors in moving fluids.

2.3 Results

2.3.1 Sensory cues for rheotaxis

In order to describe the behavioral mechanisms of flow navigation in larval zebrafish, we built a system consisting of a horizontal transparent tube in which a controlled laminar flow is induced by a linear actuator while motionless black and white stripes are projected from underneath and the behavior of the fish is recorded in three-dimensional space (Fig.2.3.1a-c). We observed that, as previously shown, 5-7 day-old larval zebrafish perform rheotaxis by orienting (Fig.2.3.1d,f,g) and swimming (Fig.2.3.1e,h,i) against the direction of the water flow [Olszewski et al., 2012]. Furthermore, we confirmed that this behavior can also occur in the absence of any visual references [Suli et al., 2012, Olive et al., 2016] (Fig.2.3.1f-i). It is important to point out that under these conditions the flow cannot be directly sensed by the animal if it is being dragged by a homogeneous current. Given that larval zebrafish swim in discrete ∼100ms-long periods of motor activity (swim bouts) separated by ∼900ms-long inactive inter-bout periods at very low Reynolds numbers (∼10) [Budick and O'Malley, 2000, McHenry and Lauder, 2005], the fish will almost immediately come to rest and assume the average velocity of the surrounding water flow at the end of each bout [Muller et al., 2000, Fuiman and Webb, 1988]. In this scenario, both fish and water move at the same speed and therefore no water flows over the animal's body. From the fish's perspective there is no oncoming water flow and, if the flow is truly homogeneous, it is physically impossible to detect it in the absence of cues from an external frame of reference [Lyon, 1904, Galilei, 1953].

Therefore, rheotaxis in darkness may rely on other sensory cues, such as touch or acceleration [Van Trump and McHenry, 2013, Arnold, 1974]. However, given that fish perform rheotaxis away from the chamber walls (Fig.2.3.1b-c and Supp. Fig.A.1.1a,b) and semicircular canals are not functional at larval stages [Münz, 1989], both touch and angular acceleration are unlikely to play a role in our experimental setup. To test the role of linear acceleration, we mounted the entire behavioral set-up on rails, and accelerated it using the same actuator as used for flow induction. We observed no orientation and position-holding behavior at all acceleration values tested, even at those significantly exceeding the ones used during rheotaxis experiments (Supp.Fig.A.1.1c-f).

Thus, we hypothesized that the navigational information required for rheotaxis had to be provided by the non-homogeneous flow properties within the behavioral chamber. In order to precisely

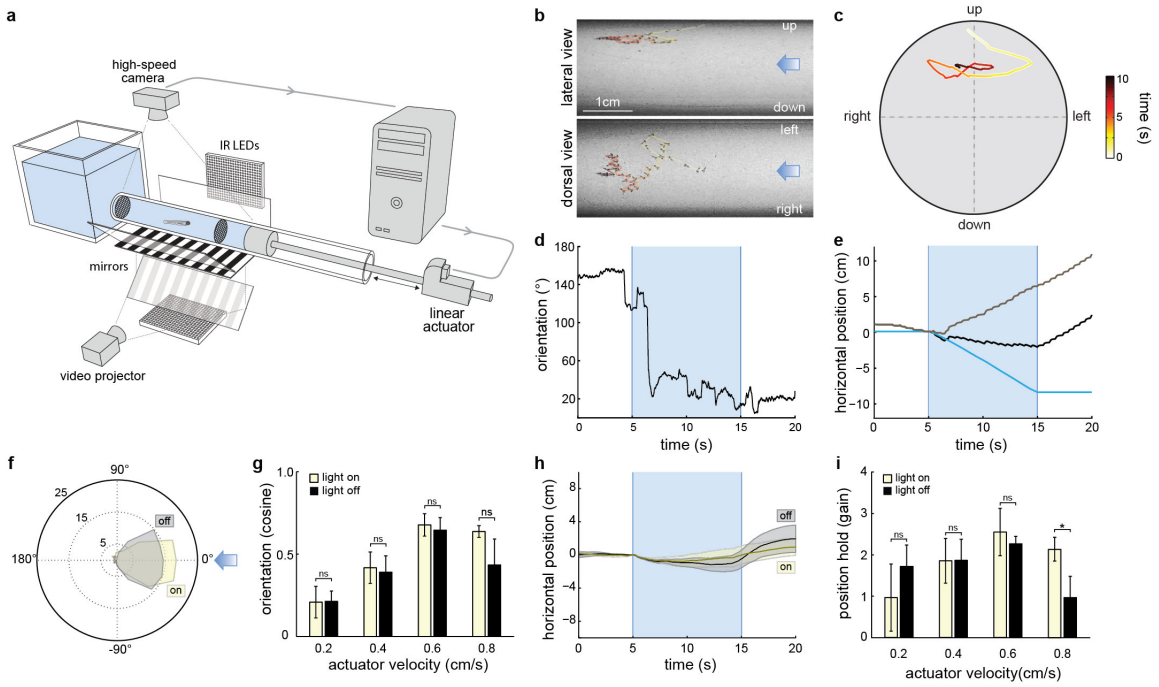

Figure 2.3.1: Larval zebrafish perform rheotaxis in the absence of visual cues| **a.**Schematic of the experimental setup. Water flow is induced by the random displacement either towards or away from the water reservoir of a computer-controlled linear actuator. Two infrared (IR) LED arrays provide illumination while visual cues are projected underneath the behavioral chamber. A high-speed camera records the behavior of the fish from above while a side mirror allows simultaneously recording of a lateral view. **b.**Time-projection of a 6-day old zebrafish larvae performing rheotaxis in the absence of visual cues. Side (upper panel) and Top (lower panel) views are shown. Flow (light blue arrows) comes from the right. **c.**Cross-sectional view of a three-dimensional reconstruction of the trial shown in (b). Tube diameter is 2.2cm. **d-e** Behavioral features of the trial shown in (b-c). Light blue indicates water flow stimulus is on. **d.**Fish orientation in relation to water flow. Zero indicates perfect orientation against flow direction. **e.**Fish position in the axis of the water flow from the observer's point of view (black trace) and the fish's point of view (grey trace). Blue trace corresponds to the displacement of the water column. **f-i.** Larval zebrafish orient and swim against incoming water flows in the absence of visual cues. **f.**Polar plot of fish orientation in the axis of the flow during stimulation. Light blue arrow represents flow direction. **g.**Cosine of the mean orientation for fish presented with different actuator velocities in the presence and the absence of visual cues. Means and SEM are shown, ns = $p>0.05$; Monte Carlo permutation test. **h.**Fish position (from the observer's point of view) in the axis of the water flow in the presence (dark trace) and the absence (light trace) of visual cues. Means (solid line) and SEM (shaded areas) are shown. **i.**Gain (numerical relationship between fish and water velocity, see Methods) for fish presented with different actuator velocities in the presence and the absence of visual cues. Means and SEM are shown, ns = $p>0.05$; * = $0.01>p$ &<0.05; Monte Carlo permutation test. n= 6 fish subjected to 12 trials at each actuator velocity (288 trials total).

measure the flow conditions in our set-up, we used Particle Image Velocimetry (PIV) and observed a radially symmetric velocity profile that develops within approximately five seconds and reaches steady state thereafter (Fig.2.3.2a, Supp.Fig.A.1.2a). To investigate the importance of flow velocity gradients in larval zebrafish rheotaxis, we performed experiments across four different gradient regimes: steep, medium and shallow gradients were created by displacing a plunger inside tubes with a large, medium and small diameter, respectively (Fig.2.3.2b). Additionally, a zero gradient regime was created by not moving the plunger within the tube, but by moving the whole set-up at constant velocity. Importantly, we observed that the ability of fish to orient and to hold position consistently improved with increasing gradient magnitudes (Fig.2.3.2c-f). Trivially, when exposed to a zero-gradient regime, fish did not perform rheotaxis (Fig.2.3.2c-f) [Galilei, 1953]. Thus, in the absence of visual stimuli, flow velocity gradients must be the main cue for rheotaxis in larval zebrafish.

It is important to note that any solid body, like that of a larval zebrafish, that is drifting in a fluid containing a velocity gradient will experience a rotational flow field (or shear) around its perimeter. Strictly, this holds only true in fluids with zero divergence ($\nabla \cdot \vec{V} = 0$). Exceptions to this rule, i.e. if there are local sinks or sources in the water, will be discussed below. This rotational flow field is directly related to the local curl of the water volume ($\nabla \cdot \vec{V}$) and their values are mathematically linked by Stokes' Theorem. In our setup, the velocity profile ($\vec{V}$) of the water flowing in our tube of radius R can be well approximated, in Cartesian coordinates, by:

$$\vec{V} = v_{max} \begin{pmatrix} 0 \\ 0 \\ 1 - \left(\frac{x^2+y^2}{R^2}\right) \end{pmatrix} \tag{2.1}$$

and the resulting, non-zero curl, is accordingly given by:

$$\nabla \times \vec{V} = \begin{pmatrix} \frac{\delta V_z}{\delta y} \\ \frac{-\delta V_x}{\delta y} \\ 0 \end{pmatrix} = \frac{2}{R^2} \begin{pmatrix} -y \\ x \\ 0 \end{pmatrix} \neq 0 \quad \text{(anywhere but the midline)} \tag{2.2}$$

The predicted spinning of an object in such a rotational flow-field can be observed in the case of a paralyzed fish shown in Supp.Fig.A.1.2b,c. Finally, Stokes' Theorem states that the integrated curl

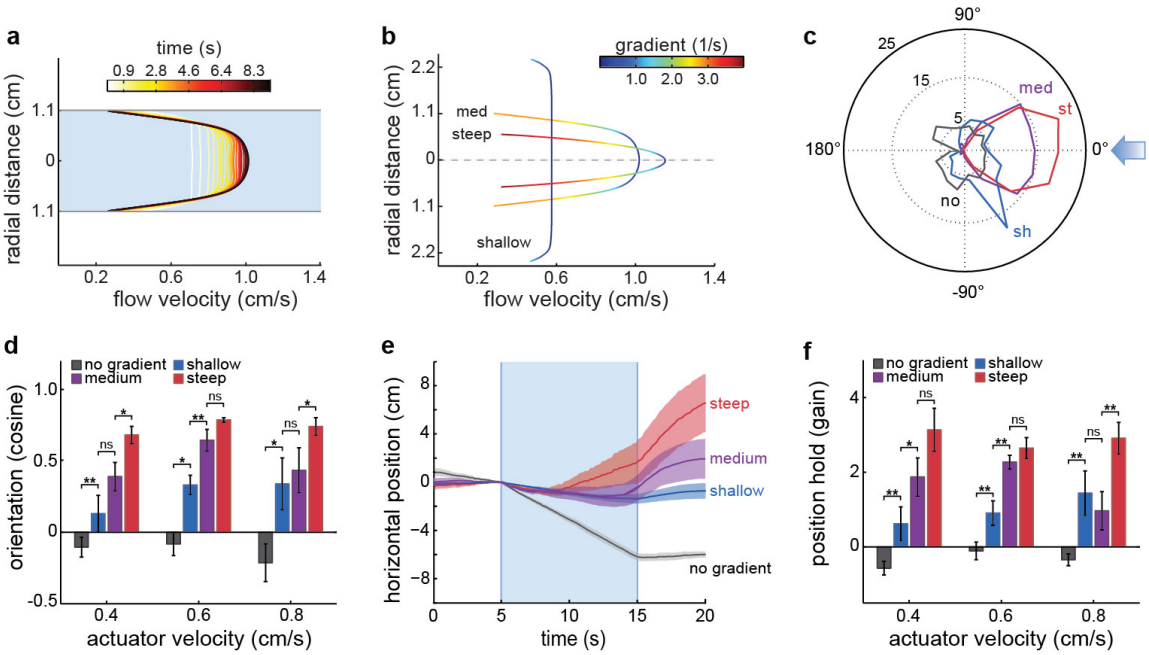

Figure 2.3.2: Flow velocity gradients are the stimulus for rheotaxis in larval zebrafish.| a-b. Water flow in the behavioral chambers. **a.**Color-coded graph of the flow velocity profile development obtained through Particle Image Velocimetry (PIV). White indicates the beginning of the flow while black indicates the final steady-state. Profiles are the result of the average flow velocities measured 5-7cm away from the flow source. **b.**Color-coded graph of velocity gradient magnitudes at the flow steady-state in tubes of large (4.76cm), medium (2.22cm) and small (1.27cm) diameters. Blue and red indicate low and high-gradient magnitudes respectively. **c.**Polar plot of fish orientation (in the axis of the flow) during different gradient profile stimulation. Light blue arrow represents stimulus direction. **d.**Cosine of the mean orientation for fish presented with different gradient conditions. Mean and SEM are shown. **e.**Horizontal positions of fish from the observer's point of view. Means (dark line) and SEM (shaded areas) are shown for different gradient profiles. **f.**Gain for fish in each of the gradient conditions. Mean and SEM are shown; * = p>0.01&<0.05; ** = p<0.01; Monte Carlo permutation test. n=6 fish subjected to 6 trials at each actuator velocity (108 trials) for each gradient condition (432 trials total). Data for medium gradient is the same as in Fig.2.3.1g,i.

over the area occupied by the fish's body (S) can be measured by a line integral around the animal's perimeter:

$$\int\int_S (\nabla \times \vec{V}) \cdot d\vec{a} = \oint_C \vec{V} \cdot d\vec{s} \tag{2.3}$$

Thus, the fish could estimate the local curl in the water at its current position by calculating a line integral of the relative flow of water around the circumference of its body (Fig.2.3.3a). We will show below, that the lateral line, a collection of mechanosensory organs distributed along the surface of the body in fish and amphibians [Münz, 1989], is perfectly suited to perform such measurements (the lateral-line integral) and that these measurements provide an elegant and accurate method of estimating local gradient values.

2.3.2 Behavioral mechanisms of flow navigation

We next focused on the behavioral mechanisms of flow navigation. Since fish cover a large range of radial distances from the tube center during the behavior, they experience significant changes in gradient magnitude during each trial, extending from a flat (zero) gradient at the center of the tube to the maximal gradient values close to the border (Fig.2.3.2b and Fig.2.3.3b-c). As larval zebrafish swim in discrete periods of motor activity [Budick and O'Malley, 2000], each swim bout will necessarily elicit a change in the gradient (delta gradient) that will define the conditions in which the subsequent bout will occur. Thus, during rheotaxis, swim bouts can be grouped into bouts that occur after increases (Fig.2.3.3b-e, red) and bouts that occur after decreases (Fig.2.3.3b-e, blue) in gradient magnitude. Note that an increase in gradient magnitude will always occur when fish swim away from the center of the tube and that a decrease in gradient magnitude will always occur when fish swim towards the center of the tube (Fig.2.3.3c and Supp.Fig.A.1.3a). This suggests a relatively simple strategy by which the fish can selectively swim against the flow: if a swim bout leads to an increase in gradient magnitude, execute a turn following the direction of flow field rotation (clockwise, top half of Fig.2.3.3c); if it leads to a decrease, then turn against it (counter-clockwise, bottom half of Fig.2.3.3c).

To test whether fish actually follow this strategy, we analyzed the distributions of turn magnitudes for bouts occurring after increases or decreases in gradient magnitude. As expected, the distribution of bouts occurring after increases in gradient magnitude was strongly skewed towards high magnitude turns that followed the direction of the rotational vector field (Fig.2.3.3d, red). How-

ever, bouts occurring after decreases in gradient magnitude showed a symmetric distribution of low magnitude turns with no obvious directionality (Fig.2.3.3d, blue). In other words, zebrafish larvae show a strong tendency to follow the direction of flow field rotation after they experience an increase in gradient magnitude, but show no directionality in their turning behavior after experiencing a decrease in gradient magnitude (Fig.2.3.3d-e). These results unveil an even simpler rheotactic algorithm in which a larval zebrafish, after experiencing a decrease in gradient magnitude, primarily swims straight. On the contrary, after experiencing an increase in gradient magnitude, it performs a high magnitude turn in the direction of flow field rotation (Fig.2.3.3d). This algorithm relies on small changes in gradient magnitude (Supp.Fig.A.1.4a-c), occurs mostly in the horizontal axis (left/right turns, yaw, Supp.Fig.A.1.4d-f) and, most importantly, allows the fish to both orient and swim against oncoming water flow (Supp.Fig.A.1.3).

Since flow velocity gradients can act as a rotating force on the animal's body [Beck et al., 2004], we investigated the possibility that the directionality of the gradient-induced turns might simply arise from a passive rotation of the fish, induced by the curl of the local flow field. To that end, we recorded the motion of a fish paralyzed with α-bungarotoxin inside the behavioral chamber. Indeed, and as indicated above, immobilized larval zebrafish experienced a consistent gradient magnitude-dependent body rotation (Supp.Fig.A.1.2b,c). However, in non-paralyzed fish, the inter-bout swim period proved too short to allow for passive body rotations that could account for the high-magnitude turns observed after increases in gradient magnitude (Supp.Fig.A.1.2d,e).

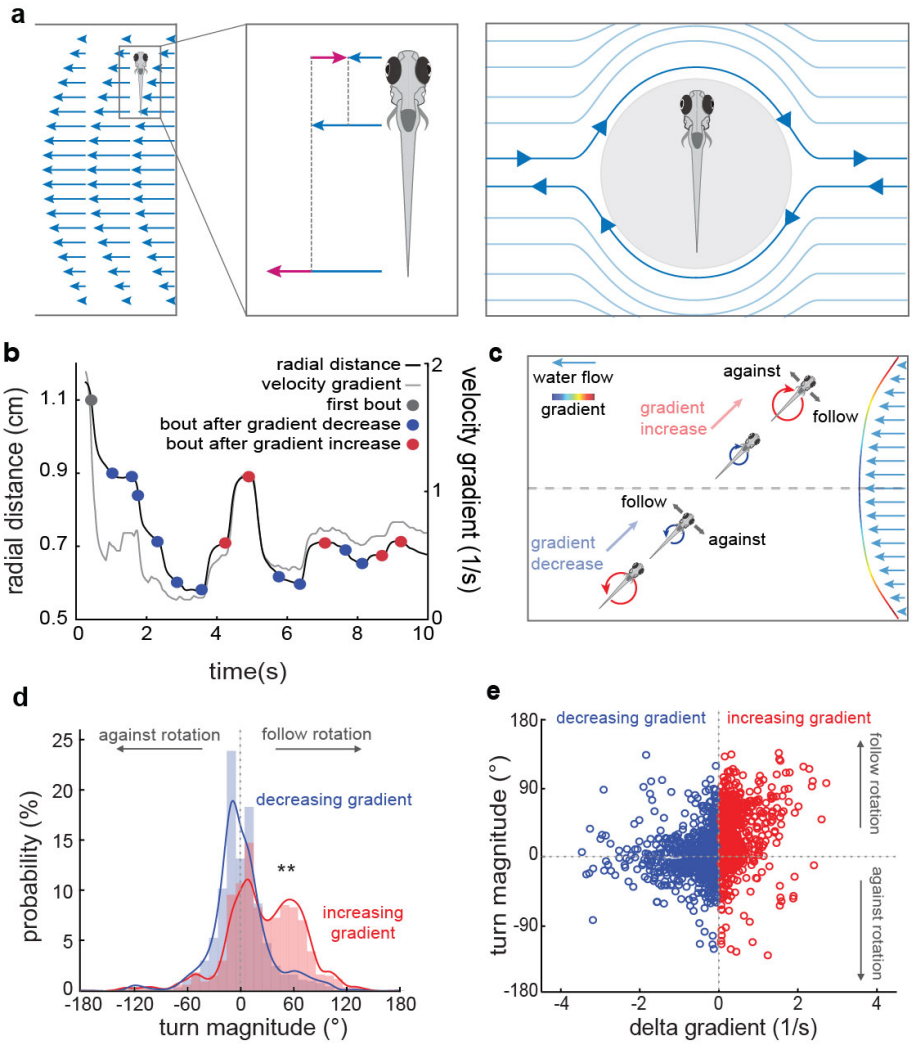

Figure 2.3.3: A behavioral algorithm for rheotaxis in larval zebrafish.| a-c. Larval zebrafish navigate velocity gradients during rheotaxis. **a.**During flow presentation, fish are immersed in a flow field of water particles moving at different velocities: high at the center and slower close to the walls (left). A fish will move at the velocity of its center of mass (center), but water particles around it will move with respect to the fish at velocities dictated by the difference in velocity between them and the fish's velocity, resulting in a rotational flow field surrounding the animal (right). **b.**Fish swimming leads to changes in radial distance (or distance from the tube's midline, grey trace) and the velocity gradient (black trace) experienced by the fish. Swim bouts occur after increases (red dots) or decreases (blue dots) in gradient magnitude. As flow profile develops over time (see Fig.2.3.2a), the relationship between radial distance and velocity gradients is not obvious in the first third of the trial. Data corresponds to the example shown in Fig.2.3.1b-e. **c.**Graphical representation of bout types during rheotaxis. **d.**Turn magnitude histogram for bouts following increases (red) and decreases (blue) in gradient magnitude. Positive turns follow the direction of flow field rotation and negative turns go against it. Histograms and fitted lines for each distribution are shown; differences in distributions assessed via Kolmogorov-Smirnov tests, ** = $p<0.01$. n = 13 fish, 341 trials. **e.**Scatter plot of turn magnitude vs delta gradient. n= 13 fish, 1916 bouts.

2.3.3 Simulations test the sufficiency of our proposed algorithm

We next generated a model to test whether this algorithm is sufficient to explain the observed rheotactic behavior. Here, a particle moves randomly in a virtual flow field which is matched to our experimental conditions with the following constraints: the path-length of each iterative step is matched to the average bout distance travelled by a larval zebrafish, the time taken for each step is set to the average bout frequency, and turn angles are drawn from the distributions described in Fig.2.3.3d. Delta gradient values are obtained by the change in position of the particle within the measured flow field described in Fig.2.3.2b. Importantly, we found that under these conditions the rheotactic algorithm elicited rheotaxis in different gradient regimes with remarkable robustness (Fig.2.3.4a-c). However, we found that under high velocity conditions the swim speed of the model fish (determined by the bout duration and frequency) was insufficient to explain the relatively high gain values of real fish (see Fig.2.3.2f). This mismatch disappeared once we accounted for the fact that during rheotaxis, larval zebrafish gradually up-regulate their swim bout displacement against the direction of the flow (Fig.2.3.4d and Supp.Fig.A.1.5a).

Interestingly, our behavioral experiments also showed that over the course of a trial, fish swim increasingly closer to the longitudinal axis of the tube and away from the high gradient areas near the walls (Supp.Fig.A.1.5b-e). This behavioral feature leads to the avoidance of high gradient regions during flow navigation and naturally emerges from the simplified rheotactic algorithm described above: a rule where fish swim primarily straight when they swim down the velocity gradient (i.e. when approaching the center of the tube) and execute large angle turns when swimming up the gradient (i.e. away from the center and towards the border) will lead to a biased random walk towards the minimal gradient values in the center of the tube. This phenomenon, also faithfully reproduced by the model (Supp.Fig.A.1.5f), is strongly reminiscent of the biased random walk during bacterial chemotaxis[Berg, 1993] and automatically leads to gradient avoidance behavior. Importantly, since high velocity gradients will consistently develop around obstacles in flowing bodies of water, an algorithm that guides the animal away from a strong gradient will automatically assist in avoiding such obstacles. Of course, such a "gradient avoidance" effect leads to a somewhat paradoxical outcome: fish will systematically veer away from the shore to the center of the stream, where there is no gradient to navigate by and where, quite disturbingly, the velocity of the current that they are trying to swim against is highest. As a consequence, we believe that our algorithm does not apply for animals

that routinely swim in the open water of larger rivers or ocean currents and applies selectively to those whose natural habitat is largely restricted to the vicinity of the shore, the reef or generally to small rivers, brooks and rivulets, where they are confined to the strong gradients present in the near wall regions [von Kármán, 1931, Carlson and Lauder, 2011].

Another argument that speaks against our algorithm being relevant for larger rivers is that there the boundary layer is not fully developed and is instead confined to the near-wall region [Tritton, 2012]. Hence, the Hagen-Poiseuille flow present in our experimental set-up, as well as the computer simulations, does not reflect accurately the velocity profile in a real stream where smaller mean velocity gradients prevail throughout most of the volume.

An additional feature of natural currents is that they are seldom purely laminar but rather, characterized by turbulences and vortices of varying degrees. It is of great interest to see how well our proposed algorithm would perform under such disorderly conditions. To that end, we equipped our simulation platform with the ability to add Karman vortex streets [Carlson and Lauder, 2011, Tritton, 2012, Barkley et al., 2015] to the laminar flow profile described in Fig.2.3.2a (Supp.Fig.A.1.6). These vortex streets are characterized by both the density of the vortices within the flowing stream and the rotational speed of each individual vortex (intensity). The maximum value of this rotational speed (100%) was set by the maximal absolute velocity of the parabolic velocity profile of the stream.

Fig.2.3.4e shows the performance of a model fish when density was set to 100%, and intensity to 50% (see Supp.Fig.A.1.6b for corresponding flow field). Remarkably, rheotactic behavior is qualitatively well maintained under these conditions. In order to probe the sensitivity of our algorithm to such turbulence, we systematically varied those two parameters (density and intensity) and tested the resulting decrease in behavioral efficiency when compared to purely laminar flow (Fig.2.3.4f-h, Supp.Fig.A.1.5f). Two features become apparent: first, performance appears to decay gracefully with an increase in both turbulence values and seems to be remarkably robust even if conditions become distinctly tempestuous (see Supp.Fig.A.1.6c). Second, while gain and orientation values depend, as expected, quite linearly on vortex density (Fig.2.3.4f,g), the performance sensitivity to intensity shows more interesting characteristics (Fig.2.3.4h). The gain values show an exquisite sensitivity to minute increases in turbulence intensity from 0% to 2%, where they drop from 2.3 to 1.5 (Fig.2.3.4h inset). They then decay linearly until they reach gain levels of ~ 1 at the 25% mark, from whence they drop to baseline levels of 0.5 at 30%. We believe that the very first drop in performance

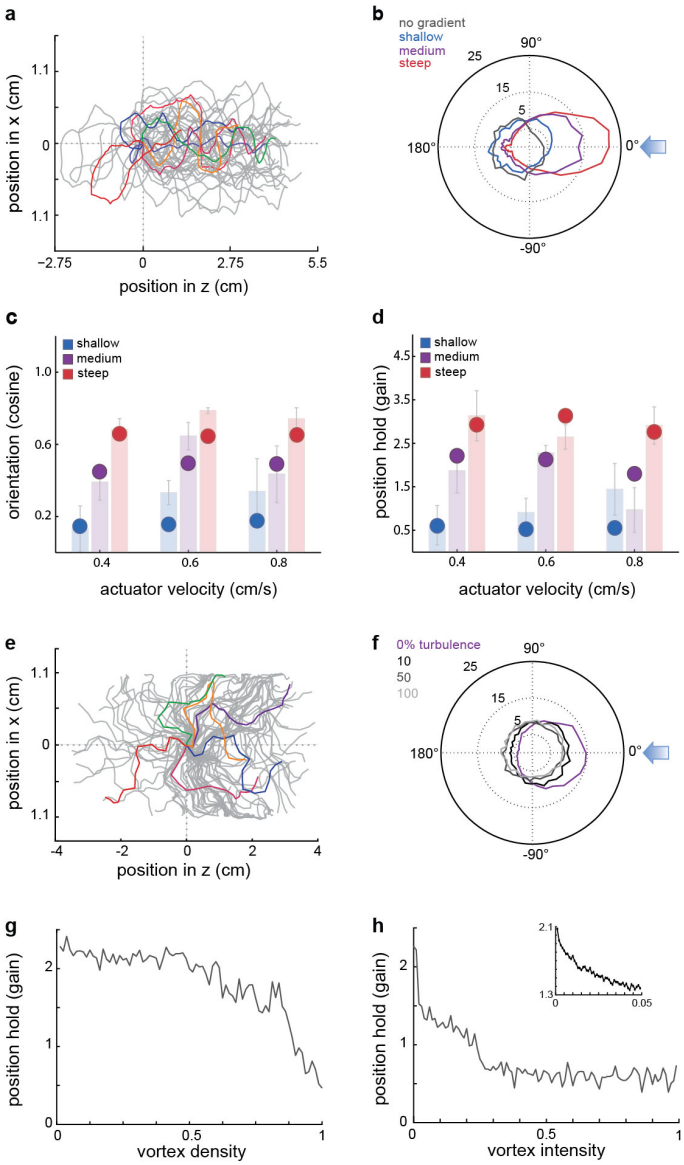

Figure 2.3.4: Model fish perform rheotaxis.| a. Trajectories of one hundred (grey) modeled fish facing a virtual flow towards the left. Five examples are colored for clarity. **b.**Polar plot of model fish orientation in the left–right axis under different gradient conditions. **c.**Comparison of cosine of the mean orientation in model (circles) and real (shaded bars) fish for increasing actuator velocities and tube diameters. Fish data is the same as in Fig.2.3.2d. **d.**Comparison of gain of model (circles) and real (shaded bars) fish for increasing actuator velocities and tube diameters. Fish data is the same as in Fig.2.3.2f. **e.**Trajectories of one hundred (grey) modeled fish facing a virtual turbulent flow towards the left (vortex density and intensity both set to 100%). Five examples are colored for clarity. **f.**Polar plot of model fish orientation in the left–right axis under different turbulent strengths. **g.**Gain of model fish as a function of increasing vortex density. Vortex intensity was kept constant at 100%. **h.**Gain of model fish as a function of increasing vortex intensity. Vortex density was kept constant at 100%. Inset: expanded view of the initial drop in gain as density increases from 0 to 0.05.

(0%-2%) is due to the different velocity gradient conditions within each vortex and a resulting deterioration of the algorithmic performance of the animal. The subsequent decay is likely caused by a physical translocation and rotation of the animal by the swirling eddies and the remaining baseline performance is permitted by the undisturbed "holes" between the vortices, which exist even at densities of 100% (Supp.Fig.A.1.6b). In summary, these extended simulations show that our algorithm is surprisingly robust to mild and moderate turbulences and can even sustain a minimal baseline performance once fully turbulent flow is established. The robustness of this effect arises from the consecutive and cumulative integration of many turn angle choices, that together average out the random perturbations induced by local vortices.

2.3.4 The role of the Lateral Line in rheotaxis

Finally, we searched for the sensory basis of gradient–dependent rheotaxis. This question, and particularly the role of the lateral line (LL) system, has been the subject of a continuous debate [Dijkgraaf, 1963, Montgomery et al., 1997, Van Trump and McHenry, 2013, Beck et al., 2004, Hofer, 1908]. In the larval zebrafish, the LL system consists of a series of mechanosensory organs (the neuromasts) located along multiple stripes in the fish's head (the anterior LL) or in single stripes along each side of the fish's tail (the posterior LL) [Ghysen and Dambly-Chaudiere, 2004]. To assess the role of the LL system in gradient induced rheotaxis, we performed chemical ablations of all neuromast hair cells using copper sulfate [Montgomery et al., 1997, Van Trump and McHenry, 2013] (Supp.Fig.A.1.7a-a'). We observed that in the absence of the LL system, turn distributions for bouts occurring after increases or decreases in gradient magnitude almost completely lost their asymmetry (Fig.2.3.3d and Fig.2.3.5a,b). Moreover, the fish's ability to orient against oncoming water flows was severely reduced (Fig.2.3.5c). These results strongly suggest that during larval zebrafish rheotaxis, the LL system acts as the gradient sensor that allows the fish to calculate the line integral of local rotational flow fields around the circumference of its body (Fig.2.3.3a). As the anterior and posterior LL systems could contribute either uniquely or in parallel to gradient sensing, we next performed unilateral as well as bilateral laser ablations of the anterior or the posterior LL primary sensory nerves (Supp.Fig.A.1.77b-d'). We observed that the lack of the posterior, but not the anterior LL system induced a significant decrease in the fish's orienting performance (Fig.2.3.5c), indicating that fish primarily use the posterior LL system for rheotaxis. Since rheotaxis occurs mostly in the

horizontal plane (yaw rather than pitch, Supp.Fig.A.1.4d-f), the receptive fields of the relevant neuromasts should be sensitive to deflections in the anterior-posterior direction. Interestingly, and in agreement with our ablation results, the posterior LL exhibits primarily antero-posterior receptive fields [López-Schier et al., 2004, Nagiel et al., 2008]. Furthermore, we find that behavioral loss was comparable in unilaterally, as well as bilaterally ablated fish (Supp.Fig.A.1.7e). This suggests that fish cannot effectively estimate the gradient, or its resulting curl, by integrating the flow profile over one side of their body only and that they need to use the corresponding negative input from the other side as a reference point [Ristroph et al., 2015].

Importantly, and as previously discussed, the vector field in our experimental conditions is divergence-free, such that its gradient is exclusively defined by the curl/shear (see Methods and Mathematical notes). However, there are instances of vector fields that have gradients with no curl and strong divergence. For example, local sources or sinks will produce fields without a curl even in the presence of obvious local velocity gradients (i.e. high speed at the center, lower speed towards the periphery). A biologically relevant example of such a sink would be the one created around the mouth of a suction feeding predator [Ferry-Graham and Lauder, 2001]. Although in such a setting our algorithm (which relies on a non-zero curl) would catastrophically fail, it has been shown that larval zebrafish can efficiently escape from local sinks, even in complete darkness, once the local gradient exceeds a certain threshold [Olszewski et al., 2012, Olive et al., 2016]. We therefore propose the existence of a different (orthogonal) algorithm based on varying flow speeds along the longitudinal axis of the fish that allows animals to detect the radial gradients typical of strong sinks. However, we believe this represents an independently evolved strategy to escape predation with little relation to the navigationally-relevant rheotactic algorithm presented here.

2.3.5 Conclusion

In summary, our experiments show that a relatively complex behavior, such as mechanosensory-based rheotaxis, can emerge from a surprisingly simple behavioral algorithm that relies on the sensing of local, gradient-induced rotational flow fields. Velocity gradients in natural environments will be present at the interface between flows and any kind of surface; thus the ecological relevance of our algorithm encompasses both rheotaxis as well as obstacle avoidance. Since flow navigation is a fundamental feature of all animals that fly or swim, the description of its elementary rules and sensory

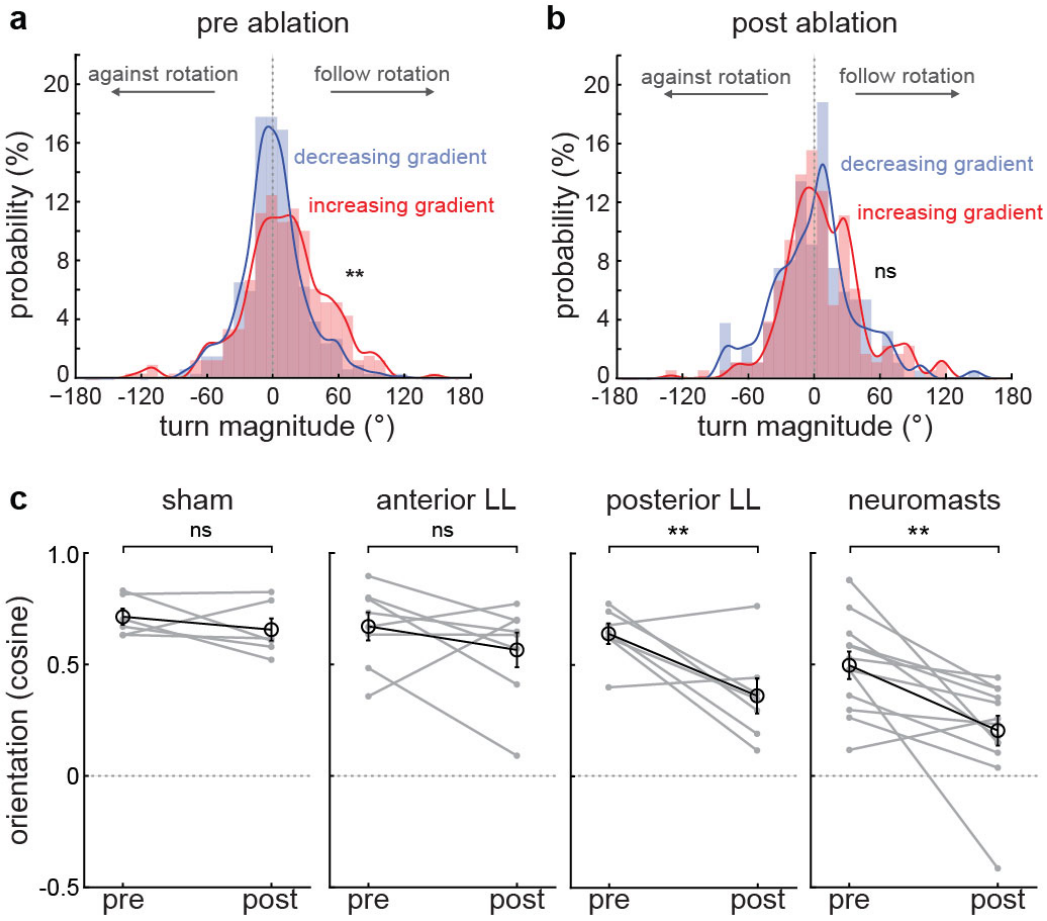

Figure 2.3.5: The mechanosensory lateral line system acts as a gradient sensor during larval zebrafish rheotaxis. **a–b.** Turn magnitude histogram **a.**before and **b.**after copper-induced chemical ablation of all neuromast hair cells. Bars and fitted lines for bouts occurring after increases (red) and decreases (blue) in experienced gradient magnitude are shown. **= p<0.01; Kolmogorov-Smirnov test. n= 12 fish. **c.**Ability to orient against water flow (Cosine of the mean orientation angle) of fish subjected to different experimental conditions. Mean and SEM of the population (black) and means of individual fish (grey) before and after treatment are shown. ns= p>0.05, ** = p<0.01; bootstrap of the mean. n= sham, 6 fish; anterior lateral line ablation, 8 fish; posterior lateral line ablation, 7 fish; chemical neuromast ablation, 12 fish. All fish were subjected to 6 trials before and after manipulations.

basis will be essential to unveil the underlying neural circuits and understand the evolution of this conserved behavior, as well as to provide efficient and robust algorithms for aquatic robot navigation [Chapman et al., 2011]. The latter has obvious applications in the development of devices assisting in the diagnostics and maintenance of oil- and water pipelines as well as the design of micro-devices that can autonomously navigate through blood vessels.

2.4 Acknowledgments

We are grateful to E. Soucy and J. Greenwood for technical support and B. Jordan for insightful discussions. We thank M. Baldwin, M. Häsemeyer and T. Dunn for critical reading of the manuscript. We also thank M. Grünthal and R. Hellmiss for contributions to figure design. This work was supported by a Pew Latin-American Fellowship to P.O, a BRAIN NIH grant U01NS090449 and NIH Pioneer award DP1 NS082121 to F.E., an HFSP grant RGP0033/2014 to F.E. and an Office of Naval Research grant N00014-09-1-0352 to George Lauder.

2.5 Methods

2.5.1 Animals

5-7 days post-fertilization (dpf) wild-type zebrafish of the WIK strain were used for all behavioral experiments, unless indicated. Animal handling and experimental procedures were approved by the Harvard University Standing Committee on the Use of Animals in Research and Training. No statistical methods were used to predetermine sample size.

2.5.2 Behavioral Chamber

A 45 cm long polycarbonate tube (1.27, 2.22 or 4.76cm inner diameter, 0.31cm wall thickness) was attached to a water reservoir and filled with aquarium water. Two 140μm mesh filters were used to contain single zebrafish larvae in a 13 cm long behavioral section while two infrared (IR) LED arrays provided illumination from below and from the sides of the tube. A high-speed camera (Pike F-032B, Allied Vision Technologies) fitted with a macro-lens (Sigma DG, USA) and a visible-light-blocking filter (to block visual cues in light-on experiments) recorded fish behavior at 200 frames per

second (fps) directly from above the behavioral section and from the reflection of a lateral IR reflecting mirror (hot mirror, Edmund Optics, USA). For experiments in which visual cues were present, stationary black & white stripes (0.5cm wide) from a mini projector (Dell M109S, USA) were reflected upward on a visible light reflecting mirror (cold mirror, Edmund Optics, USA) into a diffusive screen underneath the behavioral section. Laminar water flow was created by the displacement of a custom-made plunger attached to the rod of a computer-controlled linear actuator (Servotube Actuator STA1112, Copley Controls). For acceleration and water displacement experiments, the behavioral section of the rig was mounted on rails and attached to the actuator's rod. Behavioral trials were controlled using software custom-written in LabView (National Instruments, Austin, TX) and consisted of 5s of no stimulus, 0.1s acceleration, 9.8s water flow / water displacement stimulus, 0.1s de-acceleration and another 5s of no stimulus. For acceleration experiments, trials consisted of 2.5s of no stimulus, 1s of acceleration, 1s of water displacement, 1s of de-acceleration and another 2.5s of no stimulus. All experiments were performed by randomly moving the plunger towards or away from the water reservoir.

2.5.3 Behavioral Analysis

All behavioral analyses were performed using custom-written Matlab code (MathWorks Inc.). Rheotactic orientation was calculated as the mean of the cosines of all fish orientations during stimulus presentation. Thus, cosine = 1 represents perfect alignment against flow direction (0 degrees fish orientation) while cosine = -1 represents perfect alignment in the direction of the flow (180 degrees fish orientation). To quantify the ability to hold position against incoming flows, we calculated a relation between the velocity of the fish and the velocity of the incoming water flow (the 'gain') through the formula (fish velocity – water velocity) / water velocity. Thus, gain < 1 means fish actively swim in the direction of the flow, gain = 0 represents passive drift, gain = 1 means perfect position holding, and gain > 1 means overcompensation. This metric was used for individual bout types or, by calculating their mean, for a whole behavioral trial. Since flow stimulus onset and direction were always randomized, both cosine and whole-trial gain were calculated from a similar number of experiments in which the fish faced towards or against the direction of the flow at the beginning of the stimulus. For paralyzed fish experiments, larval zebrafish were incubated in 1mg/ml of α-bungarotoxin and then directly released into the behavioral chamber while water flow was induced. With the excep-

tion of minor necessary modifications (i.e. swimming vs paralyzed fish), all analyses were performed using the same code, independently of the experiment type.

2.5.4 Statistics

Kolmogorov-Smirnoff tests were performed through embedded functions while Monte Carlo permutation tests were custom written in Matlab (MathWorks Inc.). For the latter, we calculated the difference between the means of the two distributions to be compared; then both distributions were shuffled and a new difference in means was calculated. This was repeated through 10000 iterations and the p-value was calculated as the probability of finding the original difference of the means. No variance analyses were performed.

2.5.5 Water Flow Analysis

Particle Image Velocimetry (PIV) was performed as previously described [Drucker and Lauder, 1999]. Water velocity profiles were calculated at 50 fps (Davis software version 7.2.2, LaVision Inc., Goettingen, Germany) and analyzed using custom software written in Matlab (The MathWorks Inc.). Different flow profiles were created by the displacement of actuator-attached plugs into small (1.27-cm) and large (4.76-cm) diameter polycarbonate tubes. For behavioral analyses, flow stimulus direction was always taken as leftwards and all the time points (except for the initial acceleration) during flow development were used. As the average horizontal position of the fish during rheotaxis was 6.5 $\pm$ 0.7cm away from the flow source (either the plunger or the water reservoir), behavioral analyses were performed using the flow profile obtained at 5-7cm away from the source (Fig.2.3.2a). All time points in the development of the flow profile were matched to the time points in the behavioral movies. Since both flow profile and rheotactic behavior between experiments in which the flow was induced towards or away from the water reservoir was similar (Supp.Fig.A.1.4g-i), all trials were included in the analyses.

2.5.6 Modeling

Modeling of the rheotactic algorithm was made using software custom-written in LabView (National Instruments, Austin, TX). Flow parameters were the same as in Fig.2.3.2b and behavioral features were the same as in Fig.2.3.3d-e and Supp.Fig.A.1.5a. Briefly, the position of a particle was

moved at a fixed length at each iteration step with turn angles drawn randomly from the distributions described in Fig.2.3.3d. Delta gradient values are obtained by the change in position of the particle within the measured flow field described in Fig.2.3.2b. Additionally, under high velocity conditions, the fixed bout length of the model fish was gradually up-regulated during the course of a successful trial to account for similar observations under experimental conditions. In order to add turbulence to the model, we equipped our simulation platform with the ability to add Karman vortex streets [von Kármán, 1931, Barkley et al., 2015] to the laminar flow profile described in Fig.2.3.2a (Supp.Fig.A.1.6). The maximum value (100%) of the rotational speed of each individual vortex (intensity) was set to the maximal absolute velocity of the parabolic velocity profile of the stream. The vortex density was defined by the relative spacing of hexagonally arranged vortices with respect to each other.

2.5.7 Lateral Line Ablations

For chemical neuromast ablations, 5-7 dpf WIK larvae were used. Fish were subjected to six trials at a single actuator velocity (0.6cm/s), incubated in 1mM copper sulfate for 85 minutes and allowed to rest in fish water for 60 minutes before being subjected to six more trials. Only fish that showed a complete neuromast ablation (assessed by DiASP staining) [Schuster and Ghysen, 2013] and a constant swimming activity were included in the analysis. For 2-photon lateral line nerve ablations, 6 dpf HGn93D zebrafish larvae were subjected to six trials at a single actuator velocity (0.6cm/s) and embedded in low-melting-point agarose with one of their otic vesicles looking upwards [Pujol-Martí et al., 2012, Ahrens et al., 2012]. An image stack of the GFP-labeled lateral line (LL) nerve in the HGn93D strain was acquired and then 1-3 850nm laser pulses of 1ms duration were targeted on the anterior or the posterior central projection of the LL nerve. For sham ablations, the same treatment was performed on a single neighboring nerve innervating a dorsal neuromast. Fish were then released from the agarose and allowed to rest for 24hs to allow the regeneration of the neuromast cupula after being damaged during agarose release. In the case of bilateral LL ablations, fish were immediately mounted and ablated on their opposite side after being released from the agarose and allowed to rest for 24hs. The next day, fish were subjected to another six trials, re-embedded in agarose and another stack of the LL nerve was acquired. Only fish with normal buoyancy, constant swim activity and with clear damage to the LL nerve targeted in the treatment were included in the

analysis. All experiments were analyzed using the same code, independently of the ablation type.

2.6 Mathematical Notes

Any matrix can be written as the sum of a symmetric and an antisymmetric part. In particular, the gradient of a vector field can be decomposed into the sum of a divergence, a shear and a curl. The curl is anti-symmetric, the shear is symmetric and trace-free and the divergence is the trace. Explicitly, in three dimensions, we have:

$$\frac{\delta V_i}{\delta x_i} = \frac{1}{2}\varepsilon_{ijk}(\nabla \times \vec{V})_k + \frac{1}{3}\delta_{ij}(\nabla \cdot \vec{V}) + \sigma_{ij}; \tag{2.4}$$

where the first term is the curl, the middle term is the divergence and the last term is the shear, defined as:

$$\sigma_{ij} = \frac{1}{2}\left(\frac{\delta V_i}{\delta x_j} + \frac{\delta V_j}{\delta x_i}\right) - \frac{1}{3}\delta_{ij}(\nabla \cdot \vec{V}) \tag{2.5}$$

Shear is relevant when considering viscous fluids. The flow in our experiments has only two non-vanishing shear components, given by:

$$\sigma_{13} = \sigma_{31} = \frac{x}{R^2} \quad \text{and} \quad \sigma_{23} = \sigma_{32} = \frac{y}{R^2} \tag{2.6}$$

In our experiments, larvae compare the flow on the two sides of their body, which means that they subtract one value from the other. This is equivalent to performing the line integral shown in equation (2.3).

"We think we receive all that we perceive, but in fact, we actually give the sky its colour."

James Turrell

3

Efferent modulation in the lateral line of the larval zebrafish

3.1 Preface

The work presented in this chapter is in part the result of multiple collaborations. I would like to acknowledge the people who have contributed to this work. Ruben Portugues wrote the original software for the functional imaging assays. Experiments using heat stimuli were performed with Martin Haesemeyer, who also provided me with cell-segmentation software. Flow experiments were carried out with Maxim Nikitchenko. Mariela Petkova traced and reconstructed the electron microscopy data from samples created by David G.C. Hildebrand.

3.2 Introduction

Fish and amphibians possess a mechanosensory lateral line system that enables them to sense water motion relative to their bodies [Dijkgraaf, 1963]. This information can be used to identify moving objects in their vicinity as well as abiotic water currents, and therefore contributes to a variety of behaviors including schooling, prey capture, predator avoidance and rheotaxis [Partridge and Pitcher, 1980, McHenry et al., 2009, Montgomery et al., 1997, 2002, Suli et al., 2012]. Because fluid drag during locomotion can strongly activate the lateral line, the accurate interpretation of mechanosensory inputs requires that animals distinguish between external and self-generated stimuli.

To overcome this kind of challenge, most organisms have evolved to perform neural computations that can nullify or otherwise compensate for the expected self-generated stimulation. These involve efference copies, which are signals from motor-command centers that inform the sensory processing pathway about impending movements (see Crapse and Sommer [2008] for review). The existence of diverse centrifugal projections that contact the lateral line suggests that efference copy mechanisms are involved in this process, yet the circuitry and its consequences on behavior remain largely unknown [Metcalfe et al., 1985].

Due to their small size and optical accessibility, larval zebrafish offer a unique opportunity to perform an anatomical and functional dissection of the efferent system to the lateral line. To do this, we first described the identity and morphology of descending inputs to the lateral line. Consistent with previous observations, we identified the dopaminergic Diencephalic Efferent to the Lataeral Line (DELL) and the cholingeric Octavomedial Efferent Nucleus (OEN). Furthermore, electron microscopy studies confirmed the existence of synaptic structures between efferent terminals and hair cells. In vivo functional imaging of neuronal activity during behavior, showed that despite the significant mechanical stress on the hair cells during tail undulations, primary sensory neurons are not activated during swims. The lack of motor-correlated mechanosensory excitation is consistent with the transmission of efference copy signals that can silence self-generated stimulation. Additionally, we observed that whilst both the OEN and the DELL exhibited motor-correlated activity, DELL neurons also responded to flow and acoustic stimuli in the absence of motor outputs. Finally, we performed laser ablations of OEN neurons to establish their necessity for the suppression of sensory activity in lateral line afferent neurons during locomotion. Taken together our results identify the OEN as the source of efference copy signaling to the lateral line, and propose the hypothesis that

DELL neurons serve to enhance hair cell sensitivity during the quiescent periods following locomotion or after the occurrence of salient mechanical stimuli.

3.3 Results

Anatomy

If efference copy mechanism are in place to cancel out self-generated mechanical stimulation during locomotion, there must exist an anatomical bridge between the motor pathway and the sensory stream of the lateral line. This connection could exist at any level within both the motor and sensory pathways, so we started our search at the earliest site of information transfer in the sensory stream: the lateral line nerve. We injected fluorescent dextrans into the nerve to visualize the neurons that extend projections through it. Consistent with previous studies, we labeled the primary sensory neurons that innervate hair cells and reside in the posterior lateral line ganglion (PLLg), as well as two additional small clusters of neurons in the hindbrain and in the hypothalamus (Fig.3.3.1a) [Metcalfe et al., 1985, Bricaud et al., 2001]. These additional nuclei had been previously identified as the Octavolateral Efferent Nucleus (OEN) and the Diencephalic Efferent to the Lateral Line (DELL). Furthermore, the OEN is commonly subdivided into the Rostral and Caudal Efferent Nuclei, according to the relative positions of their somas and the location at which their axons exit the brain. Repeated dye labeling and subsequent registration of the images onto a reference brain, confirmed these subdivisions and revealed that OEN neurons may also occupy a third position in the hindbrain (Supp.Fig.B.1.1). We will identify them as the hyper-rostral OEN neurons (hrOEN) henceforth. This new position is permanent as opposed to being a corridor for neurons that are migrating to reach the already identified rostral and caudal nuclei, as demonstrated by live imaging during consecutive days (Supp.Fig.B.1.2). The significance of soma position in the OEN is currently unknown, and we will address this issue in terms of anatomy and function in later sections.

To further characterize the efferent nuclei, we sought to identify their neurotransmitter identities. To this end, we repeated dextran injections in the lateral line of transgenic larvae expressing GFP under the control of various neurotransmitter-specific promoters. Dextran-positive neurons in the hypothalamus colocalized with GFP expression under the control of the dopamine transporter promoter, demonstrating that the DELL is dopaminergic (Fig.3.3.1b) [Xi et al., 2011]. This in accor-

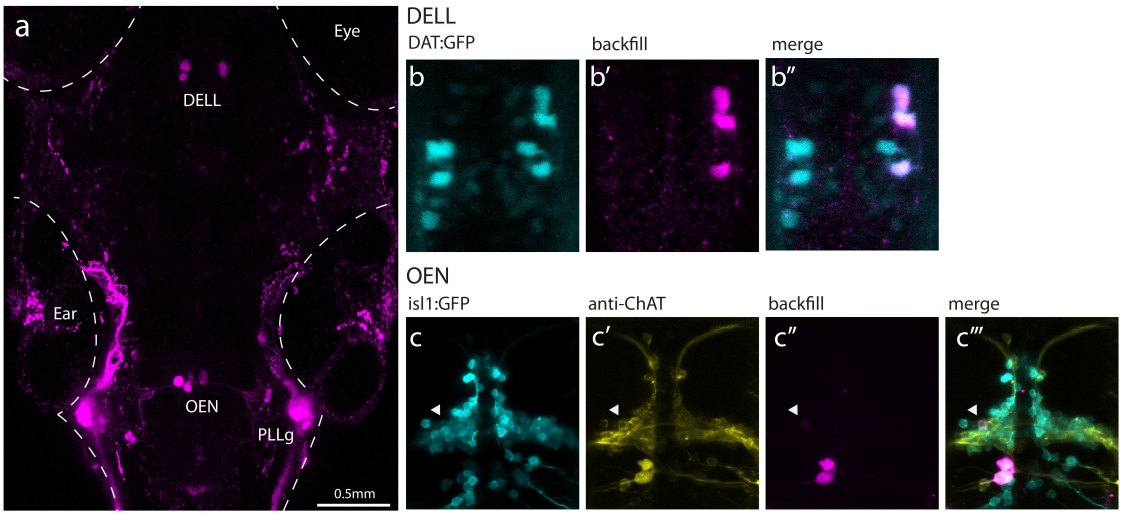

Figure 3.3.1: Afferent and efferent neurons project down the lateral line.| a-c. Maximum intensity projections of confocal images showing the anatomical location of efferent nuclei and primary sensory neurons after dye injections to the lateral line of 6 dpf zebrafish larvae. **a.**Dorsal view of a bilateral dye injection to the LL. 3 main cell clusters are labeled: the PLL ganglion (PLLg), the Octavomedial Efferent Nucleus (OEN) and the Diencephalic Efferent of the Lateral Line (DELL). **b.**Detail of the hypothalamus after LL nerve injection in DAT:GFP transgenic larvae. **c.**Detail of the hindbrain after LL nerve dye injections in isl1:GFP transgenic larvae and antibody stains against choline acetyltransferase (ChAT). Scale bars: a:0.5mm, b-c:50μm.

dance with other studies that have shown that DELL neurons are positive for the catecholaminergic marker tyrosine hydroxylase [Bricaud et al., 2001]. In the hindbrain, dextran labeling coincided with GFP expression in isl1:GFP transgenic larvae in a region that is mostly populated by cranial neurons (Fig.3.3.1c) [Higashijima et al., 2000]. Accordingly, subsequent antibody stains against choline acetyltransferase (ChAT) revealed that OEN neurons are cholinergic, as has been shown in other aquatic organisms (Fig.3.3.1c) [Russell, 1971a, Russell and Roberts, 1972, Flock and Russell, 1976].

Given that circuit architecture is closely related to circuit function, we used sparse labeling to visualize the projection patterns of individual efferent neurons. Focal electroporations were performed to label individual neurons with a membrane-tagged fluorescent protein. We observed that single DELL neurons extend ipsilaterally to innervate the inner ear, neuromasts of the head and tail, in addition to the spinal cord (Fig.3.3.2a,d). This pattern identifies them as the DC2 population of

dopaminergic neurons [Tay et al., 2011, Jay et al., 2015]. OEN neurons, by contrast, exhibit greater variability and do not send collaterals to the spinal cord (Fig.3.3.2b-d). Whilst their dendritic arbors extend bilaterally, their axons project only to the hair cells of the ipsilateral inner ear, and the anterior and posterior neuromasts (Fig.3.3.2b-d). Any combination of targets other than the inner ear alone can in fact occur (Fig.3.3.2d). Notably, efferent neurons belonging to the different OEN sub-nuclei have overlapping targets, which means that neuromast innervation is not governed by soma position in the hindbrain (Fig.3.3.2d).

Overall, tracing of individual efferent neurons revealed a large degree of divergence that does not follow a somatotopic organization (Fig.3.3.2d). This suggests that the efferent mechanisms in place must be acting in bulk, rather than being finely tuned to different regions of the body. Furthermore, electron microscopy reconstructions of neuromasts showed that unlike sensory neurons, single efferent neurons synapse onto hair cells of opposite polarities (Supp.Fig.B.1.3)[Nagiel et al., 2008, Faucherre et al., 2009]. This furthers the idea of coarse rather than fine modulation.

In summary, we confirmed the existence of two sources of descending inputs to the hair cells of the lateral line of zebrafish larvae. The first, DELL, is a dopaminergic hypothalamic nucleus and the second, the OEN, is a cholinergic nucleus with further anatomical subdivisions. Both nuclei are well poised to provide sensory modulation, and could transmit efference copy signals to compensate for self-generated simulation during locomotion.

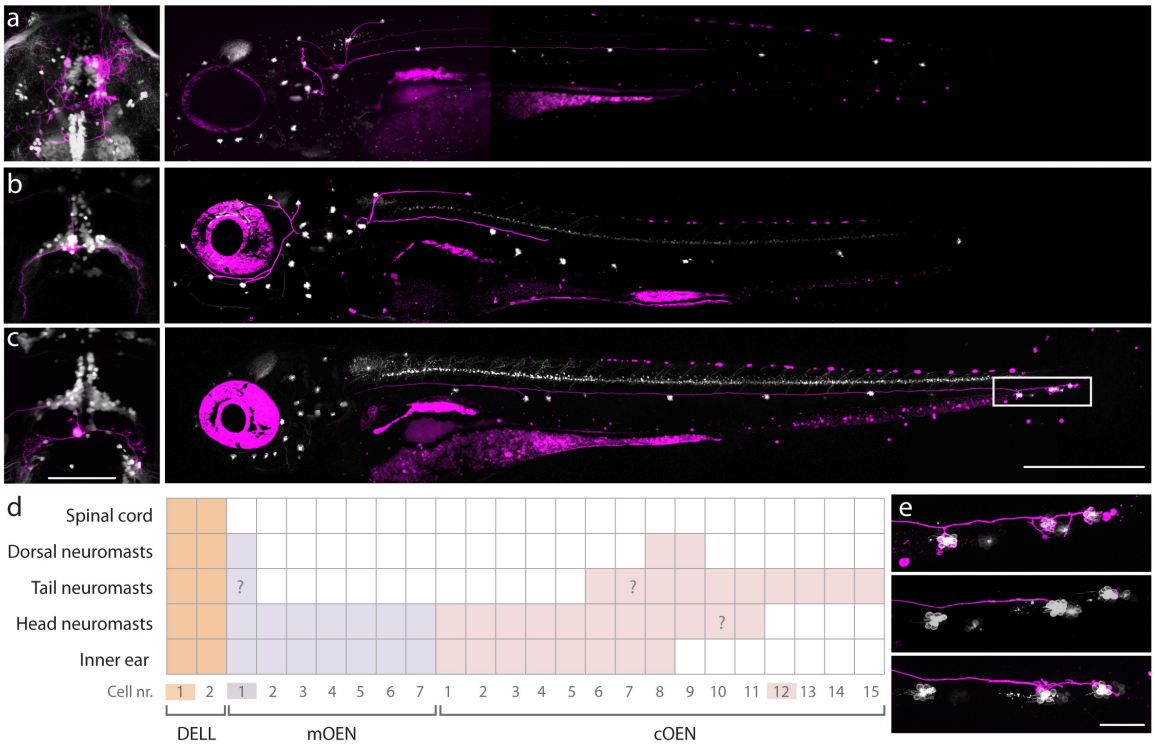

Figure 3.3.2: Focal electroporations of membrane-tagged fluorescent proteins reveal efferent neuron morphologies.| **a-c.**Projections of confocal images showing the morphology of efferent neurons of the lateral line. Dorsal and lateral views of labeled cells (magenta) performed in double transgenic larvae expressing GFP in all hair cells and in anatomical landmarks (gray). **a.**DELL neurons in the etVMAT:GFP background. **b.**Rostral and **c.**caudal OEN neurons in isl1:GFP fish. **d.**Summary matrix indicating location of targets of individual efferent neurons according to their soma positions. Highlighted cell numbers correspond to the fish in panels **a-c**. Questions marks (?) were assigned to neurons whose axons can be seen at the marked target without evidence of contact to neuromasts. **e.**Detail of caudal-most PLL neuromasts of the fish in **c.**at top:6, middle:7 and bottom: 8 days post-fertilization. Scale bars: a-c, left:100 μm, right:500 μm, e:50 μm

If efference copies are being transmitted directly to the neuromasts, then their effects should be seen in the output of the primary sensory neurons. To test this, we combined stimulus delivery and behavioral tracking with 2-photon functional imaging of transgenic larvae expressing fluorescent calcium indicators under the control of a neuronal promoter Tg(elavl3:GCaMP6s/f) [Ahrens et al., 2012, Chen and Engert, 2014]. In our assay, larval zebrafish were restrained in an agarose polymer but were free to move their tail (Fig.3.3.3a). We were interested in monitoring the activity of sensory neurons during swim events, where tail undulations can cause hair cell activation due to fluid drag [Cahn and Shaw, 1965]. Hair activation normally results in the excitation of sensory neurons but in the presence of efference copies, self-generated stimulation should be compensated for. Given that restrained larvae exhibit a low frequency of spontaneous movement, swimming was induced by projecting images of moving gratings onto a diffusive screen below the animal [Neuhauss et al., 1999, Orger et al., 2008]. Consistent with the existence of inhibitory efference copy signals, sensory neurons in the PLL ganglion displayed decreased activity during swim events, which disappeared after neuromast ablation with copper (Fig.3.3.3b-c). A possible explanation for the ability to detect this inhibition through calcium imaging is that hair cells fire spontaneously at a basal rate [Trapani et al., 2009, Trapani and Nicolson, 2011]. Thus, inhibitory signals during swims would reduce spiking and result in a decay in fluorescence. Sensory neurons, however, are responsive to external flow stimuli (Fig.3.3.3d). In the same set-up, brief local flow currents were delivered by water injections through a pipette placed immediately above the animal's head. During flow presentation, a subset of sensory neurons in the PLL ganglion were activated (Fig.3.3.3d). The partial excitation of the ganglion is in agreement with the fact that hair cells are directionally tuned, and that sensory neurons exclusively innervate neurons of a single polarity [López-Schier et al., 2004, Faucherre et al., 2009].

In summary, these experiments show that whilst sensory neurons have the ability to be activated by mechanosensory stimuli, they are not excited by hair cell deflections during swims, favoring the hypothesis that efference copy signals are transmitted directly to the neuromasts. If this is the case, then the source of the modulatory signals should be the descending efferent nuclei identified above.

A hallmark of efference copy signals is their temporal coincidence with motor outputs. Thus, we asked if neurons in the DELL or OEN exhibit this feature by monitoring their activity using the functional imaging assays described above. We extended our survey of locomotor outputs to

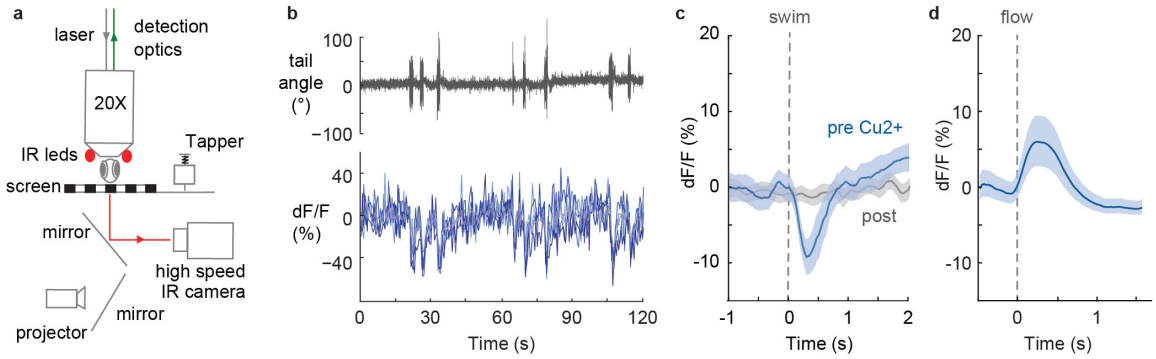

Figure 3.3.3: Functional imaging of primary sensory neurons in the PLL ganglion during head-restrained swimming.| a. Illustration of the experimental setup. Zebrafish larvae are embedded in agarose but are able to move their tail. 2-photon imaging is performed to record calcium-dependent fluorescence signals while tail position is simultaneously tracked using an infrared (IR) camera. Visual stimuli are projected onto a diffusive screen underneath the animal, taps are elicited via the impact of an electronically controlled solenoid against the stage and flow is delivered by pressure injection through a micropipette positioned above the animal's head. **b.**Example behavioral and fluorescence traces during swimming. Top: records of tail curvature to visualize locomotor events. Bottom: dF/F traces of 5 PLLg neurons. **c.**Swim triggered averages of calcium activity in sensory neurons before (blue) and after (gray) neuromast ablation with Copper Sulfate. Swims start at dotted line. Lighter traces correspond to the standard error. n=20 neurons, 2 fish. **d.**Stimulus triggered averages of calcium activity in response to a brief jet of water. n=17 neurons, 4 fish.

include startle responses in addition to swimming [Kimmel et al., 1974]. Importantly, these two behavioral modes are governed by distinct motor-command centers and therefore could, in theory, recruit efferent neurons differentially [Eaton et al., 1984, Orger et al., 2008, Severi et al., 2014, Ritter et al., 2001]. Startle responses were elicited by a mechanical tapper that hit the stage onto which the fish were tethered [Lacoste et al., 2015]. The strength of the tapper's impact against the stage was calibrated such that not all taps elicited a motor output.

Hypothalamic DELL neurons exhibited elevated activity following the onset of both swims and startle responses (Fig.3.3.4a-c). Interestingly, however, they were also activated by taps that did not trigger motor outputs, unmasking a sensory component to their activity (Fig.3.3.4c). Accordingly, DELL neurons were also excited by flow stimuli (Fig.3.3.4d). These response properties do not seem to be concordant with efference copy mechanisms, but rather, with signals involved in sensory gain modulation. Along these lines, recent electrophysiological studies have shown that dopamine increases the activity of lateral line hair cells in larval zebrafish [Toro et al., 2015]. It is interesting to speculate that perhaps, dopamine release during locomotive events ensures hair cell responsiveness

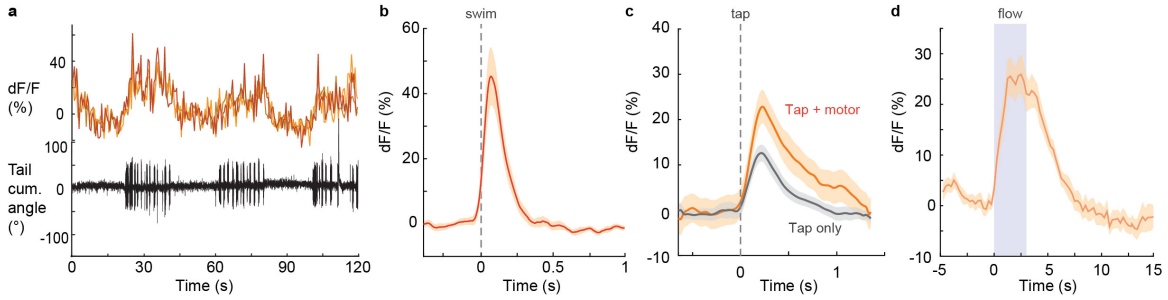

Figure 3.3.4: DELL neurons exhibit sensory and motor-correlated activity.| a. Example behavioral and fluorescence traces during swimming. Top: dF/F traces of 3 PLLg neurons. Bottom: records of tail curvature to visualize locomotor events. **b.**Swim-triggered averages of calcium activity in DELL neurons. Swims start at dotted line. Lighter traces correspond to the standard error. n=9 neurons, 3 fish. **c.**Tap-triggered averages of calcium activity in DELL neurons following taps that elicited motor outputs (orange) and taps that failed to trigger a behavioral response (grey). Tap delivery is indicated by the dotted line. n=21 neurons, 5 fish. **d.**Stimulus-triggered averages of calcium activity in response to a 3.3s water injection over the animal's body. Light-blue square corresponds to period during stimulus delivery, but a residual stimulus might have persisted after stimulus offset. n=17 neurons, 3 fish.

during the quiescent periods after a bout and facilitates neurotransmission after salient stimuli (like a tap). Notably, DELL neurons are unresponsive to noxious heat stimuli, indicating this nucleus can only be recruited by a subset of sensory modalities (data not shown).

Cholinergic OEN neurons also exhibited elevated activity during swims and startle responses (Fig.3.3.5). This activity was maintained after complete ablation of neuromasts with copper sulfate, indicating that sensory inputs are dispensable for OEN excitation. Additionally, OEN neurons showed responses exclusively to taps that elicited motor events, and did not respond to sensory stimuli such as flow or noxious heat (Fig.3.3.5c-f). The pronounced correlation between motor output and OEN activity, provides support for its role in efference copy transmission.

As mentioned earlier, an open question regarding the hindbrain efferents is whether OEN subnuclei are functionally distinct. By finding differences in the proximity of dendritic arborizations to the Mauthner cell, previous studies had proposed that OEN sub-nuclei could be differentially activated by distinct motor programs [Bricaud et al., 2001]. More specifically, they positted that caudal OEN neurons get recruited during escapes, while rostral OEN neurons get recruited during swimming. To address this issue, we analyzed the response properties of OEN neurons according to the relative position of their somas in the hindbrain. We observed that all OEN neurons that

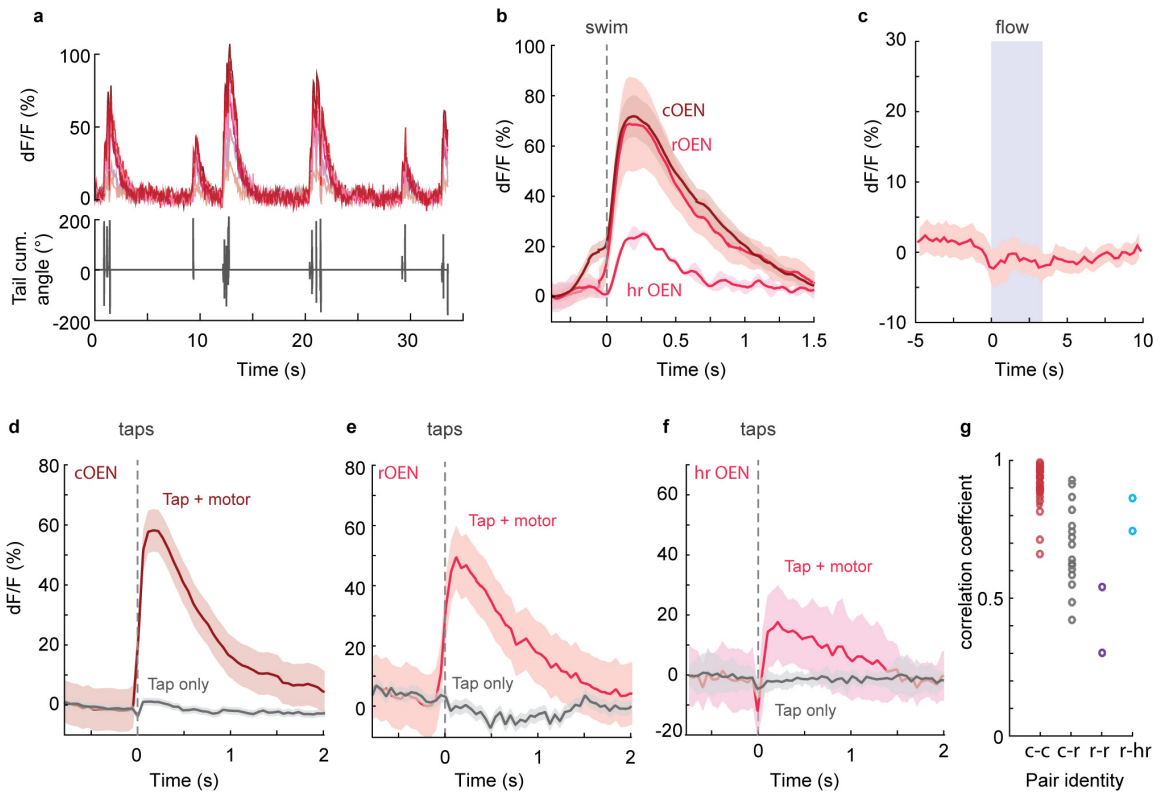

Figure 3.3.5: OEN neurons are activated by locomotor events but not to sensory stimuli.| **a.**Example behavioral and fluorescence traces during swimming. Top: dF/F traces of 7 OEN neurons. Bottom: records of tail curvature to visualize locomotor events. **b.**Swim-triggered averages of calcium activity in efferent neurons of the 3 hindbrain sub-nuclei: the caudal, rostral and hyper-rostral OEN. Swims start at dotted line. Lighter traces correspond to the standard error. n=18 neurons, 4 fish. **c.**Stimulus-triggered averages of calcium activity in response to a 3.3s water injection over the animal's body. Light-blue square corresponds to period during stimulus delivery, but a residual stimulus might have persisted after stimulus offset. Dataset includes caudal and rostral OEN neurons. n=26 neurons, 4 fish. **d-f.**Tap-triggered averages of calcium activity following taps that elicited motor outputs (red/pink) and taps that failed to trigger a behavioral response (grey) in **d.**caudal, **e.**rostral, and **f.**hyper-rostral OEN neurons. Tap delivery is indicated by the dotted line. **g.**Pairwise correlation coefficients of OEN neurons between and across sub-groups. Activity was obtained from the neurons in **b**.

project to the PLL are active during both swims and startle responses, regardless of soma location (Fig.3.3.5b,d-f). Furthermore, the activity across subgroups (caudal:rostral, rostral:hyper-rostral, etc.) is very highly correlated, suggesting that they can be thought of as one functional unit for the behaviors tested (Fig.3.3.5g).

In summary, both DELL and OEN nuclei exhibit motor-correlated activity during swims and startle responses. DELL neurons, however, also possess a sensory component to their activity that is mediated by the lateral line and the inner ear. OEN neurons do not show sensory-dependent excitation, making them the more likely mediators of efference copies to the lateral line.

To test whether the OEN is necessary for sensory inhibition during locomotion, we measured the activity of lateral line sensory neurons in the PLL ganglion before and after laser ablation of the OEN. To ensure selective targeting of these neurons, we performed unilateral dye injections in the lateral line nerve, and allowed at least 48hs for nerve regeneration [Pujol-Martí et al., 2014]. Taking advantage of the fact that efferent neurons do not cross the midline, we used the the ganglion on the contralateral side to the injection as an internal control. Before ablations, sensory neurons in both the labeled and control ganglia exhibited no difference in activity during periods of quiescence versus motor output (Fig.3.3.6c-d). Strikingly, after the ablation of OEN neurons, a subset of neurons in the ipsilateral ganglion displayed robust responses during swimming, demonstrating that OEN input is necessary for sensory inhibition during locomotion (Fig.3.3.6a-c). Neurons of the contralateral ganglion, on the other hand, continued to be silent during swim bouts (Fig.3.3.6d). So far, we have not used this approach to examine the role of DELL neurons, but given their sensory-correlated activity and the sensitizing effects of dopamine on hair cell activity, we consider it highly unlikely that they too transmit efference copies.

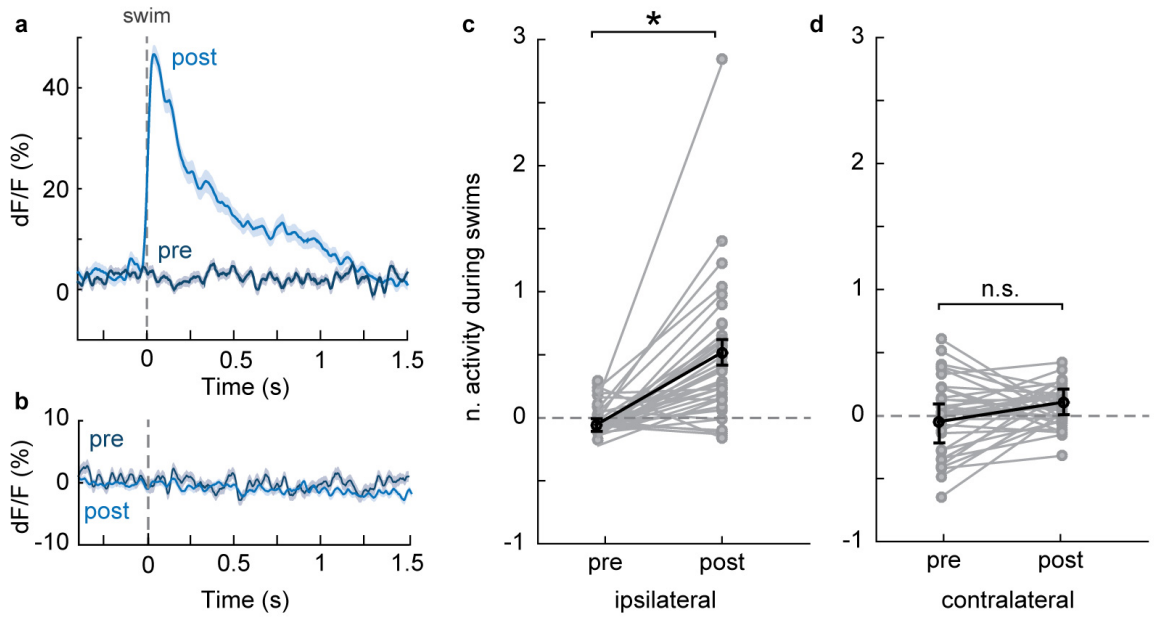

Figure 3.3.6: Sensory neurons of the PLL ganglion acquire responses to motor-evoked stimulation following ablation of OEN inputs. | **a.**Mean dF/F traces of a representative responsive sensory neuron in the PLLg before (pre) and after (post) 2-photon ablation of the ipsilateral OEN. Lighter traces correspond to the standard error of the mean (SEM). **b.**Mean dF/F traces of a representative non-responsive sensory neuron in the PLLg before (pre) and after (post) 2-photon ablation of the ipsilateral OEN. **c-d.**Plots of normalized activity during swims summarizing activity of sensory neurons in ganglia located **c.** ipsilateral or **d.** contralateral to the ablation site. The normalized activity during swims computes the difference in the average fluorescence emitted by a neuron during swims vs. quiescent periods, normalized by the average fluorescence emitted during quiescent periods ($(F_{swims} - F_{static})/F_{static}$). In this case, a score of 0 indicates no difference in activity during swims compared to inter-bouts, demonstrating no sensory-evoked activity during locomotive events. Mean and SEM of the population (black) and means of individual fish (grey) before and after treatment are shown. Paired Student's t-test. **c.** n=21 and 22 neurons, 2 fish both with p<0.01 (*). **d.** n=19 and 14 neurons, 2 fish both with p>0.05 (n.s.).

3.3.1 Conclusion

Zebrafish larvae, like other fish and amphibians, possess a mechanosesory lateral line which enables them to extract hydrodynamic information about their immediate environment. During locomotion, fluid drag elicited by the animal's own movement results in direct stimulation of the sensory organs. We observed, however, that sensory neurons of the lateral line are not activated in head-restrained larvae during tail undulations, revealing compensatory mechanisms that cancel out the self-generated stimulation. By combining cell tracing and *in vivo* functional imaging techniques, we characterized two different sources of descending inputs that innervate the peripheral sensory organs of the lateral line: the diencephalic DELL and the rhomboencephalic OEN [Metcalfe et al., 1985].

We propose that OEN neurons, transmit inhibitory efference copy signals directly onto hair cells to cancel out reafferent stimuli during locomotion (Fig.3.3.7). This simple strategy prevents informational ambiguity and most likely serves to suppress maladaptive triggering of behavioral responses. This type of cancellation could be achieved by a complete shunting of hair cell excitability during locomotion or by precise compensatory signals that allow for the detection of concomitant external cues. Whilst we have no direct evidence to support either model, the broad innervation patterns of efferent neurons may suggest that coarse inhibitory signals are in place. During swimming, neuromasts receive different inputs depending on their position in the body and their directional tuning. Given that a single efferent neuron does not selectively innervate neuromasts, it is unlikely that it could systematically send precise inhibitory signals to each one of its targets. The consequence of such a complete inhibition of the sensory stream would be a severe inability to sense exafferent cues during locomotion. However, zebrafish larvae swim in short bouts followed by longer periods of quiescence, which means that mechanosensory information can still be extracted during the inter-bout periods [Budick and O'Malley, 2000]. An interesting question that arises, then, is how the system performs in the adult zebrafish, whose locomotion is devoid of quiescent inter-bouts.

In addition, we observed dopaminergic inputs to the lateral line, originating from DELL neurons in the ventral hypothalamus (Fig.3.3.7). These neurons exhibit increased activity during locomotion, as well as in response to sensory stimuli such as flow and waves elicited by taps. The sensori-motor signature of their signal suggests a modulatory effect elicited by motion and salient mechanosensory stimuli. Furthermore, recent studies have shown that dopamine has a sensitizing

effect on hair cells via the D1b receptor [Toro et al., 2015]. By virtue of its action through G-protein coupled receptors, the effects of dopamine most likely outlast the brief occurrences of swims or stimuli, leaving the sensory system in a more receptive state during the inter-bout periods or following stimuli that might require subsequent behavioral responses. Furthermore, DELL neurons also send collaterals to the spinal cord, and have been shown to affect bout frequency, indicating a role in the regulation of spinal circuit excitability [Jay et al., 2015]. Taken together, DELL neurons seem to have a dual function in the control of basal threshold levels of both sensory and motor networks.

In summary, larval zebrafish possess parallel descending inputs that can differentially influence hair cell sensitivity. Cholinergic signals from the hindbrain transmit efference copy signals that cancel out self-generated stimulation during locomotion, while dopaminergic signals from the hypothalamus may have a role in threshold modulation. We propose that this simple circuit is involved in state-dependent gain modulation and are currently investigating its importance for sensory processing during spontaneous locomotion and mechanosensory-guided behaviors.

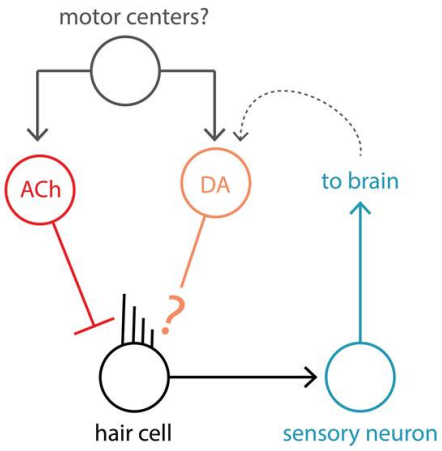

Figure 3.3.7: Proposed circuit diagram for the lateral line system of zebrafish larvae.| Upon deflection, hair cells (black) activate primary sensory neurons (blue). During locomotion, dopaminergic DELL neurons (DA, orange) and cholinergic OEN neurons (ACh, red) are activated and modulate hair cell responsiveness to stimuli. DELL neurons are activated by mechanosensory inputs through a yet uncharacterized pathway (dotted arrow).

3.4 Methods

3.4.1 Animals

4-9 days-post-fertilization (dpf) zebrafish were used for all experiments. Transgenic lines used included: isl1:GFP to visualize OEN neurons, etvMAT:GFP and DAT:GFP to label DELL neurons, Brn3c:GFP to tag hair cells of the lateral line and inner ear, and Tg(elavl3:GCaMP6s and elavl3:GCaMP6f for functional imaging experiments [Higashijima et al., 2000, Xi et al., 2011, Xiao et al., 2005, Chen and Engert, 2014]. Animal handling and experimental procedures were approved by the Harvard University Standing Committee on the Use of Animals in Research and Training. No statistical methods were used to predetermine sample size.

3.4.2 Dye labeling of efferent neurons

Larvae were anesthetized with 0.005% MS-222 (Sigma) and embedded in low melting-point agarose on their sides. Sharpened tungsten needles were used to lesion the lateral line nerve at the level of neuromast L1 and to deposit crystals containing 3kD dextrans conjugated to Alexa Fluor 647 (Invitrogen). Fish were allowed to recover for at least 24hs before proceeding with further experimentation.

3.4.3 Immunohistochemistry

24hs hours following dye labeling of efferent neurons, fish were fixed in 4% paraformaldehyde (PFA) diluted in PBS containing 0.25% Triton (PBT). They were then immunostained using standard procedures [Inoue and Wittbrodt, 2011]. Briefly, fish were washed in PBT, incubated in 150 mM Tris-HCl, pH 9, for 15 min at 70 °C, washed in PBT, permeabilized in 1% Proteinase-K during 30 min, washed in PBT, blocked in blocking solition of PBT containing, 2% normal donkey serum (NDS), 1% bovine serum albumin (BSA), 1% dimethyl sulfoxide (DMSO), 1% dimethyl sulfoxide (DMSO) and then incubated overnight at 4°C in primary antibodies diluted in blocking solution(goat anti-ChAT, 1:200, Abcam). Fish were then washed in PBT, blocked for 1 hr and incubated overnight at 4°C in secondary antibodies conjugated to Alexa Fluorophores (donkey anti-goat, 1:1000, Abcam).

3.4.4 Confocal imaging

Imaging of live or fixed tissue (after electroporation or immunohistochemistry, respectively) was performed with an upright confocal microscope (Zeiss LSM780) containing a 20×/1.0-NA water-dipping objective.

3.4.5 Focal electroporations

Focal electroporations were performed in double transgenic larvae encoding GFP in hair cells by means of the Brn3c:GFP transgene and in landmark areas to guide the electroporations (isl1:GFP or etVMAT:GFP when targeting the OEN or DELL respectively). They were performed as described by Tawk et al. [2009]. Briefly, larvae were anesthetized and embedded in low melting-point agarose dorsal-side up. Micropipettes with tip diameters of 1-2 μm were filled with a 1 μg/μl solution of plasmid DNA in distilled water. Plasmid backbones corresponded to the pCS2 expression construct and encoded mCherry or tdTomato fused to the N-terminal motif of the Src-family kinase Lyn. Micropipettes were placed near the efferent nuclei, guided by GFP expression in landmark areas, which were visualized under epi-fluorescence on a compound microscope. Plasmid delivery was achieved by 1-2 trains of voltage pulses lasting 250 ms, with 1 s intervals between them using a Grass stimulator (SD9, Grass Technologies). Pulses had an amplitude of 20 V, a duration of 2 ms and a frequency of 200 Hz. Following electroporation, larvae were allowed to recover overnight in fish water. The next day, larvae were screened and those containing labeled neurons were anesthetized and mounted in agarose to be imaged using a confocal microscope.

3.4.6 Volumetric reconstructions from serial electron microscopy data.

Volumetric reconstructions of the dorsal neuromast D2 were performed on high-resolution serial section electron microscopy images from 5.5 dpf fish. Methods and data are described in [Hildebrand et al., 2017]. The data was aligned using non-affine alignment trhough the FijiBento package on the Odyssey cluster supported by the FAS Division of Science, Research Computing Group at Harvard University [Saalfeld et al., 2012]. Image segmentation was carried out manually using a custom volume annotation and segmentation tool. Segmented images were processed for 3D modeling with MATLAB and 3Ds Max for rendering. VAST: *https://software.rc.fas.harvard.edu/lichtman/vast*.

3.4.7 *In vivo* 2-photon functional imaging

A custom built 2-photon microscope was used for all functional experiments as in Portugues et al. [2014]. The laser, a Ti:Sapphire ultra-fast laser (MaiTai, Spectra-Physics) was tuned to 950 nm, and operated at an average laser power at sample of 5–10 mW. Images were collected by scanning frames at 4 Hz and subsequent planes had a distance of 1 μm. Image acquistion, stimulus delivery and behavioral tracking were controlled using custom software written in LabView (National Instruments).

3.4.8 Chemical ablation of neuromasts

Fish were incubated in 1mM copper sulfate for 85 min and allowed to rest in fish water for 60 min. Only fish that showed a complete neuromast ablation (assessed by DiASP staining: 0.5mM in fish water for 15min) were used for additional functional imaging assays [Schuster and Ghysen, 2013].

3.4.9 Laser ablations of efferent nuclei

Fish were subjected to unilateral dye injections to the lateral line at 4dpf as previously described, and allowed to recover in freely-swimming conditions for 48hs to allow for nerve regeneration after injury [Pujol-Martí et al., 2014]. At 6 dpf, fish were embedded in low-point melting agarose to be used for functional experiments the following day. After functional experiments, we performed the ablation procedure as described in Orger et al. [2008], with the exception that anesthesia was not used. Individual efferent neurons were targeted systematically by receiving 1-3 850 nm laser pulses of 1ms, at 80% laser power. Fish were then immediately used for functional experiments to test for the effects of ablations on sensory processing. On average 5 OEN efferent neurons were ablated from the 8 that are hypothesized to exist (Supp.TableB.1.1).

"It's not enough what I did in the past - there is also the future."

Rita Levi-Montalcini

4

Conclusions & Prospects

4.1 After behavior comes the circuit

At the beginning of this work, I advocated for the power of studying behavior to guide our research on brain function. Chapter 2 delved on the characterization of rheotaxis, a robust behavior performed by zebrafish larvae. To do this, we first described the sensory cues available to inform the animal's behavior. We observed that in a body of water flowing within a pipe, all water particles do not travel at the same speed. Flow is slower at the sides than at the center of the tube, creating a graded velocity profile. By quantifying the fish's movements with respect to such gradients, we discovered that fish follow a very simple navigational algorithm. After experiencing a decrease in gradient magnitude (when moving towards the center of the tube), fish swim primarily straight. Alternatively, after experiencing an increase in gradient magnitude (when moving away from the center) fish perform large turns but only in the direction of flow field rotation. These two simple behavioral rules allow the fish to consistently turn to face the current and swim against it. In fact, these

rules are enough to recapitulate rheotaxis in a computer model of a particle in a virtual current.

Finally, we looked for the sensory modality being used during rheotaxis. The most striking candidate was the lateral line. The lateral line is a collection of mechanosensory organs distributed along the surface of the body in fish and amphibians. These organs are made up of hair cells that protrude out of the animal's body and are activated by stimuli that deflect them, such as water flow. Moreover, because they are distributed along the periphery of the animal, they are particularly well poised to sense rotational flow fields around the body. Unsurprisingly, fish without a lateral line system failed to perform rheotaxis in the dark.

Overall, by looking at behavior very closely and by thoroughly describing the physical parameters of the environment, we were able to extract the basic rules behind said behavior. Moreover, from this approach has emerged a hypothesis of how this is implemented by the brain and the properties that the neurons involved should have. The obvious next step is to test that hypothesis by examining brain activity when the animal is exposed to rotational flow fields.

Let us examine our hypothesis in more detail. We have established that zebrafish larvae must detect rotational flow fields around their bodies. This is achieved by external sensory organs around the body. Furthermore, organs on both sides are necessary for the behavior. This implies that a comparison between the left and right lateral line has to be computed. Therefore, there has to be a convergence point of bilateral inputs from the lateral line. This site could be identified by using anterograde viral-tracing whereby lateral line projections on each side of the fish are infected with virus coding for different colored fluorescent proteins [Mundell et al., 2015].

In addition, a distinguishing feature of the rotational flow field around the animal is that it moves in opposite directions on each side of the midline (Fig.4.1.1.a). A minimal wiring pattern that could detect the direction of rotation, would combine inputs from sensory hair cells that are maximally tuned to one direction on one side of the fish, and hair cells with the opposite directional tuning on the other side of the fish (Fig.4.1.1.b). This connectivity would allow for the coding of both rotational flow direction and magnitude, given that the comparator neuron would be activated as a function of the stimulus strength on both sides of the body. The existence of comparator neurons that code for direction of rotation, could be established using functional imaging during the presentation of water jets of opposing directions to either side of the body.

This wiring pattern would not be useful in the cases where water flow is rotation free, as in the case of sources and sinks. In these cases, the direction of water flow would be the same on both sides of

the fish and the comparator neuron would not be engaged. An ethological example of a sink is the mouth of a suction feeding predator [Ferry-Graham and Lauder, 2001]. Given that zebrafish larvae have been shown to sense and escape from local sinks, we propose that there must exist an additional comparator type that enables the detection of radial gradients [Olszewski et al., 2012, Olive et al., 2016].

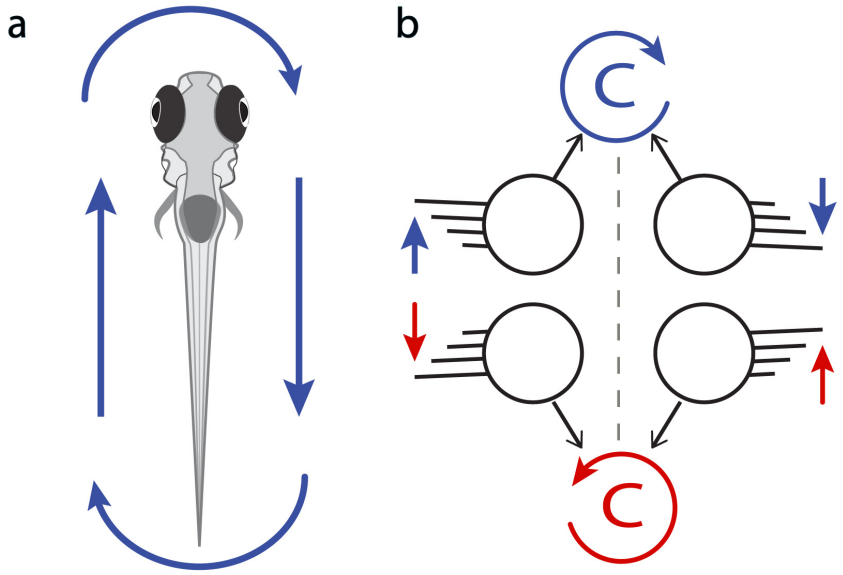

Figure 4.1.1: Hypothesized circuit wiring for rotational flow detection| a. Schematic of a clockwise rotational flow field around a larval zebrafish. **b.** Minimal circuit that could detect the direction of rotational flow fields surrounding an animal. A comparator neuron (C) receives inputs from hair cells on opposite sides of the midline (dotted line), and with opposing directional tuning. Clockwise flow rotations (blue arrows) would maximally drive 'upwards' selective hair cells on the left, and 'downwards' selective hair cells on the right. Their activation would be proportional to stimulus strength and would drive activity of the counter-clockwise comparator (C, blue) accordingly. Given that neuromasts contain hair cells of two polarities, a complementary wiring pattern would be able to detect counter-clockwise rotations (red).

Another question that still remains, concerns the process by which larvae can establish how the magnitude of the rotational flow field changes as a function of position in the arena. We proposed that this could be achieved through temporal integration by sampling the local curl before and after a bout. An alternative mechanism would involve instantaneous comparisons of the intensity of the flow vectors across the length of the animal. Both models would place testable restrictions on both

the architecture and the functional properties of the circuit.

A related problem involves when flow detection occurs in the context of swims. Because zebrafish larvae swim in discrete bouts followed by periods of quiescence, sampling during stationary periods would maximize the signal to noise ratio [Budick and O'Malley, 2000]. As we have seen in Chapter 3, sensory neurons of the lateral line are inhibited during locomotion, increasing the threshold for signal detection or making the system completely insensitive to stimuli (we will discuss both options in the next section). However, the swimming dynamics of adult zebrafish lack these periods of quiescence. Adults do however, swim actively in bursts and then coast. Given that coasting generates less reafference than active swimming, one alternative is that adults measure flow fields during coasting. This strategy has been observed in the ruffe *Gymnocephalus cernuus L.*, which seems to detect prey exclusively during coasting [Janssen, 1997]. Another solution would involve the refinement of efference copy mechanisms to the lateral line, such that exafferent stimuli can be detected and processed during locomotion. Studies in *Xenopus laevis* have shown that efference copy signals to the extraocular muscles change their patterns as the animal transitions from larval undulatory swimming to adult limb-mediated locomotion [von Uckermann et al., 2016]. It is possible that similar, plastic changes occur in the efference copy signals to the lateral line as zebrafish transition from larvae to adults.

Overall behavioral analysis has provided hints about the neuronal mechanisms underlying rheotaxis, which can now be tested using functional imaging and circuit tracing techniques.

4.2 Effects of efferent modulation on sensory coding in the lateral line

In Chapter 3 I discussed how self-generated stimulation during locomotion can cause informational ambiguity. Using retrograde labeling of the lateral line nerve, we identified two parallel descending inputs that can influence hair cell sensitivity. Functional imaging studies revealed that signals originating from the OEN in the hindbrain transmit efference copies that cancel out self-generated stimulation during locomotion. Signals from dopaminergic DELL neurons in the hypothalamus occur during locomotion and after salient mechanosensory stimuli, but we still have not tested their effects on sensory processing. To address this, we are currently performing functional imaging of the PLL ganglion before and after laser ablations of DELL neurons. Previous studies have shown a

sensitizing effect of dopamine on hair cell sensitivity [Toro et al., 2015]. An intriguing hypothesis is that dopamine release during swim bouts sensitizes the sensory system in preparation for information sampling during the quiescent inter-bout periods. It could also counteract the inhibitory effect of cholingeric inputs to prevent runaway inhibition. This phenomenon could be observed as a generalized increase in the threshold for mechanosensory excitation after DELL ablation.

With respect to the OEN, a few questions remain unanswered. As alluded to in the previous section, we would like to characterize the nature of its inhibition. Is it all-off or is it scaled to match the magnitude of each motor output? Do efference copy signals leave the animal insensitive to external cues during motion, or are they in place precisely to enable stimulus detection in spite of motion? This question can be addressed by comparing how sensory neurons respond to identical stimuli during swim bouts or quiescent periods. Activity of sensory neurons in the PPL ganglion can be measured by loose patching or calcium imaging in a paralyzed animal, in which motor output is recorded by monitoring electrophysiological activity in the dorsal root ganglia [Trapani et al., 2009, Ahrens et al., 2012]. Precise deflections of single neuromasts can be then delivered using a glass pipette connected to a piezo-electric device [Haehnel et al., 2012]. In this way we can measure how detection thresholds change as a function of motor output and the exact signature of cholinergic signals to the lateral line.

Another question involves the mechanisms by which acetylcholine results in the inhibition of hair cell excitability. Canonically, acetylcholine is thought of as the excitatory neurotransmitter of the neuromuscular junction [Fatt, 1950]. In the inner ear of rodents however, hair cell inhibition is elicited via the activation of nicotinic receptors containing $\alpha 9$ and $\alpha 10$ subunits [Elgoyhen et al., 1994, 2001]. Whilst these receptors are permeable to calcium (and hence should have a depolarizing effect), they are tightly coupled to calcium-gated SK2 channels, which hyperpolarize the cell due to potassium efflux [Dulon et al., 1998, Oliver et al., 2000, Nie et al., 2004]. Zebrafish possess two copies of each subunit and it would be interesting to test whether hair cells of the lateral line are inhibited through a similar mechanism. If this is the case, neuromasts could facilitate the study of synaptic transmission in hair cells due to their much more accessible anatomy in comparison to the cochlea.

Finally, it is worth thinking about efferent modulation of lateral line sensitivity in the context of behavior. Is it in place to prevent the maladaptive triggering of reflexes in response to the fish's own motion? Does it influence the performance of lateral-line mediated behaviors? Since the swimming

repertoire of the larval zebrafish is well characterized, we expect that changes in the statistics of the behavior after systematic ablations of the efferent nuclei will be informative in this regard [Budick and O'Malley, 2000, Dunn et al., 2016b, Portugues et al., 2015]. Furthermore, we can utilize our understanding of the behavioral algorithm followed during rheotaxis to identify failures in sensory coding after the elimination of individual efferent streams. We should note, however, that there is a caveat to this approach in reference to the DELL neurons. DELL neurons project to both the lateral line and the spinal cord, having potential modulatory effects in both thresholds for sensing and thresholds to initiate locomotive events. As such, reductions in performance after DELL ablations could be attributed to failures to detect stimuli or failures to elicit a behavioral response. Pharmacology or targeted genetic manipulations could then be used to disambiguate between the two possibilities.

In summary, further studies regarding the role that descending inputs play in sensory coding and in guiding behavior will illuminate how afferent and efferent signals encode information about the external word such that an animal can extract meaningful information and respond appropriately.

A

Appendix 1

A.1 Supplementary material for Chapter 2: A novel mechanism for mechanosensory based rheotaxis in larval zebrafish

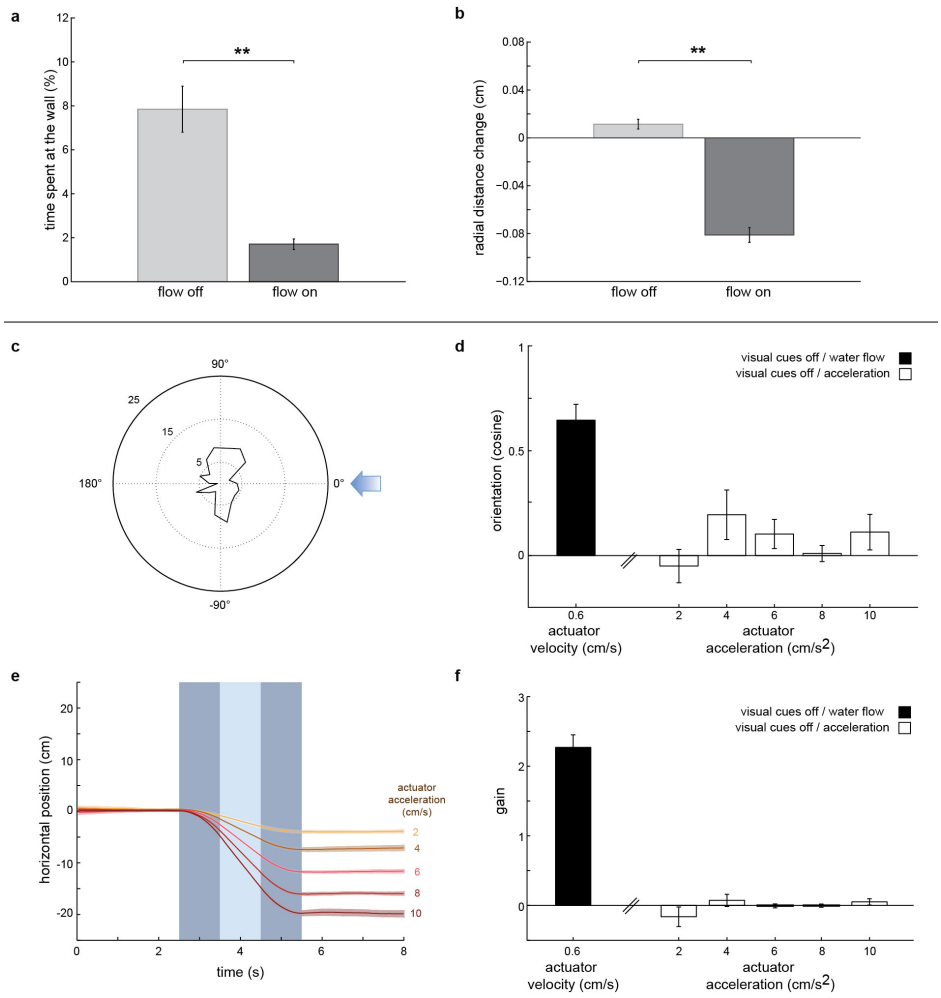

Figure A.1.1: Touch and acceleration are not relevant cues for rheotaxis in larval zebrafish.| a-b. Fish swim away from the wall during flow stimulus presentation. **a.**Percentage of time spent at the wall while water flow stimulus is off (light grey) and on (dark grey); ** = p<0.01, Monte Carlo permutation test. n= 13 fish, 341 trials. **b.** Mean radial distance change for bouts occurring in close proximity to the wall (<0.36cm, 1/3 of the tube radius) while flow is off (light grey) and on (dark grey). Negative values indicate decreases in the distance to the center of the tube. ** = p<0.01, Monte Carlo permutation test. n= 13 fish, 1364 bouts. **c-f.**Rheotactic metrics for larval zebrafish exposed to a series of stimulus consisting of an initial acceleration followed by periods of whole-tube water displacement and de-acceleration. **c.**Polar plot of fish orientation in the axis of the flow during stimulation. Blue arrow represents stimulus direction. **d.**cosine of the mean orientation for fish presented with different acceleration regimes. As a comparison, cosine of the mean orientation for fish exposed to water flow in the absence of visual cues (black bar, Fig.2.3.1g) is shown. Means and SEM are shown. **e.**Fish position (from the observer's point of view) in the axis of the water flow. Means (solid line) and SEM (shaded areas) are shown for different acceleration regimes. Dark blue represent acceleration / de-acceleration periods while light blue represents whole tube water displacement. **f.**Gain for fish presented with different acceleration regimes. As a comparison, the gain of fish exposed to water flow in the absence of visual cues (black bar, Fig.2.3.1i) is shown. Means and SEM are shown. n= 6 fish subjected to 6 trials at each acceleration regime (180 trials total).

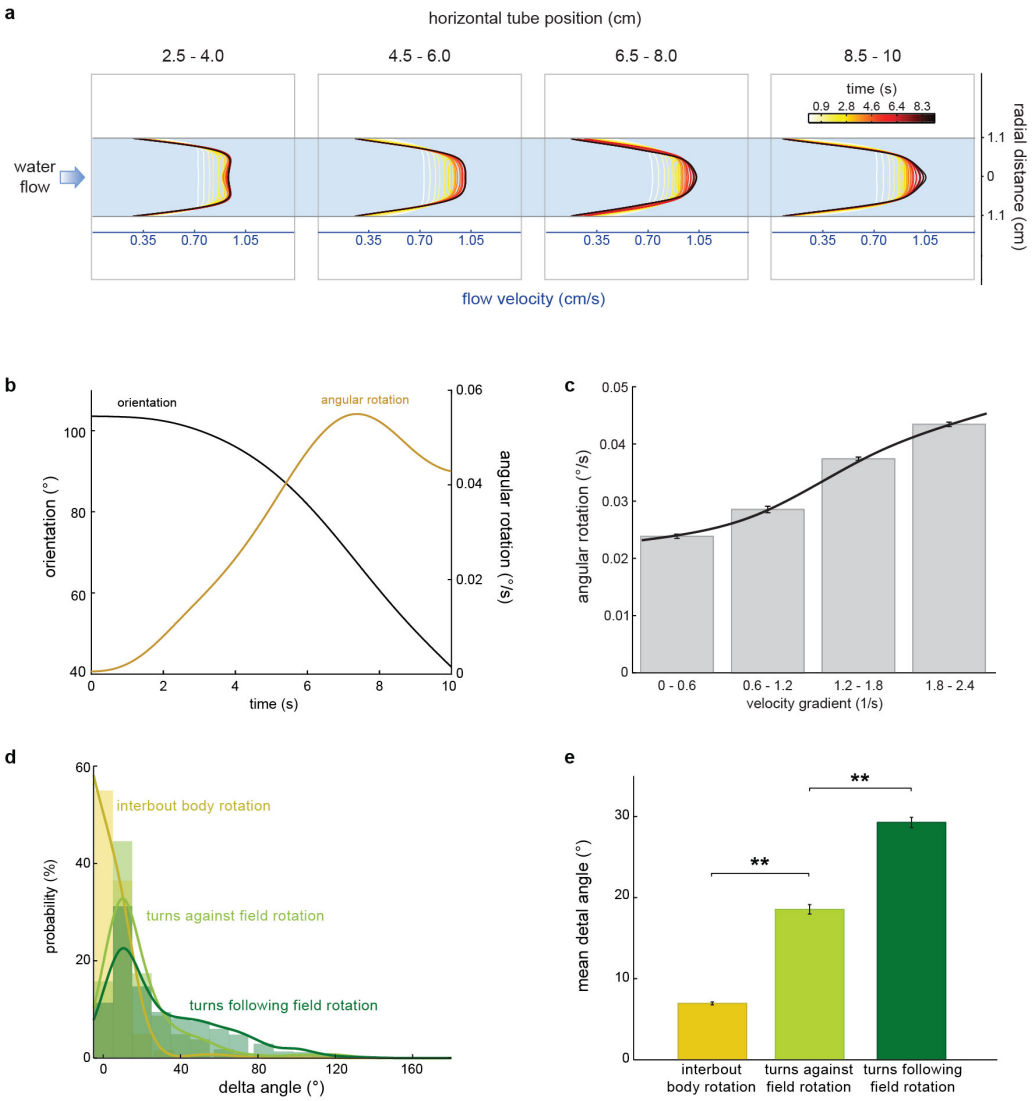

Figure A.1.2: Flow velocity gradients rotate the larval zebrafish's body.| a. Flow velocity profiles obtained through PIV at different points in the horizontal axis of the tube. Profiles are the results of averaging flow velocities at the tube positions outlined above. Color code indicates time. **b.**Orientation of a single paralyzed larval zebrafish in relation to water flow. The angular rotational velocity extracted from the black trace is superimposed in brown. **c.**Mean angular rotational velocities for different velocity gradient magnitudes. Mean and SEM for each bin (light grey) and fitted line (black trace) are shown. n= 3 fish, 18 trials. **d-e.**Inter-bout body rotation and turn magnitudes for bouts following or going against flow field rotation. **d.**Inter-bout body rotation (yellow) and turn magnitude histogram for bouts going against (light green) and following (dark green) flow rotational fields. Histograms and fitted lines for each distribution are shown. n =13 fish, 341 trials. **e.**Mean delta angle for inter-bout body rotation and turns following / going against flow field rotation. ** = p<0.01, Monte Carlo permutation test. n= 3840 inter-bout periods, 2831 bouts.

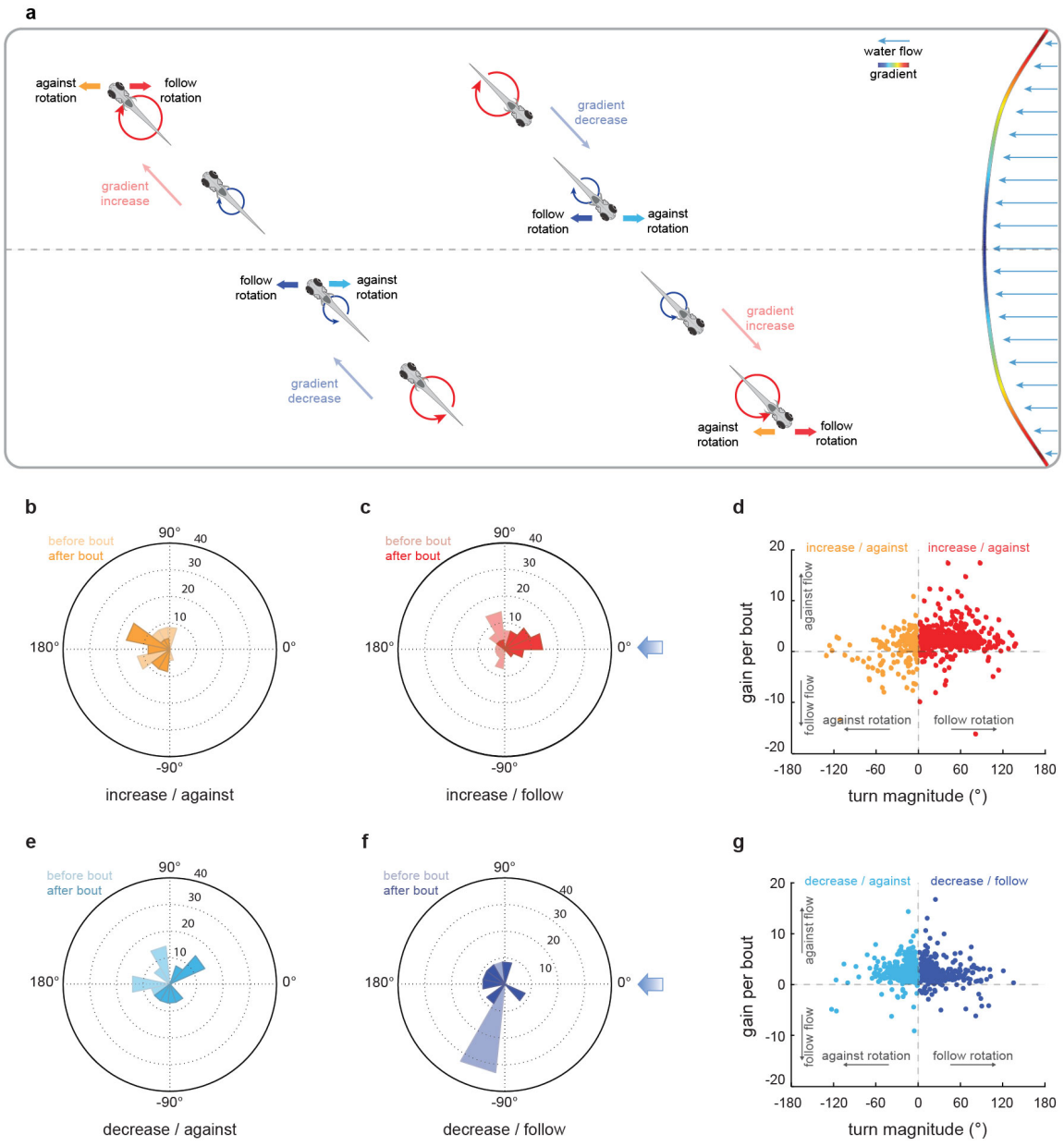

Figure A.1.3: The rheotactic algorithm allows the fish to orient and swim against water flows.| a. Graphical representation of the bout types during rheotaxis and their contribution to orientation and displacement against incoming water flows. **b,c,e,f.** Polar plots of fish orientation in the left/right axis before (light color) and after (dark color) high (>45 degrees) magnitude turns. Data is the same as in Fig.2.3.3f. **d,g.**Scatter plots of turn magnitude vs gain for bouts occurring after **d.**increases or **g.**decreases in experienced flow velocity gradient magnitude. n= 1110 bouts.

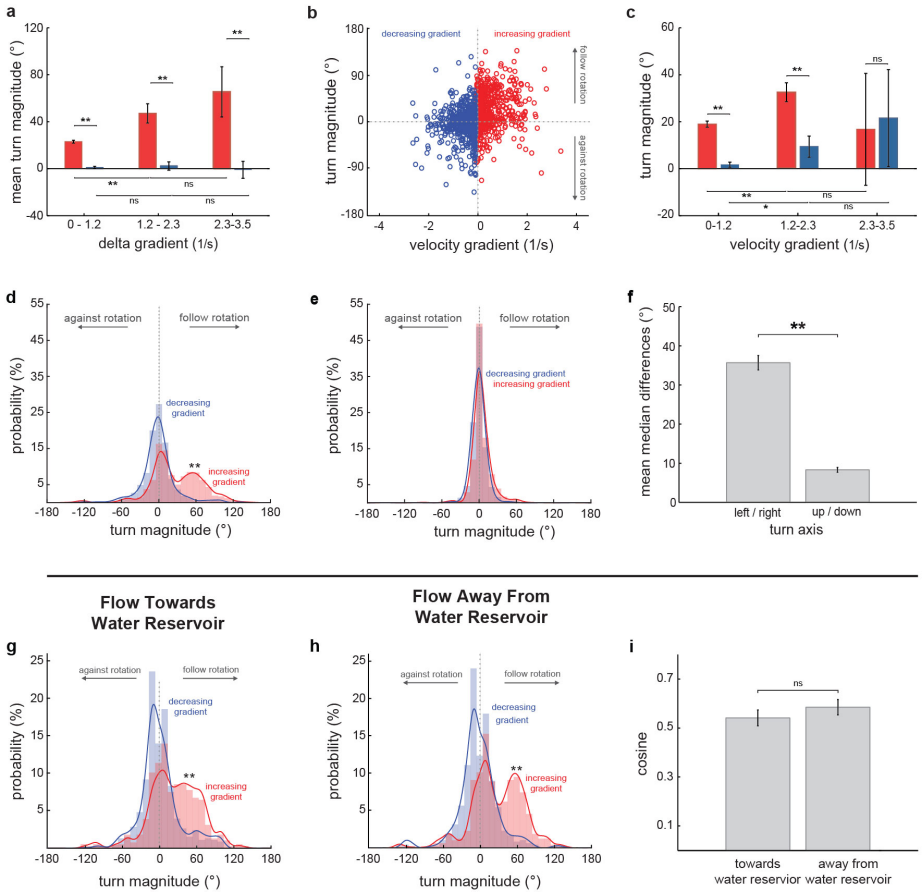

Figure A.1.4: The rheotactic algorithm depends on changes in flow gradient and is mainly composed of lateral turns.| a-c. Small differences in flow velocity gradient, not the velocity gradient itself, trigger the rheotactic algorithm. **a.**Mean turn magnitude for bouts that occur after increases or decreases in gradient magnitude, grouped by delta gradient. Data is the same as in Fig2.3.3f. Even at small delta gradient values, larval zebrafish follow flow rotation after increases but not after decreases in gradient magnitude. ns= p>0.05, ** = p<0.01, Monte Carlo permutation test. n= 13 fish, 1916 bouts. **b.**Scatter plot of flow velocity gradient versus turn magnitude for bouts occurring between 0.36 and 0.74cm away from the chamber walls (an intermediate region the fish can reach from low or high gradient areas). **c.**Mean turn magnitude for following increases or decreases in gradient magnitude, grouped by velocity gradient. Data is the same as in (b). At similar velocity gradients, bouts occurring after increases present higher turn magnitudes than bouts occurring after decreases in gradient magnitude. ns = p>0.05, ** = p<0.01, Monte Carlo permutation test. n= 13 fish, 1689 bouts. **d-e.**Turn distributions are more asymmetric in the lateral than in the vertical axes. Turn magnitude histogram for **d.**left/right and **e.**up/down turns. Bars and fitted lines for each distribution are shown. ** = p<0.01, Kolmogorov-Smirnov test. n= 13 fish, 341 trials. **f.** Mean difference between the medians of increasing (red in d, e) and decreasing (blue in d, e) gradient turn distributions. Mean and SEM are shown. ** = p<0.01, Monte Carlo permutation test. Data is the same as in (d,e). **g-i.** Turn magnitude histogram for experiments in which water flowed **g.** towards or **h.** away from the water reservoir (ftwr and fawr conditions, respectively). Bars and fitted lines for bouts occurring after increases (red) and decreases (blue) in experienced gradient magnitude are shown. ** = p<0.01; Kolmogorov-Smirnov test. **i-j.** Cosine of the mean orientation (d) for ftwr and fawr experiments. Means and SEM are shown, ns = p>0.05; * = p>0.01&<0.05; Monte Carlo permutation test. n= 13 fish; 170 and 171 trials for ftwr and awr experiments, respectively.

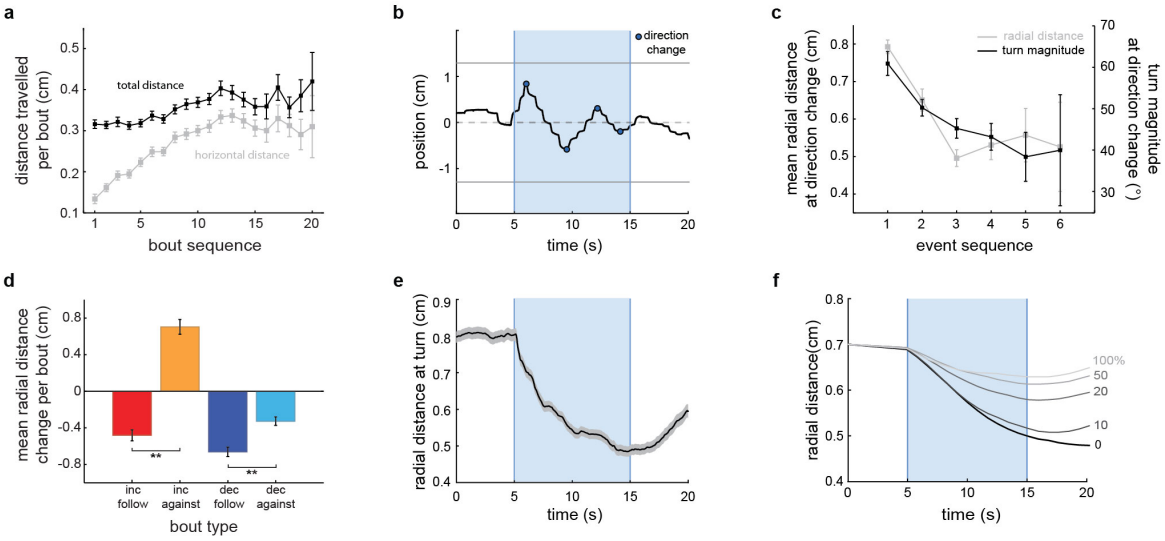

Figure A.1.5: Larval zebrafish up-regulate displacement against the flow while swimming towards the center of the tube.| a. Displacement in 3-dimensions and in the axis of the water flow for subsequent bouts during flow stimulation. Mean and SEM of each bout are shown. n= 3499 bouts. **b.**Horizontal (in the left/right axis) positions of a single fish during rheotaxis. Light blue indicates when water flow stimulus is on while dark blue dots indicate direction change events. Data corresponds to the example shown in Fig.2.3.1b-e. **c.**Radial distance and turn magnitude at consecutive swim direction changes. Mean and SEM of consecutive direction change events are shown. n= 774 direction change events. **d.**Mean radial distance change for different bout types. Mean and SEM are shown. ** = p<0.01, Monte Carlo permutation test. n= 13 fish, 1817 bouts. **e.**Radial distance over time. Mean (dark line) and SEM (shaded areas) are shown. n= 13 fish, 341trials. **f.**Radial distance over time for a modeled particle following the rheotactic algorithm.

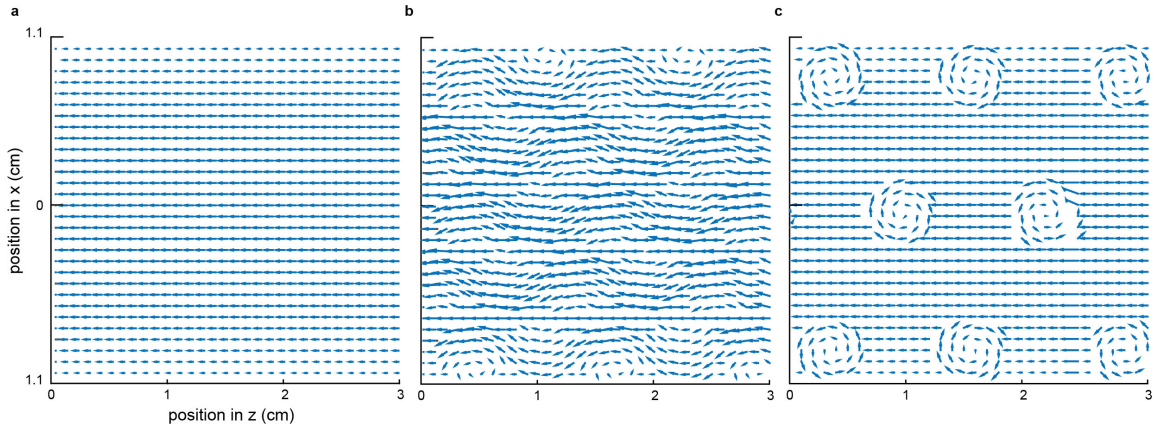

Figure A.1.6: Flow fields used for modelling rheotactic behavior.| a. Laminar flow. **b.**Karman vortex streets were added to the laminar flow profile with varying degrees of vortex intensity and density. Karman vortex streets at velocity 50% and density 100%. **c.**Static vortices set to velocity 100% and density 100%.

Figure A.1.7 ***(following page)*****: Lateral line ablations.| a-d.** Representative examples of **a-a'.**copper-mediated chemical neuromast and **b-b'.** 2-photon laser sham, **c-c'.**anterior, and **d-d'.**posterior LL nerve ablations before (left) and after (right) treatment. For chemical ablations, DiasP staining of the hair cells of a WT fish is shown. For laser ablations, Tg(HGn93D) fish expressing GFP in the LL nerves are shown. Red dotted circles indicate the region in which laser power was focused. **e.**Cosine of the mean orientation for fish subjected to unilateral laser ablations of the LL nerve. Mean and SEM of the population (black) and means of individual fish (grey) before and after treatment are shown. ns = $p>0.05$, * = $p<0.05$&>0.01; bootstrap on the mean. n= sham, 9 fish; Anterior LL ablation, 4 fish; Posterior LL ablation, 9 fish. All fish were subjected to 6 trials before and after manipulations.

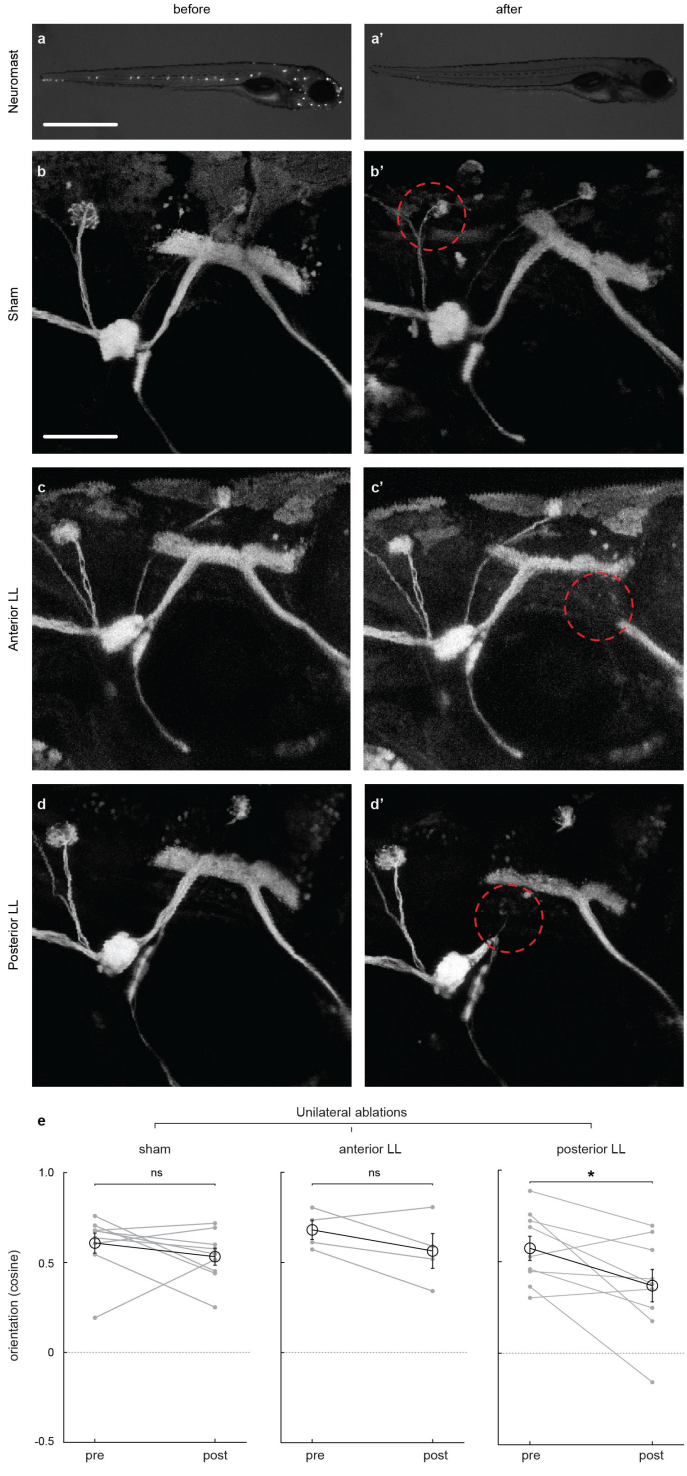
before
after
Neuromast
Sham
Anterior LL
Posterior LL
a
a'
b
b'
c
c'
d
d'
e
Unilateral ablations
sham
anterior LL
posterior LL
ns
ns
*
orientation (cosine)
1.0
0.5
0
-0.5
pre
post
pre
post
pre
post

B

Appendix 2

B.1 Supplementary material for Chapter 3: Efferent modulation in the lateral line of the larval zebrafish

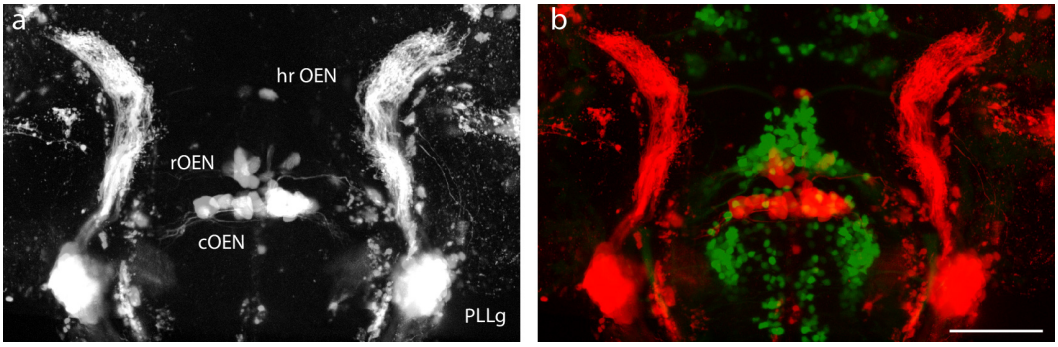

Figure B.1.1: Retrograde tracing of the LL nerve reveals 3 OEN sub-nuclei in the hindbrain.| a. Detail of the hindbrain. Registered confocal images taken after bilateral retrograde tracing of the lateral line with a fluorescent dye. Afferent neurons and their projections are visible on both PLL ganglia (PLLg), as well as efferent neurons of the OEN. They occupy 3 different positions with respect to the anterior-posterior axis and are named accordingly (caudal, rostral, and hyper-rostral). **b.**Composite image showing the registered retrograde labeled neurons (red) onto the reference brain of an isl1:gfp larva (green), in which cranio-facial motorneurons in the hindbrain are labeled. n=17 fish, 6 bilateral. Scale bar: 100 μm.

Estimations of population size

Planning for future studies that would involve ablations, it was necessary to get a sense of how large the efferent nuclei are. To this end, we used a simple capture-recapture sampling approach, which is a standard method to estimate the total number of individuals in a population. Briefly, we performed the 'capture' step by injecting a dye conjugated to a blue fluorophore at 5 dpf, at the level of the L1 neuromast. We allowed 48 hs for nerve regeneration [Pujol-Martí et al., 2014], and repeated the injection in the same location with a far red dye ('recapture'). Finally, we tallied how many neurons had been labeled in blue, red or both and used the Chapman estimator to calculate the total population size.

$$N = \frac{(m_1 + 1)(m_2 + 1)}{o + 1} + 1$$

Where N= total population size, m_1: nr. of neurons marked the first time, m_2: nr. of neurons marked the second time and o: nr. of recaptured neurons that were already marked (overlap).

We should note that Chapman was used instead of the more canonical Lincoln-Petersen estimator, to account for small population sizes and deal with cases where there were no neurons marked in both colors. This approach assumes that the population is closed, that is, that no neurons are born or die between labeling sessions. It also assumes independence of sampling, meaning that the probability of being 're-captured' is not influenced by being 'captured' the first time. We performed these experiments on transgenic animals that expressed pan-neuronal nuclear-targeted mCherry (to aid in counting neurons), as well as GFP under the isl1 promoter (to use as anatomical landmark and distinguish between the 3 hindbrain nuclei).

Efferent nucleus	Nr. of neurons (unilateral)
DELL	4 ±0.27
Rostral OEN	1 ±0.13
Medial OEN	3 ±0.22
Caudal OEN	4 ±0.29

Table B.1.1: Estimated nr. of neurons present in each nucleus innervating the PLL

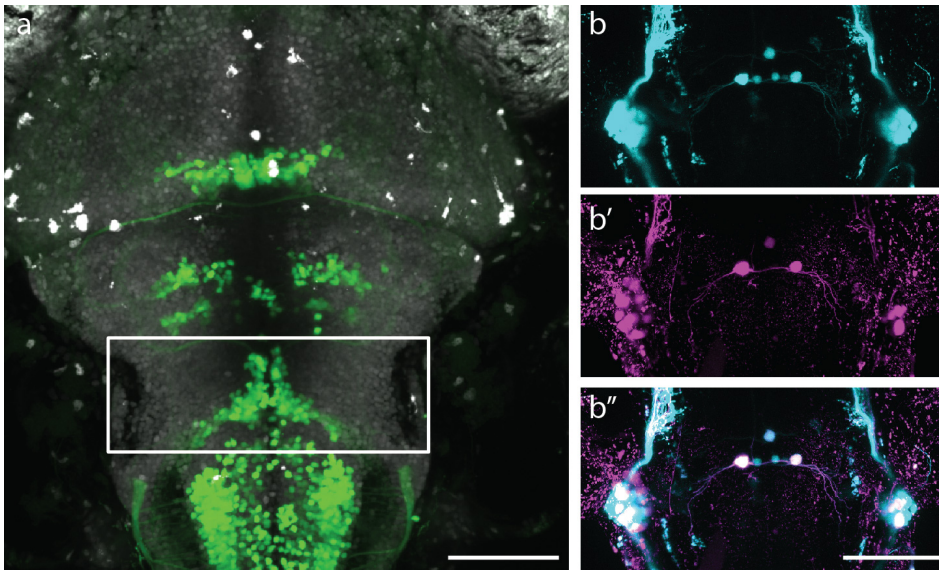

Figure B.1.2: Capture-recapture sampling to estimate population sizes.| a. Maxium intensity projections of dorsal confocal images of the brain of a double transgenic zebrafish larvae expressing nuclear-targeted mCherry pan-neuronally (grey, elavl3:h2b-mCherry) and GFP under the control of the isl1 promoter. Capture-recapture experiments were performed in this background in order to facilitate counting neurons and to assign them to the correct OEN sub-nuclei by using anatomical landmarks. **b.** Consecutive dye injections were performed. First at 5 dpf with a dye conjugated with a blue Dextran and at 7 dpf with a dye conjugated with a Dextran emitting in the far-red spectrum. Neurons labeled **b.** the first time (cyan), **b'.** the second time (magenta), and **b".** in both cases (overlap, white) were counted in order to estimate population size. Scale bars: 100 μm.

Efferent nuclei that project to the posterior LL are small, ranging from 1 to 4 neurons. Furthermore, single backfill can capture a large portion of a single population [see Table.1 for population sizes]. As a control, given that backfills also label primary sensory neurons, I used this technique to estimate the size of the posterior lateral line ganglion. It is believed that the PLLg has 30.8 ± 7.8 sensory neurons [Liao, 2010]. My estimates are close to that number, at 27 ± 2.4, validating this approach to estimate the efferent populations.

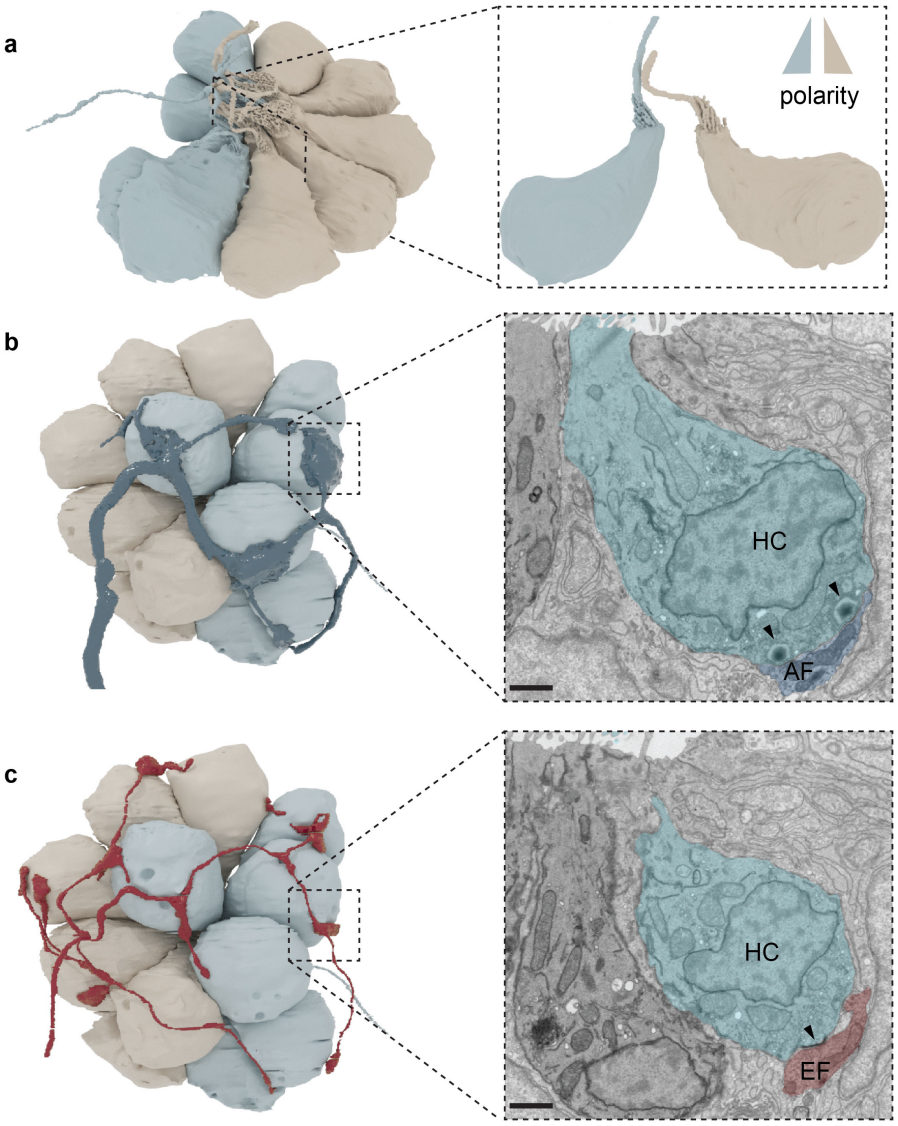

Figure B.1.3: Volumetric reconstruction of a lateral line neuromast in a 5.5 dpf fish from serial electron microscopy data.| **a.**Hair cells within a neuromast exhibit opposing polarities, as indicated by blue and beige colors. The two planar polarities are distinguished by the position of the kinocilium within the hair bundle. **b.**Afferent neurons (dark blue) innervate only hair cells of one polarity. **c.**A single efferent neuron (red) innervates hair cells of both polarities within a neuromast. Efferent and afferent terminals are distinguished by the ultrastructure of their synaptic contacts with hair cells (pseudo colored electron microscopy images). Afferents are in close apposition to ribbon synapses within hair cells, while efferent neurons are characterized by flat electron-dense contacts. Scale bars: 1 μm.

References

John C Adams, Edmund A Mroz, and William F Sewell. A possible neurotransmitter role for cgrp in a hair-cell sensory organ. *Brain research*, 419(1):347–351, 1987.

Misha B Ahrens, Jennifer M Li, Michael B Orger, Drew N Robson, Alexander F Schier, Florian Engert, and Ruben Portugues. Brain-wide neuronal dynamics during motor adaptation in zebrafish. *Nature*, 485(7399):471–477, 2012.

Misha B Ahrens, Michael B Orger, Drew N Robson, Jennifer M Li, and Philipp J Keller. Whole-brain functional imaging at cellular resolution using light-sheet microscopy. *Nature methods*, 10 (5):413–420, 2013.

Daniel Alexandre and Alain Ghysen. Somatotopy of the lateral line projection in larval zebrafish. *Proceedings of the National Academy of Sciences*, 96(13):7558–7562, 1999.

GP Arnold. Rheotropism in fishes. *Biological reviews*, 49(4):515–576, 1974.

GP Arnold and PH Cook. Fish migration by selective tidal stream transport: first results with a computer simulation model for the european continental shelf. In *Mechanisms of migration in fishes*, pages 227–261. Springer, 1984.

Jonathan J Art and Alfons BA Kroese. Effects of efferent activity during respiration on xenopus-laevis lateral line afferent responses. In *Journal of Physiology - London*, volume 332, pages P21–P22. Cambridge University Press, 1982.

Gerald P Bailey and William F Sewell. Pharmacological characterization of the cgrp receptor in the lateral line organ of xenopus laevis. *JARO-Journal of the Association for Research in Otolaryngology*, 1(1):82–88, 2000a.

Gerald P Bailey and William F Sewell. Calcitonin gene-related peptide suppresses hair cell responses to mechanical stimulation in the xenopus lateral line organ. *Journal of Neuroscience*, 20(13):5163–5169, 2000b.

Cindy F Baker and John C Montgomery. The sensory basis of rheotaxis in the blind mexican cave fish, astyanax fasciatus. *Journal of Comparative Physiology A: Neuroethology, Sensory, Neural, and Behavioral Physiology*, 184(5):519–527, 1999.

Dwight Barkley, Baofang Song, Vasudevan Mukund, Grégoire Lemoult, Marc Avila, and Björn Hof. The rise of fully turbulent flow. *Nature*, 526(7574):550–553, 2015.

James C Beck, Edwin Gilland, David W Tank, and Robert Baker. Quantifying the ontogeny of optokinetic and vestibuloocular behaviors in zebrafish, medaka, and goldfish. *Journal of neurophysiology*, 92(6):3546–3561, 2004.

Curtis C Bell. An efference copy which is modified by reafferent input. *Science*, 214(4519):450–453, 1981.

Curtis C Bell, J Bradbury, and Charles J Russell. The electric organ of a mormyrid as a current and voltage source. *Journal of Comparative Physiology A: Neuroethology, Sensory, Neural, and Behavioral Physiology*, 110(1):65–88, 1976.

Howard C Berg. *Random walks in biology*. Princeton University Press, 1993.

Isaac H Bianco, Adam R Kampff, and Florian Engert. Prey capture behavior evoked by simple visual stimuli in larval zebrafish. *Frontiers in systems neuroscience*, 5:101, 2011.

Isaac H Bianco, Leung-Hang Ma, David Schoppik, Drew N Robson, Michael B Orger, James C Beck, Jennifer M Li, Alexander F Schier, Florian Engert, and Robert Baker. The tangential nucleus controls a gravito-inertial vestibulo-ocular reflex. *Current biology*, 22(14):1285–1295, 2012.

Alexander Bowman. Plaice marking experiments shetland waters 1923–1931 (inclusive). *Journal du Conseil*, 8(2):223–229, 1933.

Francis P Bretherton and W Lord Rotschild. Rheotaxis of spermatozoa. *Proceedings of the Royal Society of London B: Biological Sciences*, 153(953):490–502, 1961.

Olivier Bricaud, Vicky Chaar, Christine Dambly-Chaudière, and Alain Ghysen. Early efferent innervation of the zebrafish lateral line. *Journal of Comparative Neurology*, 434(3):253–261, 2001.

Christian Brösamle and Marnie E Halpern. Characterization of myelination in the developing zebrafish. *Glia*, 39(1):47–57, 2002.

Seth A Budick and Donald M O'Malley. Locomotor repertoire of the larval zebrafish: swimming, turning and prey capture. *Journal of Experimental Biology*, 203(17):2565–2579, 2000.

Harold A Burgess and Michael Granato. Modulation of locomotor activity in larval zebrafish during light adaptation. *Journal of Experimental Biology*, 210(14):2526–2539, 2007.

Phyllis H Cahn and Evelyn Shaw. A method for studying lateral line cupular bending in juvenile fishes. *Bulletin of Marine Science*, 15(4):1060–1071, 1965.

Rose L Carlson and George V Lauder. Escaping the flow: boundary layer use by the darter etheostoma tetrazonum (percidae) during benthic station holding. *Journal of Experimental Biology*, 214(7):1181–1193, 2011.

Vincent Castellucci, Harold Pinsker, Irving Kupfermann, and Eric R Kandel. Neuronal mechanisms of habituation and dishabituation of the gill-withdrawal reflex in aplysia. *Science*, 167(3926): 1745–1748, 1970.

Boris Philippe Chagnaud and Sheryl Coombs. Information encoding and processing by the peripheral lateral line system. In *The Lateral Line System*, pages 151–194. Springer, 2013.

Jason W Chapman, Raymond HG Klaassen, V Alistair Drake, Sabrina Fossette, Graeme C Hays, Julian D Metcalfe, Andrew M Reynolds, Don R Reynolds, and Thomas Alerstam. Animal orientation strategies for movement in flows. *Current Biology*, 21(20):R861–R870, 2011.

Xiuye Chen and Florian Engert. Navigational strategies underlying phototaxis in larval zebrafish. *Frontiers in systems neuroscience*, 8, 2014.

Allison B Coffin, Heather Brignull, David W Raible, and Edwin W Rubel. Hearing loss, protection, and regeneration in the larval zebrafish lateral line. In *The lateral line system*, pages 313–347. Springer, 2013.

Sheryl Coombs, John Janssen, and Jacqueline F Webb. Diversity of lateral line systems: evolutionary and functional considerations. In *Sensory biology of aquatic animals*, pages 553–593. Springer, 1988.

R Cords. Das nystagmusproblem. *Münch. med. Wochenschr*, 693, 1922.

David P Corey and A James Hudspeth. Ionic basis of the receptor potential in a vertebrate hair cell. *Nature*, 281(5733):675–677, 1979.

Trinity B Crapse and Marc A Sommer. Corollary discharge across the animal kingdom. *Nature Reviews Neuroscience*, 9(8):587–600, 2008.

Keith N Darrow, Stéphane F Maison, and M Charles Liberman. Selective removal of lateral olivocochlear efferents increases vulnerability to acute acoustic injury. *Journal of neurophysiology*, 97 (2):1775–1785, 2007.

Viola M Davidson. Salmon and eel movement in constant circular current. *Journal of the Fisheries Board of Canada*, 7(7):432–448, 1949.

Filippo Del Bene and Claire Wyart. Optogenetics: a new enlightenment age for zebrafish neurobiology. *Developmental neurobiology*, 72(3):404–414, 2012.

Sven Dijkgraaf. The functioning and significance of the lateral-line organs. *Biological Reviews*, 38(1): 51–105, 1963.

John K Douglass, Lon Wilkens, Eleni Pantazelou, Frank Moss, et al. Noise enhancement of information transfer in crayfish mechanoreceptors by stochastic resonance. *Nature*, 365(6444):337–340, 1993.

Eliot Dow, Kimberly Siletti, and Albert J Hudspeth. Cellular projections from sensory hair cells form polarity-specific scaffolds during synaptogenesis. *Genes & development*, 29(10):1087–1094, 2015.

Eliot G Drucker and George V Lauder. Locomotor forces on a swimming fish: three-dimensional vortex wake dynamics quantified using digital particle image velocimetry. *Journal of Experimental Biology*, 202:2393–2412, 1999.

Didier Dulon, Lin Luo, Chunyan Zhang, and Allen F Ryan. Expression of small-conductance calcium-activated potassium channels (sk) in outer hair cells of the rat cochlea. *European Journal of Neuroscience*, 10(3):907–915, 1998.

Timothy W Dunn, Christoph Gebhardt, Eva A Naumann, Clemens Riegler, Misha B Ahrens, Florian Engert, and Filippo Del Bene. Neural circuits underlying visually evoked escapes in larval zebrafish. *Neuron*, 89(3):613–628, 2016a.

Timothy W Dunn, Yu Mu, Sujatha Narayan, Owen Randlett, Eva A Naumann, Chao-Tsung Yang, Alexander F Schier, Jeremy Freeman, Florian Engert, and Misha B Ahrens. Brain-wide mapping of neural activity controlling zebrafish exploratory locomotion. *Elife*, 5:e12741, 2016b.

Robert C Eaton, Rocco A Bombardieri, and Dietrich L Meyer. The mauthner-initiated startle response in teleost fish. *Journal of Experimental Biology*, 66(1):65–81, 1977.

Robert C Eaton, Jonathan Nissanov, and Chris M Wieland. Differential activation of mauthner and non-mauthner startle circuits in the zebrafish: implications for functional substitution. *Journal of Comparative Physiology A*, 155(6):813–820, 1984.

David E Ehrlich and David Schoppik. Control of movement initiation underlies the development of balance. *Current biology*, 27(3):334–344, 2017.

Ana B Elgoyhen, David S Johnson, Jim Boulter, Douglas E Vetter, and Stephen Heinemann. *α9*: an acetylcholine receptor with novel pharmacological properties expressed in rat cochlear hair cells. *Cell*, 79(4):705–715, 1994.

Ana B Elgoyhen, Douglas E Vetter, Eleonora Katz, Carla V Rothlin, Stephen F Heinemann, and Jim Boulter. *α10*: a determinant of nicotinic cholinergic receptor function in mammalian vestibular and cochlear mechanosensory hair cells. *Proceedings of the National Academy of Sciences*, 98(6): 3501–3506, 2001.

Raymond E Engeszer, Larissa B Patterson, Andrew A Rao, and David M Parichy. Zebrafish in the wild: a review of natural history and new notes from the field. *Zebrafish*, 4(1):21–40, 2007.

Fred H Everest and Donald W Chapman. Habitat selection and spatial interaction by juvenile chinook salmon and steelhead trout in two idaho streams. *Journal of the Fisheries Board of Canada*, 29(1):91–100, 1972.

Eric Fabricius and Karl-Jakob Gustafson. *Observations on the spawning behaviour of the grayling, Thymallus thymallus*. National Swedish Board of Fisheries, 1955.

Ryann M Fame, Carole Brajon, and Alain Ghysen. Second-order projection from the posterior lateral line in the early zebrafish brain. *Neural development*, 1(1):4, 2006.

Paul Fatt. The electromotive action of acetylcholine at the motor end-plate. *The Journal of physiology*, 111(3-4):408, 1950.

Adèle Faucherre, Jesús Pujol-Martí, Koichi Kawakami, and Hernán López-Schier. Afferent neurons of the zebrafish lateral line are strict selectors of hair-cell orientation. *PloS one*, 4(2):e4477, 2009.

Lief Fenno, Ofer Yizhar, and Karl Deisseroth. The development and application of optogenetics. *Annual review of neuroscience*, 34:389–412, 2011.

Lara A Ferry-Graham and George V Lauder. Aquatic prey capture in ray-finned fishes: a century of progress and new directions. *Journal of Morphology*, 248(2):99–119, 2001.

Robert Fettiplace and Carole M Hackney. The sensory and motor roles of auditory hair cells. *Nature Reviews Neuroscience*, 7(1):19–29, 2006.

Åke Flock. Transducing mechanisms in the lateral line canal organ receptors. In *Cold Spring Harbor Symposia on Quantitative Biology*, volume 30, pages 133–145. Cold Spring Harbor Laboratory Press, 1965.

Åke Flock and Ian J Russell. Efferent nerve fibres: postsynaptic action on hair cells. *Nature: New biology*, 243(124):89–91, 1973.

Åke Flock and Ian J Russell. Inhibition by efferent nerve fibres: action on hair cells and afferent synaptic transmission in the lateral line canal organ of the burbot lota lota. *The Journal of physiology*, 257(1):45–62, 1976.

Åke Flock and Jan Wersäll. A study of the orientation of the sensory hairs of the receptor cells in the lateral line organ of fish, with special reference to the function of the receptors. *The Journal of Cell Biology*, 15(1):19, 1962.

Gottfried S Fraenkel and Donald L Gunn. The orientation of animals: kineses, taxes and compass reactions. 1961.

Henry C Fu, Thomas R Powers, Roman Stocker, et al. Bacterial rheotaxis. *Proceedings of the National Academy of Sciences*, 109(13):4780–4785, 2012.

Lee A Fuiman and Paul W Webb. Ontogeny of routine swimming activity and performance in zebra danios (teleostei: Cyprinidae). *Animal Behaviour*, 36(1):250–261, 1988.

TW Fulton. The currents of the north sea, and their relation to fisheries. *15th Annual Report. Fish Board Scotl*, 1897.

Ethan Gahtan, Paul Tanger, and Herwig Baier. Visual prey capture in larval zebrafish is controlled by identified reticulospinal neurons downstream of the tectum. *Journal of Neuroscience*, 25(40): 9294–9303, 2005.

Galileo Galilei. *Dialogue concerning the two chief world systems, Ptolemaic and Copernican*. Modern Library Science, 1953.

Shelby D Gerking. The restricted movement of fish populations. *Biological reviews*, 34(2):221–242, 1959.

Alain Ghysen and Christine Dambly-Chaudiere. Development of the zebrafish lateral line. *Current opinion in neurobiology*, 14(1):67–73, 2004.

Alain Ghysen and Christine Dambly-Chaudière. The lateral line microcosmos. *Genes & development*, 21(17):2118–2130, 2007.

Darren Gilmour, Holger Knaut, Hans-Martin Maischein, and Christiane Nüsslein-Volhard. Towing of sensory axons by their migrating target cells in vivo. *Nature neuroscience*, 7(5):491–492, 2004.

Nicolas Gompel, Christine Dambly-Chaudière, and Alain Ghysen. Neuronal differences prefigure somatotopy in the zebrafish lateral line. *Development*, 128(3):387–393, 2001.

J Gray. Pseudo-rheotropism in fishes. *Journal of Experimental Biology*, 14(1):95–103, 1937.

Melanie Haehnel, Masashige Taguchi, and James C Liao. Heterogeneity and dynamics of lateral line afferent innervation during development in zebrafish (danio rerio). *Journal of Comparative Neurology*, 520(7):1376–1386, 2012.

Kiyoshi Hama. Some observations on the fine structure of the lateral line organ of the japanese sea eel lyncozymba nystromi. *The Journal of cell biology*, 24(2):193–210, 1965.

William Harvey. *The circulation of the blood*. Cosimo, Inc. ed.2006, 1628.

Shin-ichi Higashijima, Yoshiki Hotta, and Hitoshi Okamoto. Visualization of cranial motor neurons in live transgenic zebrafish expressing green fluorescent protein under the control of the islet-1 promoter/enhancer. *Journal of Neuroscience*, 20(1):206–218, 2000.

David GC Hildebrand, Marcelo Cicconet, Russel M Torres, Woohyuk Choi, Tran M Quan, Jungmin Moon, Arthur W Wetzel, Andrew S Champion, Brett J Graham, Owen Randlett, George S Plummer, Ruben Portugues, Isaac H Bianco, Stephan Saalfeld, Alexander D Baden, Kunal Lillaney, Randal Burns, Joshua T Vogelstein, Alexander F Schier, Wei-Chung A Lee, Won-Ki Jeong, Jeff W Lichtman, and Florian Engert. Whole-brain serial-section electron microscopy in larval zebrafish. *Nature*, in press, 2017.

Bruno Hofer. Studien über die hautsinnesorgane der fische i. *Die Funktion der Seitenorgane bei den Fischen. Ber Kgl Bayer Biol Versuchsstation München*, 1:115–168, 1908.

Sunder Lal Hora. Structural modifications in the fish of mountain torrents. *Records of the Indian Museum*, 24:31–61, 1922.

Howard C Howland. The role of the semicircular canals in the angular orientation of fish. *Annals of the New York Academy of Sciences*, 188(1):202–215, 1971.

Howard C Howland and B Howland. The reaction of blinded goldfish to rotation in a centrifuge. *Journal of Experimental Biology*, 39(3):491–502, 1962.

A James Hudspeth and David P Corey. Sensitivity, polarity, and conductance change in the response of vertebrate hair cells to controlled mechanical stimuli. *Proceedings of the National Academy of Sciences*, 74(6):2407–2411, 1977.

A James Hudspeth, Thomas M Jessell, Eric R Kandel, James Harris Schwartz, and Steven A Siegelbaum. *Principles of neural science*. 2013.

Daigo Inoue and Joachim Wittbrodt. One for all—a highly efficient and versatile method for fluorescent immunostaining in fish embryos. *PloS one*, 6(5):e19713, 2011.

John Janssen. Comparison of response distance to prey via the lateral line in the ruffe and yellow perch. *Journal of Fish Biology*, 51(5):921–930, 1997.

Michael Jay, Francesca De Faveri, and Jonathan Robert McDearmid. Firing dynamics and modulatory actions of supraspinal dopaminergic neurons during zebrafish locomotor behavior. *Current Biology*, 25(4):435–444, 2015.

F Roy Harden Jones. Fish migration: Passive drift or orientated movement? *Animal Behaviour*, 9 (3-4):239, 1961.

F Roy Harden Jones, Geoff P Arnold, M Greer Walker, and P Scholes. Selective tidal stream transport and the migration of plaice (pleuronectes platessa l.) in the southern north sea. *Journal du Conseil*, 38(3):331–337, 1979.

FR Harden Jones. Rotation experiments with blind goldfish. *Journal of Experimental Biology*, 34(2): 259–275, 1957.

Hovey Jordan. Rheotropic responses of epinephelus striatus bloch. *Amer. Jour. Physiol*, 43:438–454, 1917.

Harry Kalleberg. Observations in a stream tank of territoriality and competition in juvenile salmon and trout (salmo salar l. and s. trutta l.). *Institute of Freshwater Research Drottningholm Report*, 39: 55–98, 1958.

Eric R Kandel, Yadin Dudai, and Mark R Mayford. The molecular and systems biology of memory. *Cell*, 157(1):163–186, 2014.

Erica C Keen and AJ Hudspeth. Transfer characteristics of the hair cell's afferent synapse. *Proceedings of the National Academy of Sciences*, 103(14):5537–5542, 2006.

Charles B Kimmel, Jill Patterson, and Richard O Kimmel. The development and behavioral characteristics of the startle response in the zebra fish. *Developmental psychobiology*, 7(1):47–60, 1974.

Charles B Kimmel, William W Ballard, Seth R Kimmel, Bonnie Ullmann, and Thomas F Schilling. Stages of embryonic development of the zebrafish. *Developmental dynamics*, 203(3):253–310, 1995.

Katie S Kindt, Gabriel Finch, and Teresa Nicolson. Kinocilia mediate mechanosensitivity in developing zebrafish hair cells. *Developmental cell*, 23(2):329–341, 2012.

Alfons BA Kroese and Sietse M Van Netten. Sensory transduction in lateral line hair cells. In *The mechanosensory lateral line*, pages 265–284. Springer, 1989.

Matthew Kulpa, Joseph Bak-Coleman, and Sheryl Coombs. The lateral line is necessary for blind cavefish rheotaxis in non-uniform flow. *Journal of Experimental Biology*, 218(10):1603–1612, 2015.

Ching Kung. A possible unifying principle for mechanosensation. *Nature*, 436(7051):647–654, 2005.

Irving Kupfermann, Vincent Castellucci, Harold Pinsker, and Eric R Kandel. Neuronal correlates of habituation and dishabituation of the gill-withdrawal reflex in aplysia. *Science*, 167(3926):1743–1745, 1970.

Alix MB Lacoste, David Schoppik, Drew N Robson, Martin Haesemeyer, Ruben Portugues, Jennifer M Li, Owen Randlett, Caroline L Wee, Florian Engert, and Alexander F Schier. A convergent and essential interneuron pathway for mauthner-cell-mediated escapes. *Current Biology*, 25 (11):1526–1534, 2015.

Michael J Lannoo. Neuromast topography in ambystoma larvae. *Copeia*, pages 535–539, 1985.

Franz Leydig. *Zur Anatomie der Mannlichen Geschlechtsorgane und Analdrusen der Saugethiere*. 1850.

James C Liao. Organization and physiology of posterior lateral line afferent neurons in larval zebrafish. *Biology letters*, page rsbl20090995, 2010.

Arne Lindroth. *Distribution Territorial Bahaviour and Movements of Sea Trout Fry in the River Indalsalven*. Carl Bloms Boetryckeri, 1956.

Hernán López-Schier, Catherine J Starr, James A Kappler, Richard Kollmar, and A James Hudspeth. Directional cell migration establishes the axes of planar polarity in the posterior lateral-line organ of the zebrafish. *Developmental cell*, 7(3):401–412, 2004.

Otto Löwenstein. Experimentelle untersuchungen über den gleichgewichtssinn der elritze (phoxinus laevis l.). *Journal of Comparative Physiology A: Neuroethology, Sensory, Neural, and Behavioral Physiology*, 17(4):806–854, 1932.

EP Lyon. On rheotropism. i.—rheotropism in fishes. *American Journal of Physiology–Legacy Content*, 12(2):149–161, 1904.

EP Lyon. On rheotropism.—ii. rheotropism of fish blind in one eye. *American Journal of Physiology–Legacy Content*, 24(2):244–251, 1909.

Eva Y Ma and David W Raible. Signaling pathways regulating zebrafish lateral line development. *Current Biology*, 19(9):R381–R386, 2009.

Shinji Matsutani and Noboru Yamamoto. Centrifugal innervation of the mammalian olfactory bulb. *Anatomical science international*, 83(4):218–227, 2008.

Michelle M McClure, Peter B McIntyre, and Amy R McCune. Notes on the natural diet and habitat of eight danionin fishes, including the zebrafish danio rerio. *Journal of Fish Biology*, 69(2):553–570, 2006.

Matthew J McHenry and George V Lauder. The mechanical scaling of coasting in zebrafish (danio rerio). *Journal of Experimental Biology*, 208(12):2289–2301, 2005.

Matthew J McHenry, Karla E Feitl, James A Strother, and William J Van Trump. Larval zebrafish rapidly sense the water flow of a predator's strike. *Biology Letters*, 5(4):477–479, 2009.

Alexander Meek. Migrations in the sea. *Nature*, 95:231, 1915.

Gloria E Meredith and Barry L Roberts. Distribution and morphological characteristics of efferent neurons innervating end organs in the ear and lateral line of the european eel. *Journal of Comparative Neurology*, 265(4):494–506, 1987.

Walter K Metcalfe. Sensory neuron growth cones comigrate with posterior lateral line primordial cells in zebrafish. *Journal of Comparative Neurology*, 238(2):218–224, 1985.

Walter K Metcalfe, Charles B Kimmel, and Eric Schabtach. Anatomy of the posterior lateral line system in young larvae of the zebrafish. *Journal of Comparative Neurology*, 233(3):377–389, 1985.

Kiyoshi Miki and David E Clapham. Rheotaxis guides mammalian sperm. *Current Biology*, 23(6):443–452, 2013.

John C Montgomery and David Bodznick. An adaptive filter that cancels self-induced noise in the electrosensory and lateral line mechanosensory systems of fish. *Neuroscience letters*, 174(2):145–148, 1994.

John C Montgomery and David Bodznick. Signals and noise in the elasmobranch electrosensory system. *Journal of Experimental Biology*, 202(10):1349–1355, 1999.

John C Montgomery, Cindy F Baker, and Alexander G Carton. The lateral line can mediate rheotaxis in fish. *Nature*, 389(6654):960–963, 1997.

John C Montgomery, Fiona Macdonald, Cindy F Baker, and Alexander G Carton. Hydrodynamic contributions to multimodal guidance of prey capture behavior in fish. *Brain, behavior and evolution*, 59(4):190–198, 2002.

Yukinori Mukai and Hiroshi Kobayashi. Development of free neuromasts with special reference to sensory polarity in larvae of the willow shiner, gnathopogon elongatus caerulescens (teleostei, cyprinidae). *Zoological science*, 12(1):125–131, 1995.

Ulrike K Muller, Eize J Stamhuis, and John J Videler. Hydrodynamics of unsteady fish swimming and the effects of body size: comparing the flow fields of fish larvae and adults. *Journal of Experimental Biology*, 203(2):193–206, 2000.

Nathan A Mundell, Kevin T Beier, Y Albert Pan, Sylvain W Lapan, Didem Göz Aytürk, Vladimir K Berezovskii, Abigail R Wark, Eugene Drokhlyansky, Jan Bielecki, Richard T Born, et al. Vesicular stomatitis virus enables gene transfer and transsynaptic tracing in a wide range of organisms. *Journal of Comparative Neurology*, 523(11):1639–1663, 2015.

Heinrich Münz. Functional organization of the lateral line periphery. In *The mechanosensory lateral line*, pages 285–297. Springer, 1989.

Aaron Nagiel, Daniel Andor-Ardó, and A James Hudspeth. Specificity of afferent synapses onto plane-polarized hair cells in the posterior lateral line of the zebrafish. *Journal of Neuroscience*, 28 (34):8442–8453, 2008.

Eva A Naumann, James E Fitzgerald, Timothy W Dunn, Jason Rihel, Haim Sompolinsky, and Florian Engert. From whole-brain data to functional circuit models: the zebrafish optomotor response. *Cell*, 167(4):947–960, 2016.

Stephan CF Neuhauss, Oliver Biehlmaier, Mathias W Seeliger, Tilak Das, Konrad Kohler, William A Harris, and Herwig Baier. Genetic disorders of vision revealed by a behavioral screen of 400 essential loci in zebrafish. *Journal of Neuroscience*, 19(19):8603–8615, 1999.

Liping Nie, Haitao Song, Mei-Fang Chen, Nipavan Chiamvimonvat, Kirk W Beisel, Ebenezer N Yamoah, and Ana E Vázquez. Cloning and expression of a small-conductance ca2+-activated k+ channel from the mouse cochlea: coexpression with $a9/a10$ acetylcholine receptors. *Journal of neurophysiology*, 91(4):1536–1544, 2004.

R Glenn Northcutt. The phylogenetic distribution and innervation of craniate mechanoreceptive lateral lines. In *The mechanosensory lateral line*, pages 17–78. Springer, 1989.

Viviana A Nuñez, Andres F Sarrazin, Nicolas Cubedo, Miguel L Allende, Christine Dambly-Chaudière, and Alain Ghysen. Postembryonic development of the posterior lateral line in the zebrafish. *Evolution & development*, 11(4):391–404, 2009.

Nikolaus Obholzer, Sean Wolfson, Josef G Trapani, Weike Mo, Alex Nechiporuk, Elisabeth Busch-Nentwich, Christoph Seiler, Samuel Sidi, Christian Söllner, Robert N Duncan, et al. Vesicular glutamate transporter 3 is required for synaptic transmission in zebrafish hair cells. *Journal of Neuroscience*, 28(9):2110–2118, 2008.

Raphaël Olive, Sébastien Wolf, Alexis Dubreuil, Volker Bormuth, Georges Debrégeas, and Raphaël Candelier. Rheotaxis of larval zebrafish: behavioral study of a multi-sensory process. *Frontiers in systems neuroscience*, 10, 2016.

Dominik Oliver, Nikolaj Klöcker, Jochen Schuck, Thomas Baukrowitz, J Peter Ruppersberg, and Bernd Fakler. Gating of ca 2+-activated k+ channels controls fast inhibitory synaptic transmission at auditory outer hair cells. *Neuron*, 26(3):595–601, 2000.

Julia Olszewski, Melanie Haehnel, Masashige Taguchi, and James C Liao. Zebrafish larvae exhibit rheotaxis and can escape a continuous suction source using their lateral line. *PLoS One*, 7(5): e36661, 2012.

Michael B Orger and Gonzalo G de Polavieja. Zebrafish behavior: Opportunities and challenges. *Annual review of neuroscience*, 2017.

Michael B Orger, Adam R Kampff, Kristen E Severi, Johann H Bollmann, and Florian Engert. Control of visually guided behavior by distinct populations of spinal projection neurons. *Nature neuroscience*, 11(3):327–333, 2008.

George Howard Parker. *Hearing and allied senses in fishes*. US Government Printing Office, 1903.

Brian L Partridge and Tony J Pitcher. The sensory basis of fish schools: relative roles of lateral line and vision. *Journal of comparative physiology*, 135(4):315–325, 1980.

DH Paul and Barry L Roberts. The location and properties of the efferent neurons of the head lateral-line organs of dogfish. *Journal of Comparative Physiology A: Neuroethology, Sensory, Neural, and Behavioral Physiology*, 116(1):117–127, 1977.

James O Pickles, Spiro D Comis, and Michael P Osborne. Cross-links between stereocilia in the guinea pig organ of corti, and their possible relation to sensory transduction. *Hearing research*, 15 (2):103–112, 1984.

Harold Pinsker, Irving Kupfermann, Vincent Castellucci, and Eric R Kandel. Habituation and dishabituation of the gm-withdrawal reflex in aplysia. *Science*, 167(3926):1740–1742, 1970.

Ruben Portugues and Florian Engert. Adaptive locomotor behavior in larval zebrafish. *Frontiers in systems neuroscience*, 5:72, 2011.

Ruben Portugues, Claudia E Feierstein, Florian Engert, and Michael B Orger. Whole-brain activity maps reveal stereotyped, distributed networks for visuomotor behavior. *Neuron*, 81(6):1328–1343, 2014.

Ruben Portugues, Martin Haesemeyer, Mirella L Blum, and Florian Engert. Whole-field visual motion drives swimming in larval zebrafish via a stochastic process. *Journal of Experimental Biology*, 218(9):1433–1443, 2015.

Jesús Pujol-Martí, Andrea Zecca, Jean-Pierre Baudoin, Adèle Faucherre, Kazuhide Asakawa, Koichi Kawakami, and Hernán López-Schier. Neuronal birth order identifies a dimorphic sensorineural map. *Journal of Neuroscience*, 32(9):2976–2987, 2012.

Jesús Pujol-Martí, Adele Faucherre, Razina Aziz-Bose, Amir Asgharsharghi, Julien Colombelli, Josef G Trapani, and Hernán López-Schier. Converging axons collectively initiate and maintain synaptic selectivity in a constantly remodeling sensory organ. *Current Biology*, 24(24):2968–2974, 2014.

David W Raible and Gregory J Kruse. Organization of the lateral line system in embryonic zebrafish. *Journal of Comparative Neurology*, 421(2):189–198, 2000.

Gustaf Retzius. *Das gehörorgan der wirbelthiere*. Gedruckt in der Centraldruckerei, 1884.

GP Richardson, Ian J Russell, VC Duance, and AJ Bailey. Polypeptide composition of the mammalian tectorial membrane. *Hearing research*, 25(1):45–60, 1987.

Leif Ristroph, James C Liao, and Jun Zhang. Lateral line layout correlates with the differential hydrodynamic pressure on swimming fish. *Physical review letters*, 114(1):018102, 2015.

Dale A Ritter, Dimple H Bhatt, and Joseph R Fetcho. In vivo imaging of zebrafish reveals differences in the spinal networks for escape and swimming movements. *Journal of Neuroscience*, 21(22): 8956–8965, 2001.

Barry L Roberts and Ian J Russell. The activity of lateral-line efferent neurones in stationary and swimming dogfish. *J Exp Biol*, 57(2):435–448, 1972.

BL Roberts, Suharti Maslam, I Los, and B Van der Jagt. Coexistence of calcitonin gene-related peptide and choline acetyltransferase in eel efferent neurons. *Hearing research*, 74(1):231–237, 1994.

Ian J Russell. The role of the lateral-line efferent system in xenopus laevis. *J Exp Biol*, 54(3):621–641, 1971a.

Ian J Russell. The pharmacology of efferent synapses in the lateral-line system of xenopus laevis. *Journal of Experimental Biology*, 54(3):643–659, 1971b.

Ian J Russell. Central inhibition of lateral line input in the medulla of the goldfish by neurones which control active body movements. *Journal of comparative physiology*, 111(3):335–358, 1976.

Ian J Russell and Barry L Roberts. Inhibition of spontaneous lateral-line activity by efferent nerve stimulation. *J Exp Biol*, 57:77–82, 1972.

Ian J Russell and Barry L Roberts. Active reduction of lateral-line sensitivity in swimming dogfish. *Journal of Comparative Physiology A: Neuroethology, Sensory, Neural, and Behavioral Physiology*, 94 (1):7–15, 1974.

Stephan Saalfeld, Richard Fetter, Albert Cardona, and Pavel Tomancak. Elastic volume reconstruction from series of ultra-thin microscopy sections. *Nature methods*, 9(7):717–720, 2012.

Dora Sapède, Nicolas Gompel, Christine Dambly-Chaudière, and Alain Ghysen. Cell migration in the postembryonic development of the fish lateral line. *Development*, 129(3):605–615, 2002.

Andres F Sarrazin, Viviana A Nuñez, Dora Sapède, Valériane Tassin, Christine Dambly-Chaudière, and Alain Ghysen. Origin and early development of the posterior lateral line system of zebrafish. *Journal of Neuroscience*, 30(24):8234–8244, 2010.

Franz Eilhard Schulze. Über die nervenendigung in den sogenannten schleimkanälen der fische und über entsprechende organe der durch kiemen atmenden amphibien. *Arch Anat Physiol Lpz*, pages 759–769, 1861.

Franz Eilhard Schulze. Über die sinnesorgane der seitenlinie bei fischen und amphibien. *Archiv für mikroskopische Anatomie*, 6(1):62–88, 1870.

Kevin Schuster and Alain Ghysen. Labeling hair cells and afferent neurons in the posterior lateral-line system of zebrafish. *Cold Spring Harbor Protocols*, 2013(12):pdb–prot079467, 2013.

Kristen E Severi, Ruben Portugues, João C Marques, Donald M O'Malley, Michael B Orger, and Florian Engert. Neural control and modulation of swimming speed in the larval zebrafish. *Neuron*, 83(3):692–707, 2014.

William F Sewell and Philip A Starr. Effects of calcitonin gene-related peptide and efferent nerve stimulation on afferent transmission in the lateral line organ. *Journal of neurophysiology*, 65(5): 1158–1169, 1991.

Claude E Shannon. A symbolic analysis of relay and switching circuits. *Electrical Engineering*, 57 (12):713–723, 1938.

Sandra L Shotwell, R Jacobs, and A James Hudspeth. Directional sensitivity of individual vertebrate hair cells to controlled deflection of their hair bundles. *Annals of the New York Academy of Sciences*, 374(1):1–10, 1981.

Roger Wolcott Sperry. Neural basis of the spontaneous optokinetic response produced by visual inversion. *Journal of comparative and physiological psychology*, 43(6):482, 1950.

Arminda Suli, Glen M Watson, Edwin W Rubel, and David W Raible. Rheotaxis in larval zebrafish is mediated by lateral line mechanosensory hair cells. *PloS one*, 7(2):e29727, 2012.

Thomas Szabo and Alfred Fessard. Physiology of electroreceptors. In *Electroreceptors and Other Specialized Receptors in Lower Vertrebrates*, pages 59–124. Springer, 1974.

Marcel Tawk, Isaac H Bianco, and Jonathan DW Clarke. Focal electroporation in zebrafish embryos and larvae. *Zebrafish: Methods and Protocols*, pages 145–151, 2009.

Tuan Leng Tay, Olaf Ronneberger, Soojin Ryu, Roland Nitschke, and Wolfgang Driever. Comprehensive catecholaminergic projectome analysis reveals single-neuron integration of zebrafish ascending and descending dopaminergic systems. *Nature communications*, 2:171, 2011.

Andrew W Thompson, Gilles C Vanwalleghem, Lucy A Heap, and Ethan K Scott. Functional profiles of visual-, auditory-, and water flow-responsive neurons in the zebrafish tectum. *Current Biology*, 26(6):743–754, 2016.

Lin Tian, S Andrew Hires, and Loren L Looger. Imaging neuronal activity with genetically encoded calcium indicators. *Cold Spring Harbor Protocols*, 2012(6):pdb–top069609, 2012.

Cecilia Toro, Josef G Trapani, Itallia Pacentine, Reo Maeda, Lavinia Sheets, Weike Mo, and Teresa Nicolson. Dopamine modulates the activity of sensory hair cells. *Journal of Neuroscience*, 35(50): 16494–16503, 2015.

Kuniaki Toyoshima and Akitatsu Shimamura. Comparative study of ultrastructures of the lateral-line organs and the palatal taste organs in the african clawed toad, xenopus laevis. *The Anatomical Record*, 204(4):371–381, 1982.

Josef G Trapani and Teresa Nicolson. Mechanism of spontaneous activity in afferent neurons of the zebrafish lateral-line organ. *Journal of Neuroscience*, 31(5):1614–1623, 2011.

Josef G Trapani, Nikolaus Obholzer, Weike Mo, Susan E Brockerhoff, and Teresa Nicolson. Synaptojanin1 is required for temporal fidelity of synaptic transmission in hair cells. *PLoS Genet*, 5(5): e1000480, 2009.

David J Tritton. *Physical fluid dynamics*. Springer Science & Business Media, 2012.

Chintan A Trivedi and Johann H Bollmann. Visually driven chaining of elementary swim patterns into a goal-directed motor sequence: a virtual reality study of zebrafish prey capture. 2013.

William J Van Trump and Matthew J McHenry. The morphology and mechanical sensitivity of lateral line receptors in zebrafish larvae (danio rerio). *Journal of Experimental Biology*, 211(13): 2105–2115, 2008.

William J Van Trump and Matthew J McHenry. The lateral line system is not necessary for rheotaxis in the mexican blind cavefish (astyanax fasciatus). *Integrative and comparative biology*, page icto64, 2013.

Neil J Vickers. Mechanisms of animal navigation in odor plumes. *The Biological Bulletin*, 198(2): 203–212, 2000.

Heinrich A Vischer. The development of lateral-line receptors in eigenmannia (teleostei, gymnotiformes). i. the mechanoreceptive lateral-line system (part 1 of 2). *Brain, behavior and evolution*, 33(4):205–213, 1989.

Erich Von Holst. Relations between the central nervous system and the peripheral organs. *The British Journal of Animal Behaviour*, 2(3):89–94, 1954.

Theodore von Kármán. Mechanische ähnlichkeit und turbulenz, nachr. ges. wiss gottingen, math. phys. klasse; 1930, 5. *English translation, NACA TM*, 611:58–76, 1931.

Géraldine von Uckermann, François M Lambert, Denis Combes, Hans Straka, and John Simmers. Adaptive plasticity of spino-extraocular motor coupling during locomotion in metamorphosing xenopus laevis. *Journal of Experimental Biology*, 219(8):1110–1121, 2016.

Jacqueline F Webb. Gross morphology and evolution of the mechanoreceptive lateral-line system in teleost fishes (part 1 of 2). *Brain, behavior and evolution*, 33(1):34–43, 1989a.

Jacqueline F Webb. Neuromast morphology and lateral line trunk canal ontogeny in two species of cichlids: an sem study. *Journal of Morphology*, 202(1):53–68, 1989b.

Mario F Wullimann and Benedikt Grothe. The central nervous organization of the lateral line system. In *The lateral line system*, pages 195–251. Springer, 2013.

Yanwei Xi, Man Yu, Rafael Godoy, Gary Hatch, Luc Poitras, and Marc Ekker. Transgenic zebrafish expressing green fluorescent protein in dopaminergic neurons of the ventral diencephalon. *Developmental Dynamics*, 240(11):2539–2547, 2011.

Tong Xiao, Tobias Roeser, Wendy Staub, and Herwig Baier. A gfp-based genetic screen reveals mutations that disrupt the architecture of the zebrafish retinotectal projection. *Development*, 132 (13):2955–2967, 2005.

Yasumasa Yamada and Kiyoshi Hama. Fine structure of the lateral-line organ of the common eel, anguilla japonica. *Cell and Tissue Research*, 124(4):454–464, 1972.

Steven J Zottoli and Craig Van Horne. Posterior lateral line afferent and efferent pathways within the central nervous system of the goldfish with special reference to the mauthner cell. *Journal of comparative neurology*, 219(1):100–111, 1983.

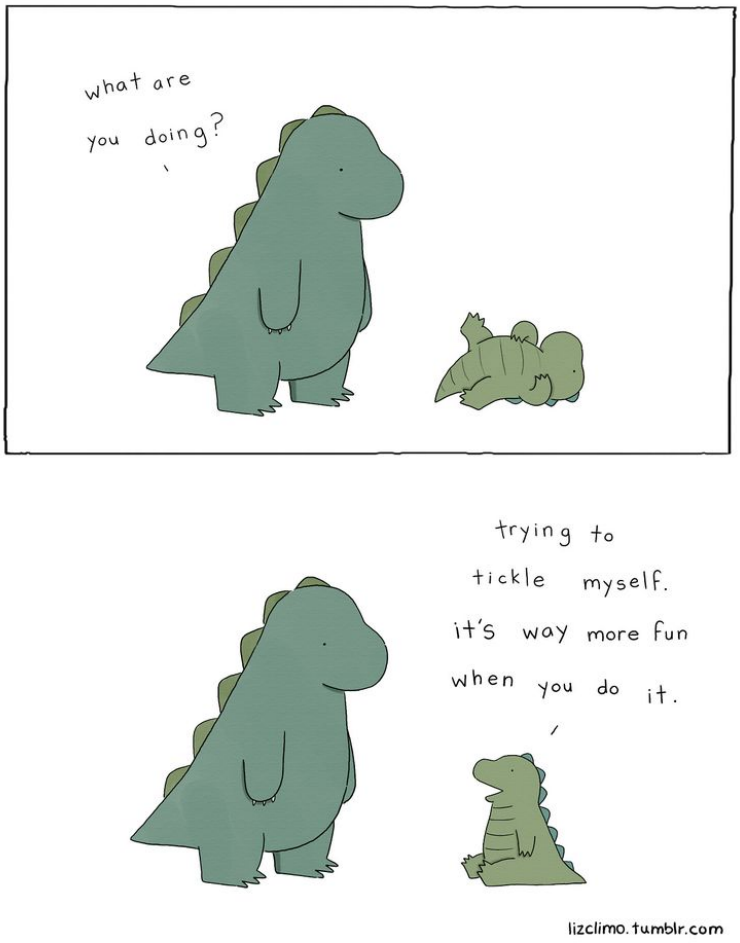

**With permission from the artist Liz Climo.*

Colophon

This thesis was typeset using LaTeX, originally developed by Leslie Lamport and based on Donald Knuth's TeX. The body text is set in 11 point Arno Pro, designed by Robert Slimbach in the style of book types from the Aldine Press in Venice, and issued by Adobe in 2007. A template, which can be used to format a PhD thesis with this look and feel, has been released under the permissive MIT (X11) license, and can be found online at github.com/suchow/ or from the author at suchow@post.harvard.edu.